

THE EFFECT OF PARTICLES ON THE CRITICAL  
LENGTH IN SUBSONIC AND SUPERSONIC  
GAS-PARTICLE FLOW IN A  
VERTICAL CONSTANT  
AREA TUBE

By

DAVID MICHAEL ADAMS

Bachelor of Science  
Texas A. and M. University  
College Station, Texas  
1959

Master of Science  
Texas A. and M. University  
College Station, Texas  
1960


Submitted to the Faculty of the Graduate School  
of the Oklahoma State University  
in partial fulfillment of  
the requirements for  
the Degree of  
DOCTOR OF PHILOSOPHY  
May, 1965

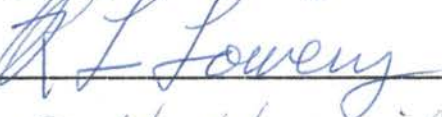
MAY 28 1965


THE EFFECT OF PARTICLES ON THE CRITICAL  
LENGTH IN SUBSONIC AND SUPERSONIC  
GAS-PARTICLE FLOW IN A  
VERTICAL CONSTANT  
AREA TUBE

Thesis Approved:

  
\_\_\_\_\_  
Thesis Adviser

\_\_\_\_\_  


\_\_\_\_\_  


\_\_\_\_\_  


\_\_\_\_\_  
  
Dean of the Graduate School

581331

## PREFACE

In this investigation the governing physical one-dimensional differential equations for subsonic and supersonic adiabatic gas-particle flow in a constant area tube were solved by finite difference computer techniques. Primary considerations were to evaluate the effect of the governing variables and starting conditions on the critical length and the local and critical exit properties of the gas and particles. The critical length is the maximum length that a gas-particle mixture may be transported. An experimental system was designed and operated for air and spherical glass particles flowing in a vertical constant area tube. Critical conditions were maintained for all test runs. The experimental results for the critical conditions were compared to corresponding analytical solutions.

The work herein was supervised by Dr. J. H. Boggs, Head, School of Mechanical Engineering, Oklahoma State University, and Dr. J. D. Parker, Associate Professor, School of Mechanical Engineering, Oklahoma State University. The author expresses grateful appreciation to Dr. Boggs and Dr. Parker for their advice and many suggestions, and for making available the facilities and equipment of the Mechanical Engineering Laboratory and the Oklahoma State University

Computing Center. Acknowledgement is also due the men of the Mechanical Engineering Laboratory for their aid in the construction and operation of the test apparatus described in this study, and to Dr. R. L. Lowery for his help with the instrumentation of the apparatus. Special thanks is given to Henderson E. Miller who assisted in the writing of the computer program for the analytical equations given herein.

## TABLE OF CONTENTS

Chapter	Page
I. INTRODUCTION . . . . .	1
II. REVIEW OF THE LITERATURE . . . . .	5
III. ANALYTICAL ANALYSIS . . . . .	31
IV. ANALYTICAL RESULTS . . . . .	49
Presentation of Results . . . . .	49
Discussion of Results . . . . .	59
V. EXPERIMENTAL ANALYSIS . . . . .	86
Derivation of Semi-Empirical Equations . . . . .	86
The Experimental System . . . . .	94
VI. EXPERIMENTAL RESULTS . . . . .	101
Presentation of Results . . . . .	101
Discussion and Comparison to Analytical Solutions . . . . .	109
Comparison of Results From the Literature to Analytical Solutions . . . . .	115
VII. INTERPRETATION OF RESULTS . . . . .	119
Summary and Conclusions . . . . .	119
Suggestions for Future Study . . . . .	123
BIBLIOGRAPHY . . . . .	125
APPENDIX . . . . .	133
A. Computer Program and Input Data . . . . .	133
B. Experimental Data . . . . .	151

LIST OF TABLES

Table	Page
I. Effect of Property Variations on the Critical Length . . . . .	61
II. Effect of the Parameters of the System on the Critical Length. . . . .	85
III. Properties of Gas-Particle Mixtures . . . . .	138
IV. Computer Input Data . . . . .	140
V. Computer Program . . . . .	142
VI. Experimental Single-Phase Data . . . . .	152
VII. Experimental Two-Phase Data . . . . .	153
VIII. Experimental Two-Phase Data . . . . .	154
IX. Experimental Equipment . . . . .	155

## LIST OF FIGURES

Figure	Page
1. Thermodynamic System . . . . .	33
2. Local Velocity, Temperature, Pressure, and Mach Number Characteristics of Subsonic Gas-Particle Flow . . . . .	51
3. Local Velocity, Temperature, Pressure, and Mach Number Characteristics of Supersonic Gas-Particle Flow . . . . .	54
4. Mixture Enthalpy-Entropy Diagram for Subsonic and Supersonic Gas-Particle Flow . . . . .	57
5. The Effect of Particles on the Subsonic and Supersonic Critical Lengths . . . . .	60
6. ASME Nozzle . . . . .	87
7. Instrumentation and Test Section . . . . .	99
8. Air Flow Nozzle Apparatus and Air Filter . . . . .	99
9. Over-all View of Experimental Apparatus . . . . .	100
10. Local Velocity, Temperature, Pressure, and Mach Number Characteristics of Subsonic Air Flow . . . . .	102
11. Local Velocity, Temperature, Pressure, and Mach Number Characteristics of Supersonic Air Flow . . . . .	104
12. Local Velocity, Temperature, Pressure, and Mach Number Characteristics of Subsonic Air-Particle Flow . . . . .	105
13. Local Velocity, Temperature, Pressure, and Mach Number Characteristics of Subsonic Air-Particle Flow . . . . .	107

LIST OF FIGURES (Continued)

Figure	Page
14. Dependency of the Wall Friction Factor on the Mach Number of Air . . . . .	111
15. Dependency of Air-Particle Pressure Drop on the Particle to Air Mass Flow Ratio . . . . .	116



TABLE OF NOMENCLATURE

A	Particle to air specific heat ratio, dimensionless, $A = c_{p1}/c_{g1}$ .
$A_t$	Total cross-sectional area of flow, in. <sup>2</sup> .
$A_g$	Effective cross-sectional area of flow for the gas, in. <sup>2</sup> .
$A_p$	Effective cross-sectional area of flow for the particles, in. <sup>2</sup> .
$A_{pf}$	Projected frontal area of a particle, in. <sup>2</sup> .
$A^o$	Area ratio, dimensionless, $A^o = A_t/A_{g1}$ .
B	Acceleration of gravity parameter, dimensionless, $B = 2gd_t/V_{g1}^2$ .
$C_d$	Drag coefficient of particles, dimensionless, $C_d = F_p^2 g_c / A_{pf} \rho_g (V_g - V_p)^2$ .
C	Gas to particle density ratio, dimensionless, $C = \rho_{g1}/\rho_p$ .
$CF_d$	Discharge coefficient of nozzle, dimensionless.
$c_{gs}$	Speed of sound in the gas, ft./sec.
$c_p$	Specific heat of the particles, Btu/lb. <sub>m</sub> <sup>o</sup> R.
$c_g$	Constant pressure specific heat of the gas Btu/lb. <sub>m</sub> <sup>o</sup> R.
$c_g^o$	Specific heat ratio of the gas, dimensionless, $c_g^o = c_g/c_{g1}$ .

TABLE OF NOMENCLATURE (Continued)

$c_p^o$	Specific heat ratio of the particles, dimensionless, $c_p^o = c_p/c_{p1}$ .
$d_p$	Diameter of particles, in.
$d_t$	Diameter of tube, in.
$d_{nt}$	Diameter of nozzle throat, in.
$D$	Tube to particle diameter ratio, dimensionless, $D = d_t/d_p$ .
$F_p$	Viscous and form drag forces acting on a particle, lb. <sub>f</sub> .
$f$	Wall friction factor, dimensionless, $f = \frac{dP}{g} \frac{2g_c R T}{g} \frac{d_t}{dx} \frac{V_g^2}{g}$ .
$g$	Local acceleration of gravity, ft./sec. <sup>2</sup> .
$g_c$	32.174 lb. <sub>m</sub> ft./sec. <sup>2</sup> lb. <sub>f</sub> .
$h_m$	Enthalpy of the gas-particle mixture, Btu/lb. <sub>m</sub> <sup>o</sup> R.
$h_m^o$	Enthalpy ratio, dimensionless, $h_m^o = h_m/c_{gl} T_{gl}$ .
$K_g$	Thermal conductivity of gas, Btu/hr. <sup>o</sup> F ft.
$K_g^o$	Thermal conductivity ratio of gas, dimensionless, $K_g^o = K_g/K_{g1}$ .
$M_g$	Mach number of gas, dimensionless, $M_g = V_g/c_{gs}$ .
$m_p$	Mass flow rate of particles, lb. <sub>m</sub> /min.
$m_g$	Mass flow rate of gas, lb. <sub>m</sub> /min.
$Nu_p$	Nusselt number of gas, dimensionless, $Nu_p = \frac{h_p d_p}{K_g}$ ( $h_p$ - convective film coefficient over particles).

TABLE OF NOMENCLATURE (Continued)

N	Number of particles passing a given location per unit time, particles/sec.
$Pr_g$	Prandtl number of gas, dimensionless, $Pr_g = c_g \mu_g / K_g$ .
$Pr_{gl}$	Reference Prandtl number of particles, dimensionless, $Pr_{gl} = c_{gl} \mu_{gl} / K_{gl}$ .
$P_g$	Pressure of gas, lb. <sub>f</sub> /in. <sup>2</sup> .
$P_g^0$	Pressure ratio of gas, dimensionless, $P_g^0 = P_g / P_{gl}$ .
$P_a$	Atmospheric Pressure, lb. <sub>f</sub> /in. <sup>2</sup> .
$Re_p$	Reynolds number of particles, dimensionless, $Re_p = d_p (V_g - V_p) \rho_g / \mu_g g_c$ .
$Re_{pl}$	Reference Reynolds number of particles, dimensionless, $Re_{pl} = d_p V_{gl} \rho_{gl} / \mu_{gl} g_c$ .
$Re_t$	Reynolds number of tube, dimensionless, $Re_t = d_t V_g \rho_g / \mu_g g_c$ .
$R_g$	Gas constant of gas, ft. lb. <sub>f</sub> /lb. <sub>m</sub> <sup>o</sup> R.
$s_m$	Entropy of gas-particle mixture, Btu/lb. <sub>m</sub> <sup>o</sup> R.
$s_m^0$	Entropy ratio, dimensionless, $s_m^0 = s_m / c_{gl}$ .
$S_p$	Particle slip, dimensionless, $S_p = V_p / V_g$ .
$T_g$	Temperature of gas, <sup>o</sup> R.
$T_g^0$	Temperature ratio of gas, dimensionless, $T_g^0 = T_g / T_{gl}$ .
$T_p$	Temperature of particles, <sup>o</sup> R.
$T_p^0$	Temperature ratio of particles, dimensionless, $T_p^0 = T_p / T_{gl}$ .
$V_g$	Velocity of gas, ft./sec.

TABLE OF NOMENCLATURE (Continued)

$V_g^0$	Velocity ratio of gas, dimensionless, $V_g^0 = V_g/V_{g1}$ .
$V_{g1}$	Reference velocity of gas, $V_{g1} = \sqrt{2g_c c_{g1} T_{g1}}$ , ft./sec.
$V'_p$	Volume of a particle, in. <sup>3</sup> .
$V_p$	Velocity of particles, ft./sec.
$V_p^0$	Velocity ratio of particles, dimensionless, $V_p^0 = V_p/V_{g1}$ .
$x$	Local tube position co-ordinate, ft.
$x_t$	Length of tube, ft.
$x_t^0$	Tube length to tube diameter ratio, dimensionless, $x_t^0 = x/d_t$ .
$x_{max}$	Critical length, ft.
$x_{max}^0$	Critical length to tube diameter ratio, dimensionless, $x_{max}^0 = x_{max}/d_t$ .
$x^0$	Local tube position to tube diameter ratio, dimensionless, $x^0 = x/d_t$ .
$X$	Particle to gas mass flow ratio, dimensionless, $X = m_p/m_g$ .
$Z$	Specific heat ratio parameter of the gas, dimensionless, $Z = 2\gamma/(\gamma-1)$ .

Greek Symbols

$\gamma$	Specific heat ratio of the gas, dimensionless, $\gamma = c_g/c_v$ ( $c_v$ -constant volume specific heat).
$\rho_g$	Density of the gas, lb. <sub>m</sub> /ft. <sup>3</sup> .
$\rho_p$	Density of the particles, lb. <sub>m</sub> /ft. <sup>3</sup> .

TABLE OF NOMENCLATURE (Continued)

$\mu_g$	Viscosity of the gas, lb. <sub>f</sub> sec./ft. <sup>2</sup> .
$\mu_g^o$	Viscosity ratio of the gas, dimensionless, $\mu_g^o = \mu_g / \mu_{gl}$ .
$\Delta P_p$	Total pressure drop of the gas over the particles per unit length of tube, lb. <sub>f</sub> /in. <sup>2</sup> ft.

Superscripts

o	Dimensionless quantities that refer to reference conditions.
---	--

Subscripts

p	Particles.
g	Gas.
l	Reference conditions.
m	Gas-particle mixture.
i	Inlet of tube.
e	Exit of tube.

## CHAPTER I

### INTRODUCTION

The two-phase flow of a gas and solid particles is one of the most important and frequently encountered types of flow, especially in the area of solid propellant rocket nozzles, pipeline flow, and various industrial applications. Much analytical and experimental work has been done in order to predict the effect of the presence of the solid particles, which is often significant, on the characteristics of single-phase gaseous flow. More specifically, most of the studies on gas-particle systems have attempted to evaluate such factors as:

1. The effect of particles on the thrust and efficiency of solid propellant rocket nozzles.
2. The effect of particles on the performance of heat exchangers.
3. The effect of particles on the attenuation and speed of sound and shock waves propagating in a gas.
4. The effect of particles on the pressure and temperature changes of a gas flowing in a tube.

5. Maximum particle mass flow and two-phase flow stoppage in gas-particle systems.
6. The total changes and local variations in the properties of the gas and particles in gas-particle flow systems.
7. The governing parameters and variables in gas-particle flow and their individual effects on the characteristics of the system.

In general, the most important parameters and variables in any gas-particle system are the particle to gas mass flow ratio, the particle drag and heat transfer coefficients, the particle-particle and particle-gas interactions, the particle distribution, the properties of the particles and gas, and the particle-gas interactions with a boundary.

The number of practical applications involving gas-particles systems is almost unlimited. One important application is the adiabatic transportation of a gas and solid particles in a constant area tube that has a high diameter ratio where the diameter ratio is defined as the tube length divided by the tube diameter. The restriction to high diameter ratio tubes is very important because, in one-dimensional Fanno flow of an ideal gas with constant properties in a constant area, the maximum distance that the gas can be transported is limited by tube wall friction (1). The maximum tube length, or critical length, is determined by the length of tube necessary for wall friction to expand or compress the gas from a given inlet Mach

number (subsonic or supersonic) to a limiting Mach number equal to one at the exit of the tube. If the tube is operating under sub-critical conditions, the tube length is less than the critical length. For critical conditions, the tube length equals the critical length. It is an impossible situation for the tube length to be greater than the corresponding critical length. The addition of solid particles into a gaseous stream flowing through a constant area tube would affect the critical length and the local and exit properties of the gas, among other things. Consequently, it is important to know the effect of the particles and variables of the system on the critical length so that the practical design of such a two-phase flow system can be more accurately accomplished.

Since little analytical or experimental work has been done on gas-particle systems operating under critical conditions, it is the purpose of this investigation to analyze this problem both analytically and experimentally. The problem is limited to subsonic and supersonic adiabatic flow of air and solid spherical particles in a vertical constant area circular tube where the tube operates under critical conditions. Simplifying assumptions and finite difference computer solutions are employed in the analysis. The results are focused on the critical length, as affected by the variables of the system, and the local and critical exit properties of the air and particles. The conditions for choking, or two-phase flow stoppage, and sub-critical



conditions are discussed in relation to critical conditions. The experimental analysis is limited to subsonic flow and to the measurement and calculation of local and critical exit air properties. Particle and air mass flow rates are measured for two-phase flow in a tube of fixed length. Since the tube is operated critically and has a fixed length, the critical length is constant and equals the tube length. The experimental results and those obtained for sub-critical flow from the literature are compared to analytical solutions.

## CHAPTER II

### REVIEW OF THE LITERATURE

Many investigations have been undertaken to understand the mechanism and flow characteristics of multi-phase, multi-component flow. The three individual phases are the gaseous, liquid, and solid phase where each phase may have more than one component. Since the purpose of this study is to investigate the characteristics of two-phase two-component gas-particle flow in a vertical constant area tube, only the pertinent literature in this area will be reviewed. The less important literature in this area and literature in other related areas will be discussed briefly for the purpose of supplying additional background material.

Two of the most important properties of a gas-particle system that determines whether or not particles can be transported in a vertical tube are the terminal velocity of the particles  $V_{pt}$  and the particle slip  $V_{ps}$ . The terminal velocity of a particle is defined as the maximum velocity obtainable in free fall in a fluid or gaseous medium. At the terminal point, the particle acceleration is zero since the gravity forces equal the viscous and form drag forces over the particle. The particle slip is defined as the difference between the velocity of the gas and the

particle  $V_g - V_p$ . Ideally, for particles to be transported upwards in a vertical tube with a uniform gas velocity distribution the particle slip  $V_{ps}$  must be greater than the terminal velocity of the particles  $V_{pt}$ , i.e.,  $(V_g - V_p > V_{pt})$ . If the diameter of the particles is very small, the terminal velocity of the particles and the corresponding particle slip are small, i.e.,  $V_g - V_p \approx V_{pt} \approx 0$ . However, for finite sized particles, the particle slip must be greater than the terminal velocity so that the particles can be accelerated by the viscous and form drag forces which are in excess of the gravitational forces acting on the particles. These forces are generated as a result of the relative velocity between the gas and the particles. The gas velocity at which particles can no longer be supported is essentially equal to the terminal velocity of the particles, i.e.,  $V_g - V_p = V_{pt}$ . Thereafter, the particles fill the tube and choking results.

Croft (2) presented an equation for the determination of the terminal velocity of spherical particles. His equation, based on the assumption that viscous and form drag forces equal gravitational forces, is given as

$$V_{pt} = \sqrt{\frac{2V_p^3 g (\rho_p - \rho_g)}{C_{d,pf} K_w^2 \rho_g}} \quad \text{where}$$

$K_w$  = Flow boundary factor

and the other variables are defined as in this study. The

effect of a flow boundary or a wall resulting from particle-wall collisions becomes important when the ratio of the diameter of the particle  $d_p$  to the diameter of the tube  $d_t$  exceeds 0.2. The equations for  $K_w$ , which are valid only for streamlined flow, show that the flow boundary factor increases as  $\frac{d_p}{d_t}$  increases and has a limiting value equal to one for very small particles. Therefore, for a given diameter tube, increasing the particle diameter tends to decrease the terminal velocity of the particles  $V_{pt}$  because of the wall effect. However, the net change in  $V_{pt}$  may be an increase because  $V_{pt}$  is greater for larger particles, i.e., the effect of gravity forces acting on the larger particles may be greater than the wall effect. Croft also presented equations for the drag coefficient of single spherical particles  $C_d$  which are similar to those used in this investigation. In addition to the wall effect, other factors affect  $V_{pt}$  such as turbulence, multi-particle interactions, and irregularly shaped particles.

To account for irregularly shaped particles in the equations for  $C_d$ , Waddell (3) defines a particle circularity  $\Phi$  and a particle sphericity  $\$$  by the following relations:

$$\Phi = \frac{C_p^c}{C_p} \quad \text{and}$$

$$\$ = \frac{S_p}{S} \quad \text{where}$$

$c$  = Circumference of a circle of the same area  
as the plane figure

$C_p$  = Actual perimeter of the plane figure

$s$  = Surface area of a sphere having the same  
volume as a particle whose surface area  
is  $S$ .

The maximum value for both  $\phi$  and  $\psi$  is equal to one for a sphere. He also defines a true nominal particle diameter  $d_{pn}$  on which  $C_d$  and the particle Reynolds number  $Re_p$  are based. It is defined as

$d_{pn}$  = Diameter of a sphere of a volume equal to that  
of the particle, irrespective of the latter's  
shape.

Based on the above definitions, Waddell showed experimentally that the drag coefficient  $C_d$  for irregularly shaped particles is generally greater than for spherical particles at the same effective particle Reynolds number and that this effect increases as  $\phi$  and  $\psi$  increase. Therefore, the effect of irregularly shaped particles tends to decrease the terminal velocity of the particles.

To account for multi-particles in the equations for  $C_d$  as affected by particle-particle and particle-wall interactions, Torobin and Gauvin (66) review the results obtained by others. Briefly, they show that free stream turbulence increases  $C_d$  for single particles. However, for multi-particles  $C_d$  is decreased because of particle-particle and particle-wall interactions even though the turbulence

generated between multi-particles has the opposite effect for single particles. The effect of multi-particles tends to increase the terminal velocity of the particles. This review is discussed more completely on page 28.

Alves (4) suggested that the total pressure drop in a gas-particle system consists of the following components:

1. That required to accelerate the gas.
2. That required to accelerate the particles by viscous and form drag forces.
3. That required to support the gas.
4. That required to support the solid particles.
5. That required to overcome the friction of the gas on the tube walls.
6. That required to keep the particles in suspension.

Although gas-particle and fluid-particle fluidized beds are not pertinent to this investigation, their characteristics are important for the prediction of choking in steady two-phase flow. Leva, Grummer, Weintraub, and Pollchik (5) and Wilhelm and Kwauk (6) presented similar pressure drop-velocity curves for gas-particle and fluid-particle beds. They showed that at inlet gas or fluid velocities great enough to give a pressure drop equal to the weight of the particles in the bed, the bed expands from the fixed state of minimum bed height so that all the particles are no longer touching and the bed is in the fluid state. A further increase in velocity is accompanied

by a further increase in bed expansion, or voidage of particles, and the pressure drop across the entire bed in both cases remains equal to the weight of the bed. The velocity is increased and the pressure drop across the bed remains constant until a velocity is reached, the terminal velocity of the particles, beyond which the particles flow upward out of the bed in a steady stream (uniform particle diameter only). Thus, there is a net steady particle flow in the bed which can be considered to be gas-particle flow thru a vertical tube. However, during fluidization the particles are moving upwards in the core of the bed and downwards near the wall because of the velocity distribution of the gas in the bed, according to Chin-Yung Wen and Hashinger (7). According to results given by Zenz (8), the same effect was noticed just after the bed was fluidized and particles flowed upwards. As the gas velocity was increased the gas turbulence decreased, the holdup and downward motion of the particles in the bed decreased, and the particle flow continued through a decreasingly dense mass of slower moving and falling particles in the bed. The pressure drop decreased to a minimum and then increased as the gas velocity increased. Of course, even at higher gas velocities the particles would tend to decrease in velocity or fall downward in the tube (bed) because of the lower gas velocities near the wall of the tube. However, the turbulence of the gas stream and the spin of the particles would tend to force the particles towards the center of the tube

where they would be accelerated upwards. The topic of turbulent diffusion in fluidized beds of particles is discussed more completely analytically by Hanratty, Latinen, and Wilhelm (9).

Vogt and White (10) reported a semi-empirical study on the pressure losses in vertical and horizontal pipes carrying suspensions of solid particles in air. An equation was developed that correlated their experimental data as well as data obtained from the literature. The equation for both horizontal and vertical flow is given as

$$\alpha - 1 = A \left( \frac{d_t}{d_p} \right)^2 \left( \frac{\rho_g X}{\rho_p Re_t} \right)^k \quad \text{where}$$

$\alpha$  = Two-phase pressure drop divided by the single-phase pressure drop both at the same gas velocities

and A and k are functions of the dimensionless group

$$\sqrt{\frac{(\rho_p - \rho_g) \rho_g g d_p^3}{3\mu_g}}$$

and the other variables are defined as in this study. The particle material used was sand, steel shot, clover seed, and wheat which flowed thru a 0.5 inch diameter iron pipe. No particle velocity measurements were taken.

An excellent semi-empirical study was presented by Hariu and Molstad (11) on the pressure drop in vertical



glass tubes with air as the flowing medium and sand and silica-alumina cracking catalyst as the particle materials. The particle to air mass flow ratio was varied from 6 to 30. A comparison of a portion of their results for sub-critical flow with analytical results obtained from this study is made later.

Farbar (12) reported a study on the flow characteristics of air-particle mixtures in a horizontal and vertical glass tube that had an inside diameter of 0.67 inch and length between pressure taps of 2 feet. Particle materials used were alumina and silica catalysts that varied in size from less than 10 microns to greater than 220 microns. The particle to air mass flow ratio  $X$  was varied from 0 to 16. His results for the total air pressure drop across the tube showed an increase with  $X$  and the inlet air velocity. No correlation of experimental data was attempted. His results, when based on the ratio of pressure drops  $\alpha$ , were similar to those given by Vogt and White above.

Boatright (13) reported on air and sand flowing in vertical Lucite tube that had an inside diameter of 0.301 inch and a length between pressure taps of 10 feet. The average particle diameter was 500 microns and the particle to air mass flow ratio varied from 4 to 9. Inlet air velocities varied from 110 to 155 feet per second. Pressure drop correlation was based on the ratio  $\alpha$  of the two-phase pressure drop to that of the air only at essentially the same inlet air volume flow rates. The proposed correlation

is given by

$$\alpha = 2.213 + 0.0152(X)Re_t \frac{\rho_g}{\rho_p} .$$

Since the inlet air velocities for equal volume flow rates were not the same, the data was somewhat scattered. No particle velocity measurements were taken.

Boggs and Fitch (14) presented a report on two-phase systems that review the studies by Croft, Waddell, Alves, Wilhelm and Kwauk, Zenz, Vogt and White, Hariu and Molstad, Farbar, and others. Results on gas-liquid and liquid-particle systems are also reviewed.

Richardson and McLeman (15) conveyed air and solid particles through a horizontal brass pipeline, 1.0 inch in diameter and 110 feet long. Particle materials used were Perspex, sand, coal, brass, aluminum, and lead. The particle velocity was measured by interrupting the flow of particles for a fraction of a second by the introduction of an air pulse into the system. The time taken for the pulse to travel between two points a known distance apart was then measured electronically. The pressure drop was measured between each 10 feet interval and generally showed an increase along the pipe, although the data was somewhat scattered. The velocities of the particles and the pressure drops were correlated in terms of the physical properties of the solid particles and the flow rate of the air.

Electrostatic effects, resulting from frictional generation of static electricity, were noted that caused erratic pressure drop data for some of the materials tested. Khudiakow and Chukanov (16) found that electrostatic retardation of particle movement could become large enough to completely halt the flow of the particle phase in vertical gas-particle systems.

An excellent mathematical paper on turbulent gas-particle flow was presented by Soo (17). Particle velocity and concentration of solid particles were calculated for the case of low particle to gas mass flow ratios, small particles, and negligible gravity effects. The velocity distribution of the gas stream was assumed to be unchanged by the presence of the particles. His results may be summarized as follows:

1. Constant exchange of solid particles between the regions near the wall and near the center of the pipe gives rise to a velocity of the solid particles that is higher than that of the fluid near the wall and lower than that of the fluid near the center of the pipe.
2. The mass flow distribution of the solids increases from the wall to the center of the pipe.
3. The mass concentration of the solid particles decreases from the wall to the center of the pipe.

The empirical constants needed in the mathematical formulation were determined from data by Soo and Regalbuto (18) for air and glass bead flow in a horizontal pipe. The analytical correlation for the distributed mass flow of solid particles and the corresponding experimental results agreed satisfactorily.

Hino (19) presented a mathematical study on turbulent flow with suspended particles. Two fundamental equations were derived which were the energy equation for flow with suspended particles, which considered all of the effects of suspended particles, and the acceleration balance equation of turbulent motion. Using these equations, general formulas were derived for the changes in the characteristic turbulence quantities such as the Von Karman constant, the intensity of turbulence, the life time of eddies, and the diffusion coefficient. Reasonable agreement between the theory developed and experimental results was obtained. The results showed that for flow with suspensions of neutrally buoyant particles the Von Karman constant, the decay time of turbulent eddies, and the diffusion coefficient decreased, and the intensity of turbulence increased as the volume concentration of the suspended particles increased. For sediment laden streams, all of the above factors decreased. No experimental data was available for sediment laden streams, however. Since the Von Karman constant was changed, the fluid velocity profile was affected. The profile was affected very little for low particle concentrations.

The intensity of turbulence for sediment laden streams decreased only slightly. This could be expected since the density and corresponding inertia of the particles were large compared to the stream values.

In most practical applications of two-phase flow, the particle size distribution is not uniform. To account for this in any experimental correlation and analytical analysis, the particle size distribution must be known. Although most of the studies to date have not considered this, Lebedev and Makirov (20) have developed a mathematical method that yields nomograms and which permits the determination of the particle size distribution in suspensions, fogs, and clouds from only three measurements of the relative intensity of light scattered at small angles.

The frequent use of the standard incompressible wall friction factor curves for gas flow has been shown to be questionable by Chen (21), especially at high gas Mach numbers. For gaseous flow in smooth tubes, the wall friction factor  $f$  is commonly accepted to be a function only of the tube Reynolds number  $Re_t$ . However, he shows that an additional dependency on the gas Mach number exists. Basically, he shows that  $f$  can be greater or lower than the standard values, depending on the gas Mach number. His qualitative results are discussed more completely on page 111.

Many studies have been undertaken to find the effect of particles on the rates of heat transfer in gas-particle and liquid-particle systems. Generally, it has been shown

by several investigators that the rates of heat transfer can be increased by the addition of particles into a gaseous or liquid stream flowing in vertical or horizontal tubes (22 thru 29). The effect of the particles on the velocity and temperature profiles and particle-wall interactions became more important in controlling the rates of heat transfer as the particle diameter decreased and the particle to gas or particle to liquid mass flow ratio increased. Since the rates of heat transfer were increased, the effect of the particles was to flatten the temperature profile.

Other important two-phase flow systems are gas-liquid and solid-liquid flow in constant and variable area tubes and gas-particle flow in variable areas. Netzer (30) and Smigielski (31) presented studies on the flow of gases and liquid droplets in converging and converging-diverging nozzles. Their works concentrated on predicting the local liquid and gas velocities, static pressure, and droplet diameter as a function of the axial distance along the nozzle. Analytical and experimental results were compared. The analysis of this type of flow is especially complicated because of the variance in droplet diameter due to evaporation or condensation, distortion, and separation of the droplets. The distortion and separation of the droplets result from the relationship between the forces tending to accelerate or decelerate the droplets and the surface tension binding forces of the droplets.

Karplus (32, 33) investigated the velocity of sound in a liquid containing gas bubbles and in a mixture of water and steam. For both types of flow, he showed that the velocity of sound decreased radically when steam or air bubbles were injected into water. The minimum in the speed of sound was, in each case, lower than the speed of sound corresponding to either phase individually. A slow pressure rise in the system generally caused a shock wave to be produced very rapidly. However, the shock waves were expected to be severely attenuated when passing thru the mediums.

Vogrin (34) reported on air and water flowing in a converging-diverging nozzle. The primary consideration was to determine the effects of accelerating the liquid phase by the gaseous phase. These effects were measured experimentally in terms of the nozzle exit water velocity, exit gas-liquid slip ratio, and exit acceleration factor. An accurate gamma-ray attenuation technique was employed to measure the void fraction where the void fraction is defined as the ratio of the gas volume to the total mixture volume.

Studies to evaluate the critical mass flow function for liquid-metal systems and superheated steam have been conducted by Fauske (35) and Murdock and Bauman (36), respectively. Stepanoff (37) presented a paper concerned with the prediction of the performance (head, capacity, and efficiency) of centrifugal pumps handling solid-liquid mixtures.

Levy (38) gave an analytical study on the prediction of the pressure drop and density and velocity distributions in a vapor-liquid system. He treated it as a continuous medium and applied it to the methods and assumptions commonly used in single-phase turbulent liquid flow. His results for horizontal pipe flow were:

1. The ratio of the two-phase pressure drop to the total liquid pressure drop, greater than one, decreased as the ratio of the mean fluid density to the liquid density increased and the effect was more pronounced as the liquid Reynolds number increased where the Reynolds number was based on the total flow and the properties of the liquid.
2. The velocity profiles were not as flat as in single-phase turbulent fluid flow. They were much more curved and became even more so as the mean fluid density was decreased, i.e., as the liquid flow rate was reduced.
3. The density profiles indicated that as the mean fluid density decreased a larger fraction of available liquid located itself near the pipe wall. This effect was reduced for larger fluid Reynolds numbers.
4. The ratio of the two-phase friction factor to that of the single-phase liquid friction



factor, greater than one, decreased with increased mean fluid density and liquid Reynolds number.

Recent attention has been given to gas-particle flow in a rocket nozzle. Hoglund (39) presented an excellent review on the recent advances in gas-particle nozzle flow. The primary considerations were the particle lag problem and the parameters and characteristics of multi-particles. Other studies were given by Travis (40) and Gilbert, Allport, Dunlap, Crowe, Wrenn, and Rogers (41). In most of the investigations, the primary concern was to evaluate the effect of the particles on the thrust and efficiency of rocket nozzles. Glauz (42) presented a method by which the region at which the gas Mach number equalled one in a convergent-divergent nozzle could be accurately predicted. He shows that this region lies downstream of the throat of the nozzle. Soo (43) gave an important analytical paper on gas-particle flow in a nozzle. Duct flow and normal shocks were also discussed. Other studies on normal shock waves in gas-particle flow were given by Kriebel (44) and Carrier (45).

The effect of particles on the attenuation and propagation of sound waves in a gas have been studied by Dobbins and Temkin (46), Chu (47), Wood (48), Soo (49), Knudsen, Wilson, and Anderson (50), Epstein and Carhart (51), Bradfield (52), and Zink (53). Briefly, it has been shown that the presence of particles in a gas reduces the speed

of sound as the particle to gas weight ratio is increased. A minimum exists which is lower than the speed of sound in either the gas or the solid individually. A mixture Mach number has not yet been defined for gas-particles systems in which the velocities of the gas and particles are not equal. The attenuation of sound waves increases as the particle to gas weight ratio increases. However, the attenuation is also frequency dependent. For low frequency sound waves, the attenuation is less than for higher frequency waves because the energy dissipated by friction is less for low frequency waves. At low frequencies where the suspended particles can take part in the acoustic displacements of the gas, the relative motion between the gas and the particles becomes small. The production of viscous waves becomes small and, consequently, so does the viscous attenuation. At high frequencies, the particles become essentially fixed in space and ultimately increase the viscous attenuation compared to lower frequencies. Therefore, smaller particles reduce the attenuation. The speed of sound is also affected by frequency. For common gases such as air and oxygen, the speed of sound is decreased slightly as the frequency increases. For a gas such as helium, the reduction is considerable. Chu and Parlange (54) developed a macroscopic theory on two-phase flow with mass, momentum, and energy exchange. The theory was applied to systems that depart slightly from local thermodynamic equilibrium. An example of wave propagation in a two-phase medium with

viscous and thermal relaxation was calculated.

The most difficult measurements in gas-particle flow are the properties of the particles, especially the particle velocity  $V_p$ . Three commonly used methods for measuring  $V_p$  are:

1. Direct measurement of  $V_p$ .
2. Calculation of  $V_p$  from direct measurements of the mixture density  $\rho_m$ .
3. Calculation of  $V_p$  from direct measurements of the effective cross-sectional area of the particles  $A_p$  or the void fraction  $\alpha_v$  where  $\alpha_v$  is defined as the ratio of the effective cross-sectional area of the gas  $A_g$  divided by the total cross-sectional area  $A_t$ .

Several methods have been used or can be proposed for the measurements of  $V_p$ ,  $A_p$ ,  $\alpha_v$ , or  $\rho_m$  which are:

1. Gamma-ray attenuation for  $\alpha_v$  (34).
2. Interruption of the flow stream by a sound pulse for  $V_p$  (15).
3. Trapping a known volume of gas-particle mixture for  $\rho_m$  (11).
4. Photographic techniques for  $A_p$  or  $V_p$  (62, 63).
5. Buoyancy manometers for  $\rho_m$  (32).
6. Gas-particle capacitance measurements for  $\rho_m$  or  $A_p$ . Scott (55) used this method for gas flow only.
7. Particle pitot tube for  $V_p$  and the gas velocity  $V_g$  (56).

8. Transportation of particles through a coil for  $\rho_m$ ,  $V_p$ , or  $A_p$ .
9. Particle effect on the index of refraction of the gas for  $\rho_m$  or  $A_p$ .

The use of any of the above methods is governed primarily by the cost, application, ease of operation, and the desired accuracy.

Since experimental establishment of the magnitude of the drag and heat transfer coefficients for spheres has proceeded for many years, it might be expected that these values are known quite precisely. Most of the work that has been done involves single spheres moving at constant velocities in a turbulent free incompressible fluid of effectively infinite extent. The dependency of the drag and heat transfer coefficients on deviations from the above restrictions has been difficult to determine. For multi-particle flow in gaseous or fluid streams, additional factors are introduced such as particle-particle and particle-gas interactions and particle-boundary interactions if a flow boundary exists.

Millikan (57) was one of the first investigators to adequately describe the fall of a small spherical body in a gas. From his experimental and analytical results, and others, the well-known standard drag curve of the particle drag coefficient as a function of the particle Reynolds number was established (78). Corrsin and Lumley (58) presented the total differential momentum equation for the

viscous unsteady motion of a sphere moving in a turbulent fluid. No solutions were given, however.

Peskin (59) presented an excellent analytical study on the intensity of motion and the diffusivity of a single spherical particle suspended in an incompressible turbulent fluid. The statistical behavior of particle motion was considered for an isolated particle subject to drag forces only and for the case in which other similar particles present in the field exerted pressure forces on the particle. Satisfactory experimental agreement was observed.

His conclusions were:

1. Dynamic friction, which is the tendency of many particles to decelerate one given particle, was present in the system and had the effect of reducing the diffusivity of a particle.
2. The intensity of particle motion  $V_p^2$  was reduced because of dynamic friction.
3. The diffusivity of an isolated particle  $x_p^2$  in a turbulent fluid was less than the eddy diffusivity of turbulence of the stream.
4. For the combined diffusivity of an isolated particle and the interaction diffusivity, the slower and larger particles were affected by the particle-particle interactions while the faster particles behaved as if there were no other particles present (high dynamic friction).

5. For larger particles, the diffusivity approached zero.

Rubinow and Keller (60) solved the Navier-Stokes equations for the motion of a fluid around a spinning sphere at low particle Reynolds numbers. The force and torque on the sphere were computed. It was found that in addition to the drag force determined by Stoke's theory, the sphere experiences a force  $F_L$  orthogonal to its direction of motion and axis of spin. This force was given by

$$F_L = \pi d_p^3 \rho_g V_p w (1 + Re_p) / 6 \quad \text{where}$$

$w$  is the angular velocity of the sphere and the other symbols are defined as in this study. For viscous fluid-particle flow in a circular tube, it was shown that the particles were not concentrated along the axis of the tube but at a radius of about one-half the radius of the tube. This was caused by particle spin and the transverse force resulting from the non-uniformity of the fluid velocity profile.

Haberman (61) reported solutions for subsonic potential compressible flow past a sphere inside a circular duct. Results were given for the velocity and pressure distribution on the surface of the sphere and the critical free stream Mach numbers at which the maximum local velocity reached the local speed of sound.

Soo and co-workers (62, 63) developed experimental and computational methods which allowed them to measure the

statistical properties of both the particles and the fluid for gas-particle flow in a horizontal square plexiglass test section. A tracer diffusion technique employing helium was used to determine the gas-phase turbulent motion and a photo-optical technique was used for the determination of the motion of the particles. The experiments showed that:

1. For a two-phase turbulent stream of the loading from 0.01 to 0.06 lb<sub>m</sub> of solid per lb<sub>m</sub> of air and particle size below 250 micron, the stream turbulence is not significantly affected by the presence of the particles.
2. The particle motion is non-isotropic, even where the stream motion is isotropic, mainly due to gravity and wall effects.
3. The intensity of particle motion is greatly affected by the distribution of the stream intensity in the duct.
4. The probability of a particle-stream encounter has a significant effect on the particle diffusivity which, in the cases studied, is of the order of  $10^{-2}$  of the eddy diffusivity of the stream.
5. The particle Reynolds number is in all cases below 10, hence the Stoke's approximation of drag is a reasonable one.

Soo and Tien (64) presented an analytical study on the

effect of a wall on gas-solid turbulent motion. Their conclusions were:

1. The intensity of motion of the solid particles is affected by the presence of the wall and the distribution of turbulent intensity of the stream near the wall.
2. The intensity of motion of the solid particles can be significantly higher than the turbulence intensity of the main stream.
3. The particle diffusivity is not significantly affected by the wall.
4. The intensity of particle motion increases toward the wall. The scale of turbulence of particle motion decreases towards the wall.
5. The effect of the wall on the main stream is more predominant for low duct Reynolds numbers than for high Reynolds numbers.
6. The intensity of motion of the stream increases toward the wall and reduces to zero at the wall.
7. The spinning motion of the solid particles resulting from fluid velocity gradients induces a force (Magnus effect) which causes the solid particles to move away as they approach the wall.

Electrostatic forces and inter-particle pressure forces were neglected in the analysis.

Ranz, Talandis, Gutterman (65) investigated the mechanics of particle bounce from a surface. They showed



that during particle bounce energy exchange can occur between a particle and surface and between the translational and rotational energies of the particle. There is a certain probability that a particle striking at a low angle will bounce at a high angle, and vice versa, and be carried far out into the main stream. The lateral velocity of high angle bounce in a tube represents kinetic energy lost because the particle must be reaccelerated axially. Thus, the particle bounce contributes to the general lagging of the particle behind the gas flow.

Torobin and Gauvin (66) presented an important review on the characteristics of single and multi-particles in gas-particle flow. The review is in six parts, the first four of which are concerned with the mechanics of single particles in fluids free from turbulent motion. Part V considers the effects of fluid turbulence on the particle drag coefficient. The results for a single fixed and single moving sphere showed that free stream turbulence tends to increase the drag coefficients and cause a regression of the critical point. The range of particle Reynolds number was from 1 to 1000. Part VI involves the review of studies on the multi-particle behavior in turbulent fluids. The following conclusions are noteworthy:

1. Multi-particle drag coefficients are generally less than for single particles.
2. The conventional friction factor equations for solids free flow are not applicable to two-phase

flow. Friction factors greater and lower than the standard single-phase values were observed.

3. The velocity profile and turbulence level of the stream can be significantly affected by the presence of particles.
4. Electrostatic forces can be very significant in gas-particle systems and can cause large variation in pressure drop data.

Kada and Hanratty (67) employed the tracer diffusion technique to study the effect of solids on the fluid turbulence in a vertical solids-liquid system. They showed that the solids do not have a large effect on the diffusion rate unless there is an appreciable slip velocity between the solids and the fluid and unless the solids concentration is high enough.

Torobin and Gauvin (68, 69) developed an experimental installation for the quantitative measurement of the drag coefficient of single spheres moving with a turbulent fluid. A hot wire anemometer was used to measure the turbulence parameters of the fluid and a radiotracer technique was employed for the determination of the particle velocity history. Their results showed that the drag coefficient is a function of the particle Reynolds number and relative intensity but not of acceleration and relative macro and micro variations.

Little mentioned thus far are the heat and mass transfer from single and multi-particles. Although many studies

have been undertaken to find the heat transfer characteristics of particles, the correlations differ. Drake (70) proposed the following relationship as a form suitable for heat transfer data correlation for single spheres:

$$\text{Nu}_p = 2.0 + 0.459(\text{Re}_p)^{0.55}(\text{Pr}_g)^{0.33}$$

where the variables are defined as in this study. No similar relationship exists for multi-particles. Other studies on heat and mass transfer from spheres are given by Yuge (70), Pasternak and Gauvin (72), Johnson (73), Yen and Thodos (74), and Klyachke (75).

## CHAPTER III

### ANALYTICAL ANALYSIS

Analytical solutions in closed form for gas-particle flow have been rather limited because of the complexity of the governing differential equations and the uncertainty in predicting some of the effects of the particles on the gaseous stream and the multi-particle characteristics. Therefore, the use of finite difference techniques, an IBM 1410 computer, and many simplifying assumptions are utilized to solve the governing differential equations. As mentioned earlier, the analysis is concentrated on the critical length, as affected by the variables of the system, and the local and critical exit properties of the air and particles. In addition, the analysis is extended to include a discussion of choking and sub-critical flow.

The basic simplifying assumptions used in this investigation are:

1. Steady, one-dimensional flow with tube wall friction.
2. The particles do not interact or contribute to the pressure of the system.
3. Constant area tube with no external heat transfer.

4. No particle radiation, only convection.
5. The particle distribution is uniform over all cross-sections and  $m_p = A_p V_p \rho_p$ .
6. The particles have a uniform temperature and size and are spherical.
7. The gas is a perfect gas with constant specific heat  $c_g$ , viscosity  $\mu_g$ , and thermal conductivity  $K_g$ .
8. The particles have constant properties but the volume occupied by them is not negligible.
9. Drag and gravity forces are the only forces acting on the particles.
10. No external shaft or shear work.
11. The gas is inviscid except for wall and particle frictional forces.
12. The local acceleration of gravity is constant.
13. The standard drag and heat transfer curves for single particles apply for multi-particles.
14. The single-phase wall friction factor curves apply for gas-particle flow.

The thermodynamic system, co-ordinate system, and elemental control volume ( $A_t dx$ ), on which the governing differential equations are based, are shown below in Figure 1. If the gas-particle flow proceeds to the critical condition, the critical length  $x_{max}$  equals the tube length  $x_t$ , whereas for sub-critical flow the tube length  $x_t$  is always less than the critical length.

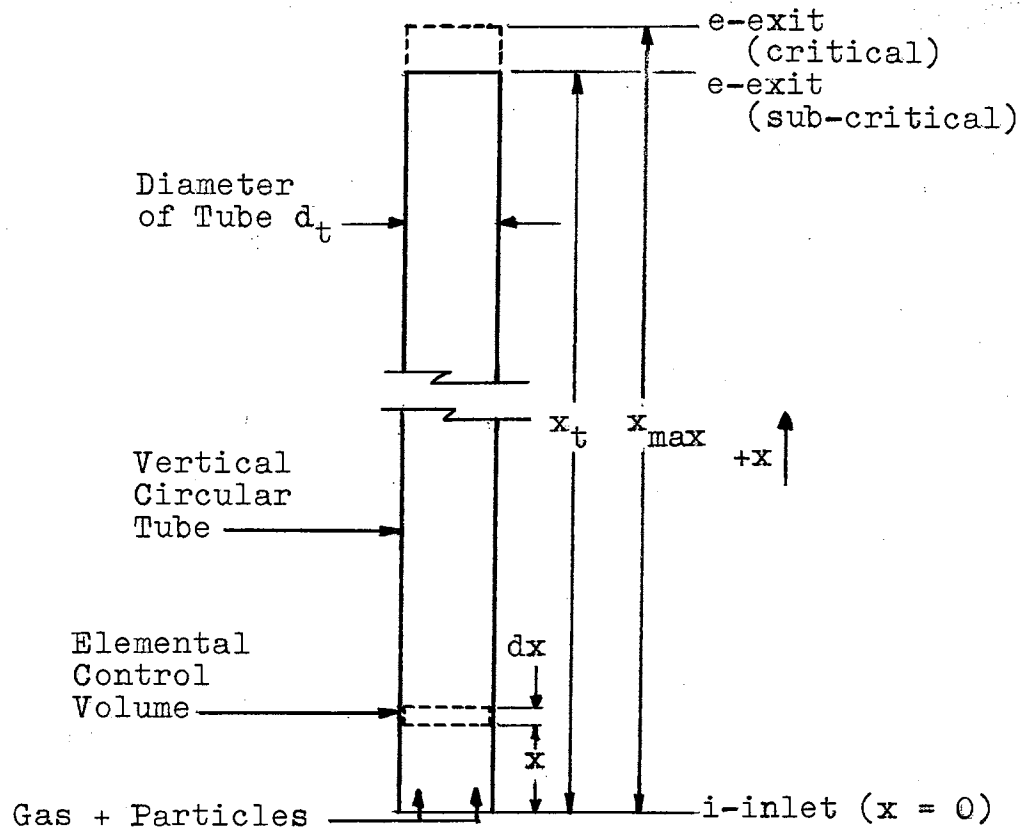


Figure 1. Thermodynamic System

The governing differential equations based on the above elemental control volume are derived as follows:

Over-all Energy Equation

For adiabatic, steady, one-dimensional flow with no external shaft or shear work, the energy equation in differential form for the gas and particles yields:

$$d \left[ m_g \left( h_g + \frac{V^2}{2g_c} + \frac{gx}{g_c} \right) + m_p \left( h_p + \frac{V^2}{2g_c} + \frac{gx}{g_c} \right) \right] = 0 \text{ where}$$

$$h_g = \text{Enthalpy of the gas} = c_g T_g \text{ and}$$

$$h_p = \text{Enthalpy of the particles} = c_p T_p.$$

Substituting these values into the energy equation, dividing by  $m_g$  and  $c_g$ , and rearranging gives:

$$d\left[\left(T_g + \frac{V_g^2}{2g_c c_g}\right) + \frac{m_p}{m_g}\left(\frac{c_p}{c_g} T_p + \frac{V_p^2}{2g_c c_g}\right)\right] = -\left(1 + \frac{m_p}{m_g}\right) \frac{g dx}{g_c c_g}. \quad (1)$$

### Continuity Equation

It was assumed on page 32 that  $m_p = A_p V_p \rho_p$  for the particles. To justify this assumption, consider the elemental control volume in Figure 1 and the following assumptions:

1. Particles are spheres with a uniform diameter  $d_p$ .
2. Particles are uniformly distributed over the length  $dx$  and across the cross-sectional area of the tube  $A_t$ .
3. The particle diameter  $d_p$  is small compared to  $dx$  and the velocities of the gas and particles are uniform across  $A_t$ .

Therefore, the number of particles at any given instant along the length  $dx$  of the elemental control volume would be

$$\frac{N_p(\text{particles})}{dx(\text{length})} = m_p \left(\frac{\text{mass}}{\text{time}}\right) \frac{1}{m_p} \left(\frac{\text{particle}}{\text{mass}}\right) \frac{dt}{dx} \left(\frac{\text{time}}{\text{length}}\right).$$

Then, the volume occupied by the particles would be

$\Delta V_p = A_p dx$  where  $A_p$  is the effective cross-sectional area occupied by the particles. The above equation becomes

$$\frac{N_p}{dx A_p} = \frac{N_p}{\Delta V_p} = \frac{m_p}{m'_p} \frac{1}{A_p V_p} .$$

Noting that the density of the particles is  $\rho_p = \frac{N_p m'_p}{dx A_p}$ ,

there results

$$\rho_p = \frac{N_p m'_p}{dx A_p} = \frac{m_p}{A_p V_p} , \text{ or}$$

$$m_p = A_p V_p \rho_p .$$

Now, for an ideal gas (one dimensional)

$$m_g = \frac{A_g V_g P_g}{R_g T_g} .$$

In logarithmic form, this equation becomes

$$\ln m_g = \ln A_g + \ln V_g + \ln P_g - \ln R_g - \ln T_g .$$

Since  $m_g$  and  $R_g$  are constant, differentiating the above equation gives

$$\frac{dA_g}{A_g} + \frac{dV_g}{V_g} + \frac{dP_g}{P_g} - \frac{dT_g}{T_g} = 0 .$$

For the particles, this same analysis would give for

$$\rho_p = \text{constant}$$



$$\ln m_p = \ln A_p + \ln V_p + \ln \rho_p \quad \text{and}$$

$$\frac{dA_p}{A_p} = - \frac{dV_p}{V_p}.$$

Since the total cross-sectional area of the tube equals the sum of the effective cross-sectional areas of the gas and particles, there results for  $A_t = A_p + A_g =$  constant

$$\frac{dA_g}{A_g} = \frac{d(A_t - A_p)}{(A_t - A_p)} = \frac{dA_t}{A_t \left(1 - \frac{A_p}{A_t}\right)} - \frac{dA_p}{A_p \left(\frac{A_t}{A_p} - 1\right)} = \frac{1}{\left(\frac{A_t}{A_p} - 1\right)} \frac{dV_p}{V_p}.$$

Eliminating  $\frac{dA_g}{A_g}$  from the continuity equation for the gas and substituting  $A_p = \frac{m_p}{V_p \rho_p}$  yields

$$\frac{dP_g}{P_g} = \frac{1}{\left(1 - \frac{A_t V_p \rho_p}{m_p}\right)} \frac{dV_p}{V_p} - \frac{dV_g}{V_g} + \frac{dT_g}{T_g} \quad (2)$$

or upon integrating

$$\frac{P_g V_g}{T_g V_p} \left( \frac{A_t V_p \rho_p}{m_p} - 1 \right) = G' = \text{Constant}. \quad (3)$$

Thus, the factor  $\left(1 - \frac{A_t V_p \rho_p}{m_p}\right)$  accounts for the volume occupied by the particles.

### Over-all Momentum Equation

For steady one-dimensional flow considering only

pressure, wall friction, and gravity forces the momentum equation in differential form for gas-particle flow gives:

$$\begin{aligned}\Sigma F_x &= [P_g - (P_g + dP_g)]A_t - \tau_w dA_w - \frac{g}{g_c} (\rho_p \Delta V_p + \rho_g \Delta V_g) \\ &= \frac{m_p}{g_c} [(V_p + dV_p) - V_p] + \frac{m_g}{g_c} [(V_g + dV_g) - V_g]\end{aligned}$$

where

$$\tau_w dA_w = \text{Wall friction forces} = \frac{fP_g V_g^2 A_t dx}{2g_c R_g T_g d_t} \quad (79),$$

$$\Delta V_p = \text{Elemental particle volume,}$$

$$\Delta V_g = \text{Elemental gas volume,}$$

$$\rho_p \Delta V_p = \text{Elemental particle mass} = \frac{m_p dx}{V_p}, \text{ and}$$

$$\rho_g \Delta V_g = \text{Elemental mass of gas} = \frac{m_g dx}{V_g}.$$

Therefore, the momentum equation becomes

$$-dP_g A_t - \frac{fP_g V_g^2 A_t dx}{2g_c R_g T_g d_t} - \frac{gm_g}{g_c} \left( \frac{m_p}{V_p m_g} + \frac{1}{V_g} \right) dx = \frac{m_g}{g_c} \left( \frac{m_p}{m_g} dV_p + dV_g \right).$$

where

$$m_g = A_g V_g \rho_g = A_t \left( 1 - \frac{A_p}{A_t} \right) \rho_g = A_t \left( 1 - \frac{m_p}{A_t V_p \rho_p} \right) \frac{V_g P_g}{R_g T_g}.$$

Substituting the continuity Equation (2) and the above equation for  $m_g$  into the momentum equation yields

$$A_t P_g \left[ \frac{1}{\left(1 - \frac{m_p}{A_t V_p \rho_p}\right)} \frac{dV_p}{V_p} + \frac{dV_g}{V_g} - \frac{dT_g}{T_g} \right] - \frac{f P_g V_g^2 A_t dx}{2 g_c R_g T_g dt} - \frac{g A_t V_g P_g}{g_c R_g T_g} dx$$

$$\left(1 - \frac{m_p}{A_t V_p \rho_p}\right) \left(\frac{m_p}{m_g V_p} + \frac{1}{V_g}\right) = \frac{A_t V_g P_g}{g_c R_g T_g} \left(1 - \frac{m_p}{A_t V_p \rho_p}\right) \left(\frac{m_p}{m_g} dV_p + dV_g\right).$$

Cancelling  $A_t P_g$  and rearranging the above equation, there results

$$- \frac{a'}{V_p} \frac{dV_p}{dx} + \frac{b'}{V_g} \frac{dV_g}{dx} - \frac{1}{T_g} \frac{dT_g}{dx} + c' = 0 \quad \text{where} \quad (4)$$

$$a' = \left[ \frac{1}{\left(1 - \frac{m_p}{A_t V_p \rho_p}\right)} + \left(1 - \frac{m_p}{A_t V_p \rho_p}\right) \frac{m_p V_g V_p}{m_g g_c R_g T_g} \right],$$

$$b' = \left[ 1 - \left(1 - \frac{m_p}{A_t V_p \rho_p}\right) \frac{V_g^2}{g_c R_g T_g} \right], \text{ and}$$

$$c' = \left[ - \frac{f V_g^2}{2 g_c R_g T_g dt} - \left(1 - \frac{m_p}{A_t V_p \rho_p}\right) \frac{g V_g}{g_c R_g T_g} \left(\frac{m_p}{m_g V_p} + \frac{1}{V_g}\right) \right].$$

### Particle Momentum Equation

For one-dimensional flow considering only drag and gravity forces, the momentum equation in differential form for each particle yields:

$$\Sigma F_x = F_p - \frac{g m'_p}{g_c} = \frac{m'_p}{g_c} \frac{dV_p}{dt} = \frac{m'_p}{g_c} \frac{dV_p}{dx} V_p \quad \text{where}$$

$$A_{pf} = \text{Frontal area of particle} = \frac{\pi d_p^2}{4},$$

$$m'_p = \text{Mass of particle} = \frac{\rho_p \pi d_p^3}{6},$$

$F_p$  = Viscous and form drag forces acting on the particle, and

$$C_d = \text{Particle drag coefficient} = \frac{F_p}{\frac{\rho_g A_{pf}}{2g_c} (V_g - V_p)^2}.$$

Substituting the above values into the particle momentum equation results in

$$V_p \frac{dV_p}{dx} = \frac{3C_d \rho_g (V_g - V_p)^2}{4\rho_p d_p} - g. \quad (5)$$

### Particle Energy Equation

For one-dimensional flow considering only particle internal energy and convection heat transfer, the energy equation in differential form for each particle gives:

$$\frac{Q_c}{m'_p} = - \frac{dU_p}{dt} = -V_p \frac{dU_p}{dx} \quad \text{where}$$

$$U_p = \text{Internal energy of particle} = c_p T_p.$$

Let  $h_p$  = Heat transfer coefficient of particle,

$$A_{ps} = \text{Surface area of particle} = \pi d_p^2,$$

$$\text{Nu}_p = \text{Nusselt number of particle} = \frac{h_p d_p}{K_g}, \text{ and}$$

$$\begin{aligned} \frac{Q_c}{m_p} &= \text{Specific convection heat transfer} \\ &= \frac{h_p A_{ps}}{m_p} (T_p - T_g). \end{aligned}$$

Substituting the above values into the particle energy equation gives

$$V_p \frac{dT_p}{dx} = \frac{6\text{Nu}_p K_g}{d_p^2 \rho_p c_p} (T_g - T_p). \quad (6)$$

To non-dimensionalize the above equations, the following parameters are used (See Table of Nomenclature):

$$A^o = \frac{A_t}{A_{gl}}, V_g^o = \frac{V_g}{V_{gl}}, V_p^o = \frac{V_p}{V_{gl}}, V_{gl} = \sqrt{2g_c c_{gl} T_{gl}}, T_g^o = \frac{T_g}{T_{gl}},$$

$$T_p^o = \frac{T_p}{T_{gl}}, P_g^o = \frac{P_g}{P_{gl}}, c_g^o = \frac{c_g}{c_{gl}}, c_p^o = \frac{c_p}{c_{pl}}, \mu_g^o = \frac{\mu_g}{\mu_{gl}},$$

$$K_g^o = \frac{K_g}{K_{gl}}, x^o = \frac{x}{d_t}, A = \frac{c_{pl}}{c_{gl}}, B = \frac{2gd_t}{V_{gl}^2}, C = \frac{\rho_{gl}}{\rho_p}, D = \frac{d_t}{d_p},$$

$$\text{Re}_{pl} = \frac{d_p V_{gl} \rho_{gl}}{\mu_{gl} g_c}, \text{Pr}_{gl} = \frac{c_{gl} \mu_{gl}}{K_{gl}}, \frac{R_g}{c_{gl}} = \frac{\gamma - 1}{\gamma}, Z = \frac{2\gamma}{\gamma - 1}, X = \frac{m_p}{m_g}.$$

The subscript 1 refers to arbitrary reference

conditions. Since the properties of the gas and particles,  $c_g$ ,  $\mu_g$ ,  $K_g$ , and  $c_p$ , were assumed constant, the corresponding reference values,  $c_{g1}$ ,  $\mu_{g1}$ ,  $K_{g1}$ , and  $c_{p1}$ , were equated to them, respectively. Thus,  $c_g^0 = c_p^0 = \mu_g^0 = K_g^0 = 1$ . In addition, the reference temperature,  $T_{g1}$ , and pressure,  $P_{g1}$ , were assumed equal to the inlet temperature,  $T_{gi}$ , and pressure,  $P_{gi}$ , of the gas. Thus,  $T_{gi}^0 = P_{gi}^0 = 1$ . Some of the above parameters were first suggested by Soo (43). Equations (1) thru (6) in non-dimensional form become:

#### Over-all Energy Equation

$$d[(T_g^0 + V_g^{02}) + X(AT_p^0 + V_p^{02})] = -(1+X)Bdx^0. \quad (7)$$

#### Continuity Equation

Assuming that the effective cross-sectional area of the gas referred to reference conditions is based on the same mass flow rate of the gas

$$A_{g1} = \frac{\dot{m}_g}{V_{g1} \rho_{g1}},$$

and the continuity equation becomes

$$\frac{dP_g^0}{P_g^0} = \left[ \frac{1}{\left(1 - \frac{XC}{P}\right)} \frac{dV_p^0}{V_p^0} - \frac{dV_g^0}{V_g^0} + \frac{dT_g^0}{T_g^0} \right] \quad \text{or} \quad (8)$$

$$\frac{p^o v^o}{T^o v^o} \left( \frac{A^o v^o}{XC} - 1 \right) = G = \text{Constant (Integrated)}. \quad (9)$$

### Over-all Momentum Equation

$$- \frac{a}{v_p^o} \frac{dv_p^o}{dx^o} + \frac{b}{v_g^o} \frac{dv_g^o}{dx^o} - \frac{1}{T_g^o} \frac{dT_g^o}{dx^o} + c = 0 \quad (10)$$

where

$$a = \left[ \frac{1}{\left(1 - \frac{XC}{A^o v_p^o}\right)} + \left(1 - \frac{XC}{A^o v_p^o}\right) XZ \frac{v_p^o v_g^o}{T_g^o} \right],$$

$$b = \left[ 1 - \left(1 - \frac{XC}{A^o v_p^o}\right) Z \frac{v_g^o}{T_g^o} \right], \text{ and}$$

$$c = - \left[ \frac{fZv_g^o}{2T_g^o} + \left(1 - \frac{XC}{A^o v_p^o}\right) BZ \frac{v_g^o}{2T_g^o} \left( \frac{X}{v_p^o} + \frac{1}{v_g^o} \right) \right].$$

### Particle Momentum Equation

$$\frac{dv_p^o}{dx^o} = \frac{3CDC_d G (v_g^o - v_p^o)^2}{4v_g^o \left( \frac{A^o v_p^o}{XC} - 1 \right)} - \frac{B}{2v_p^o}. \quad (11)$$

### Particle Energy Equation

$$\frac{dT_p^o}{dx^o} = \frac{6CDNu_p}{ARe_{pl} Pr_{gl} v_p^o} (T_g^o - T_p^o). \quad (12)$$

In addition to the above governing differential equations, other equations are needed. The required equations in non-dimensional form are:

Mixture Enthalpy

$$h_m^o = h_{mi}^o + \frac{AX(T_p^o - T_{pi}^o) + (T_g^o - T_{gi}^o)}{(1+X)} \quad \text{where (13)}$$

$$h_m^o = \frac{h_m}{c_{gl} T_{gl}}$$

and the inlet mixture enthalpy is based on the same standard temperature and pressure for all solutions.

Mixture Entropy

$$s_m^o = s_{mi}^o + \frac{AX \ln \frac{T_p^o}{T_{pi}^o} + \ln \frac{T_g^o}{T_{gi}^o} - \frac{2}{Z} \ln \frac{P_g^o}{P_{gi}^o}}{(1+X)} \quad (14)$$

where

$$s_m^o = \frac{s_m}{c_{gl}}$$

and the inlet mixture entropy is based on the same standard temperature and pressure for all solutions.

Area Ratio

$$A^o = \frac{A_t}{A_{gl}} = \frac{T_g^o}{P_g^o V_g^o} \left( 1 + \frac{X C P_g^o V_g^o}{V_p^o T_p^o} \right). \quad (15)$$

Mixture Mass Flow per Unit Area

$$\frac{\dot{m}}{A_t} = \frac{V_{gl} P_{gl}}{A^o} (1+X). \quad (16)$$



Mach Number of Gas

$$M_g = \frac{V_g}{c_{gs}}$$

where  $c_{gs}$  = Speed of sound in an ideal gas =  $\sqrt{\gamma g_c R_g T_g}$ .

Therefore,

$$M_g = \frac{V_g^o}{(T_g^o \gamma / Z)^{0.5}} \quad (17)$$

Particle Reynolds Number

$$Re_p = \frac{d_p (V_g - V_p) \rho_g}{\mu_g g_c} = \left(1 - \frac{V_p^o}{V_g^o}\right) \frac{V_g^o p_g^o Re_{pl}}{T_g^o} \quad (18)$$

Tube Reynolds Number

$$Re_t = \frac{d_t V_g \rho_g}{\mu_g} = \frac{D Re_{pl} V_g^o p_g^o}{T_g^o} \quad (19)$$

Particle Drag Coefficient

It was assumed earlier that the standard drag curve for single particles apply for multi-particles. From Reference (78), the standard drag curve was approximated by four straight lines which can be shown to be:

$$C_d = \frac{24}{Re_p} \quad 0.1 \leq Re_p < 1 \quad (20)$$

$$= \frac{24}{(Re_p)^{0.75}} \quad 1.0 \leq Re_p < 10$$

$$= \frac{13.5}{(\text{Re}_p)^{0.5}} \quad 10 \leq \text{Re}_p < 1000$$

$$= 0.44 \quad 1000 \leq \text{Re}_p < 100,000$$

### Particle Nusselt Number

It was assumed earlier that the standard heat transfer curves for single particles apply for multi-particles. From Drake (70) the relationship suggested is

$$\text{Nu}_p = 2 + 0.459(\text{Re}_p)^{0.55}(\text{Pr}_g)^{0.33} \quad \text{where} \quad (21)$$

$\text{Pr}_g = \text{Pr}_{gl}$ , since the properties of the gas were assumed constant and equal to the values at the reference conditions.

### Wall Friction Factor

It was assumed earlier that the single-phase wall friction factor curves apply for gas-particle flow. From Reference (79), the equations given are

$$f = \frac{0.316}{(\text{Re}_t)^{0.25}} \quad \text{Re}_t < 100,000 \quad (22)$$

$$= \frac{0.1382}{(\text{Re}_t)^{0.177}} \quad \text{Re}_t > 100,000$$

where the second equation is a simplified approximation to the one given.

Since the simultaneous solution of Equations (7), (10), (11), and (12) in closed form for the dependent variables

$V_g^0$ ,  $V_p^0$ ,  $T_g^0$ , and  $T_p^0$  as functions of the independent variable local tube position  $x^0$  is beyond mathematical treatment, a finite difference technique and an IBM 1410 computer were used to obtain the required solutions. Several finite difference techniques for solving ordinary differential equations exist, but the one chosen for its simplicity and accuracy was that proposed by Runge and Kutta (76, 77) about 1895 (see Appendix A).

Once the above four variables are calculated at any position  $x^0$ , the remaining variables  $P_g^0$ ,  $h_m^0$ ,  $s_m^0$ ,  $A^0$ ,  $m_m/A_t$ ,  $M_g$ ,  $Re_p$ ,  $Re_t$ ,  $C_d$ ,  $Nu_p$ , and  $f$  are calculated at  $x^0$  from Equations (9), (13), (14), (15), (16), (17), (18), (19), (20), (21), and (22), respectively. The above variables at  $x^0$  are then used to determine the same variables at the next elemental position  $x^0 + dx^0$ .

To begin the computer solution at the inlet of the tube where  $x_i^0 = 0$ , the knowledge of the following starting conditions and parameters is required:

$$A, B, C, D, Re_{pl}, Pr_{gl}, V_{gi}^0, V_{pi}^0, T_{gi}^0, T_{pi}^0, P_{gi}^0, Z, \text{ and } X.$$

In each case, the solution was continued at each successive interval until the critical length  $x_{max}^0$  was reached. The accuracy of the Runge-Kutta method depends on the interval of integration  $dx^0$ . In general, the smaller the increment  $dx^0$  the better the accuracy. Therefore, the smallest possible intervals were used for the subsonic and supersonic solutions that yielded reliable results and that did not

require excessive computer time. Large intervals were used at first and then decreased until the results did not vary significantly. In order for the subsonic and supersonic solutions to have any relative meaning, the inlet stagnation enthalpies and the mass flow rates of the gas and particles were assumed equal. Appropriate equations were derived to determine the supersonic inlet conditions necessary to satisfy the assumptions.

In single-phase flow the critical length is reached when all of the derivatives of the gas properties with respect to the tube position  $x^0$  become infinite (1). This was also observed for the two-phase flow. Thus, the program termination point involved finite difference integration along curves whose slopes approached infinity. To accurately predict the critical length and the corresponding exit properties, a backup routine was used that would decrease the size of the integration interval  $dx^0$  greatly just before the critical length  $x_{max}^0$  was reached. To insure proper program termination, seven tests were used that indicated when the critical length was reached. They are:

1. Sign change of the denominator of the equation for  $\frac{dV_g^0}{dx^0}$  (see Appendix A).
2. Disorder of the denominator of the equation for  $\frac{dV_g^0}{dx^0}$ .
3. Disorder of the Mach number of the gas  $M_g$ .
4. Failure of  $T_p^0$  to be greater than 0.

5. Failure of  $T_g^0$  to be greater than 0.
6. Failure of  $P_g^0$  to be greater than 0.
7. Entropy maximum.

See Appendix A for the computer program corresponding to the above analysis.

## CHAPTER IV

### ANALYTICAL RESULTS

The governing physical equations for gas-particle flow thru a vertical constant area tube were presented in Chapter III. Since finite difference techniques were employed for their solutions, each computer solution was obtained for a given set of governing variables of the system and starting conditions  $c_g$ ,  $c_p$ ,  $K_g$ ,  $\mu_g$ ,  $d_t$ ,  $d_p$ ,  $V_{pi}$ ,  $V_{gi}$ ,  $T_{pi}$ ,  $T_{gi}$ ,  $P_{gi}$ ,  $g$ ,  $\gamma$ ,  $\rho_p$ ,  $m_p$ , and  $m_g$ . From these quantities and the reference conditions the dimensionless parameters and starting conditions given on page 46 were formulated.

#### Presentation of Results

To study the effect of the above quantities on the critical length, two sets of data were considered. The first set, or particle mass variation data set, was based on varying only the particle to air mass flow ratio  $X$ . The solutions were obtained for air and spherical glass particles flowing in a vertical constant area circular tube. The conditions at the inlet of the tube were maintained constant and the particle to air mass flow ratio varied from 0.001 to 30.0. The average particle diameter was 0.0185 inch and the inside diameter of the tube was 0.5

inch. The second set, or property variation data set, was based on varying individually each of the governing variables and starting conditions given on the previous page (excluding  $m_g$  and  $m_p$ ). The reason for choosing this method, rather than individually changing the non-dimensional parameters given on page 46, is that the effects on the critical length are easier to explain as will be seen later. However, the discussion will be extended to evaluate the general effects of the non-dimensional parameters on the critical length. The solutions for the property variation data set were obtained for only one value of particle to air mass flow ratio of  $X = 10$ . Typical starting conditions and governing variables were chosen which closely approximated those values encountered in the experimental results presented later. See Appendix A for values of the starting conditions, governing variables, computer input data, and the computer program.

The results for the particle mass variation data set for subsonic and supersonic flow are shown in Figures 2 and 3, respectively. In each of the curves, the independent variable  $x^0$  is the abscissa while the dependent variables  $V_g^0$ ,  $V_p^0$ ,  $T_g^0$ ,  $T_p^0$ ,  $P_g^0$ , and  $M_g$  are the ordinates. Several curves are shown, each one corresponding to a different particle to air mass flow ratio  $X$ . The mixture enthalpy  $h_m^0$  - entropy  $s_m^0$  diagram is shown in Figure 4 for subsonic and supersonic flow and various values of  $X$ . Lastly, the effects of the particle to air mass flow ratio on the

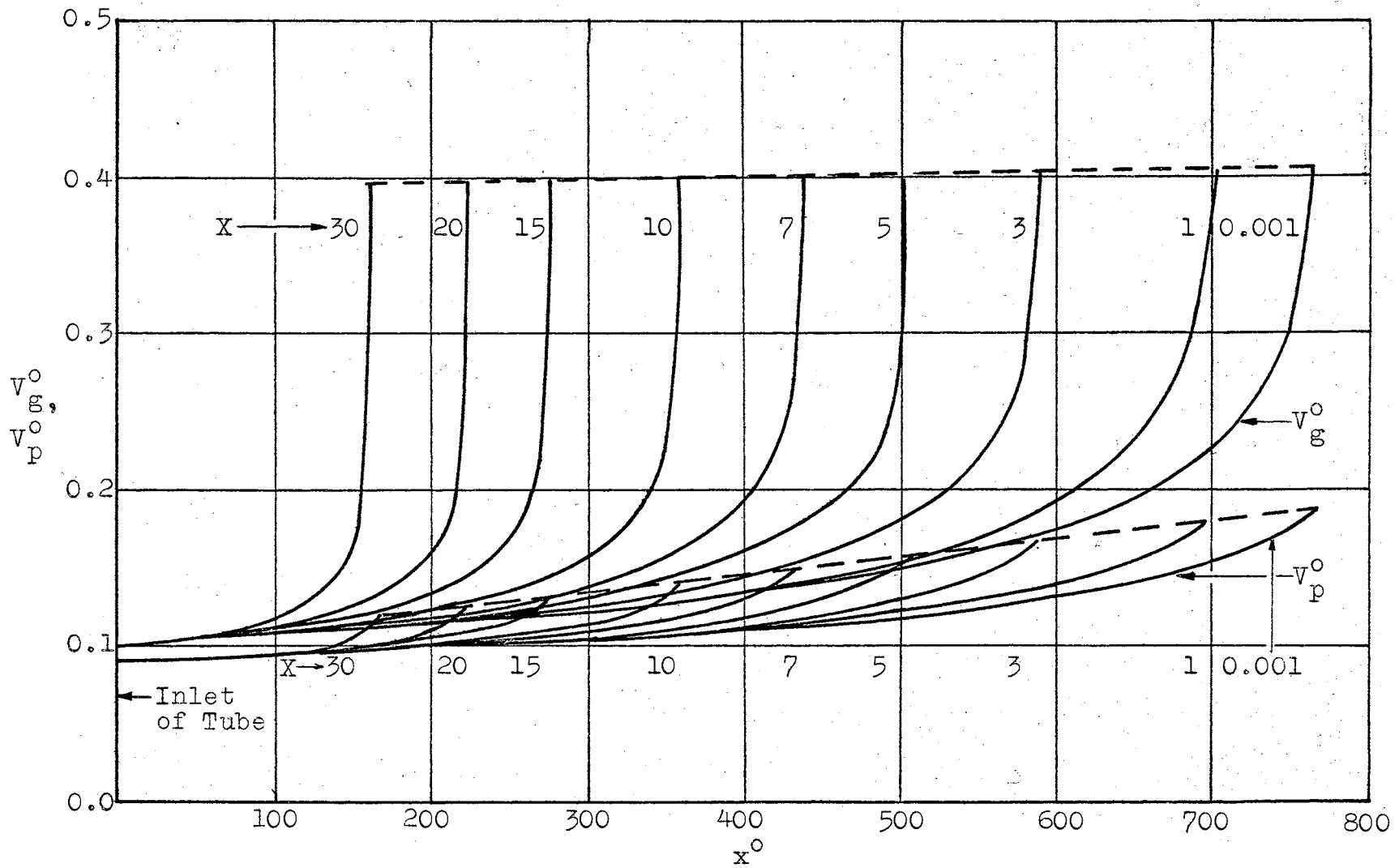


Figure 2. Local Velocity, Temperature, Pressure, and Mach Number Characteristics of Subsonic Gas-Particle Flow



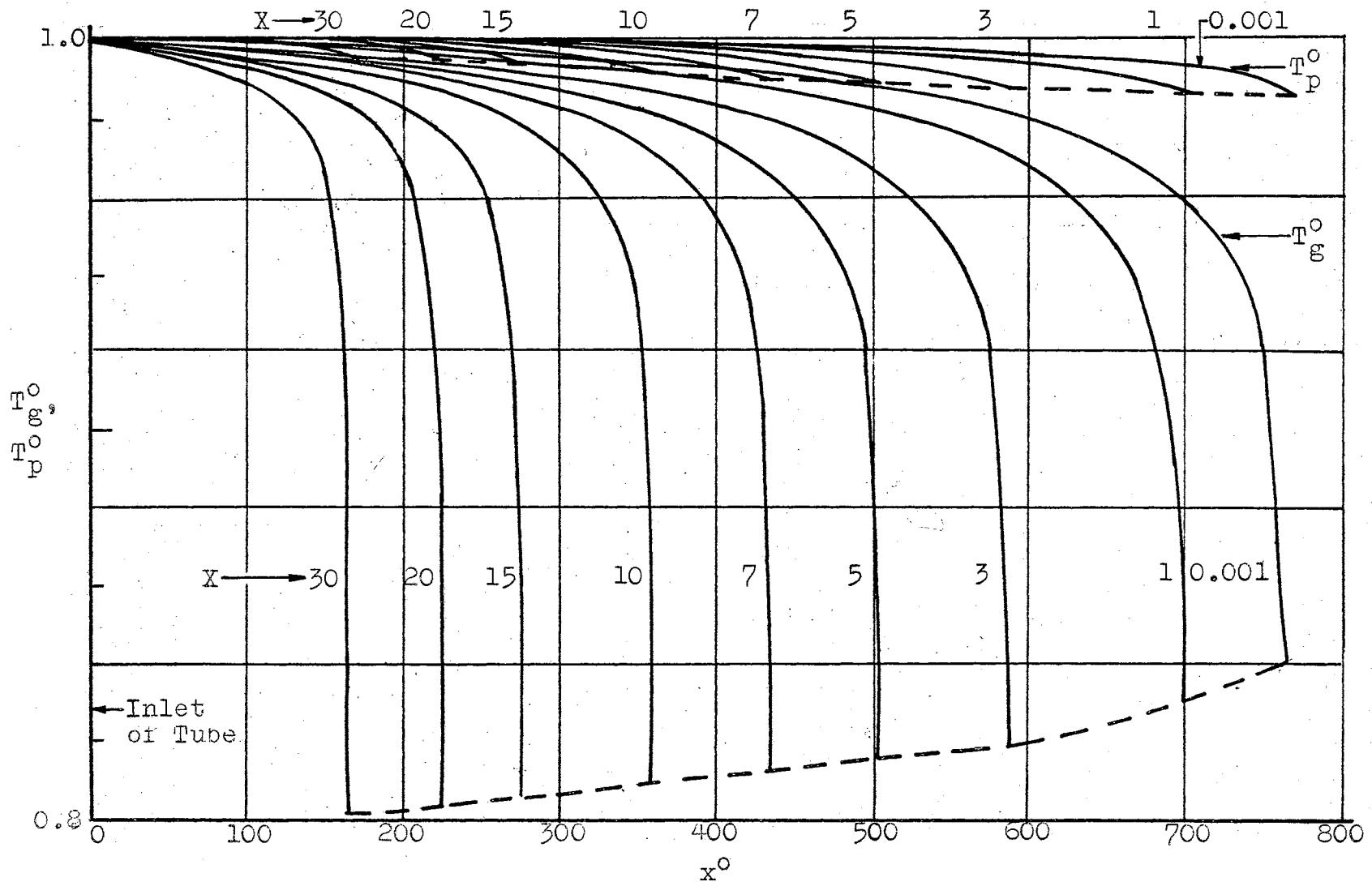


Figure 2. Continued

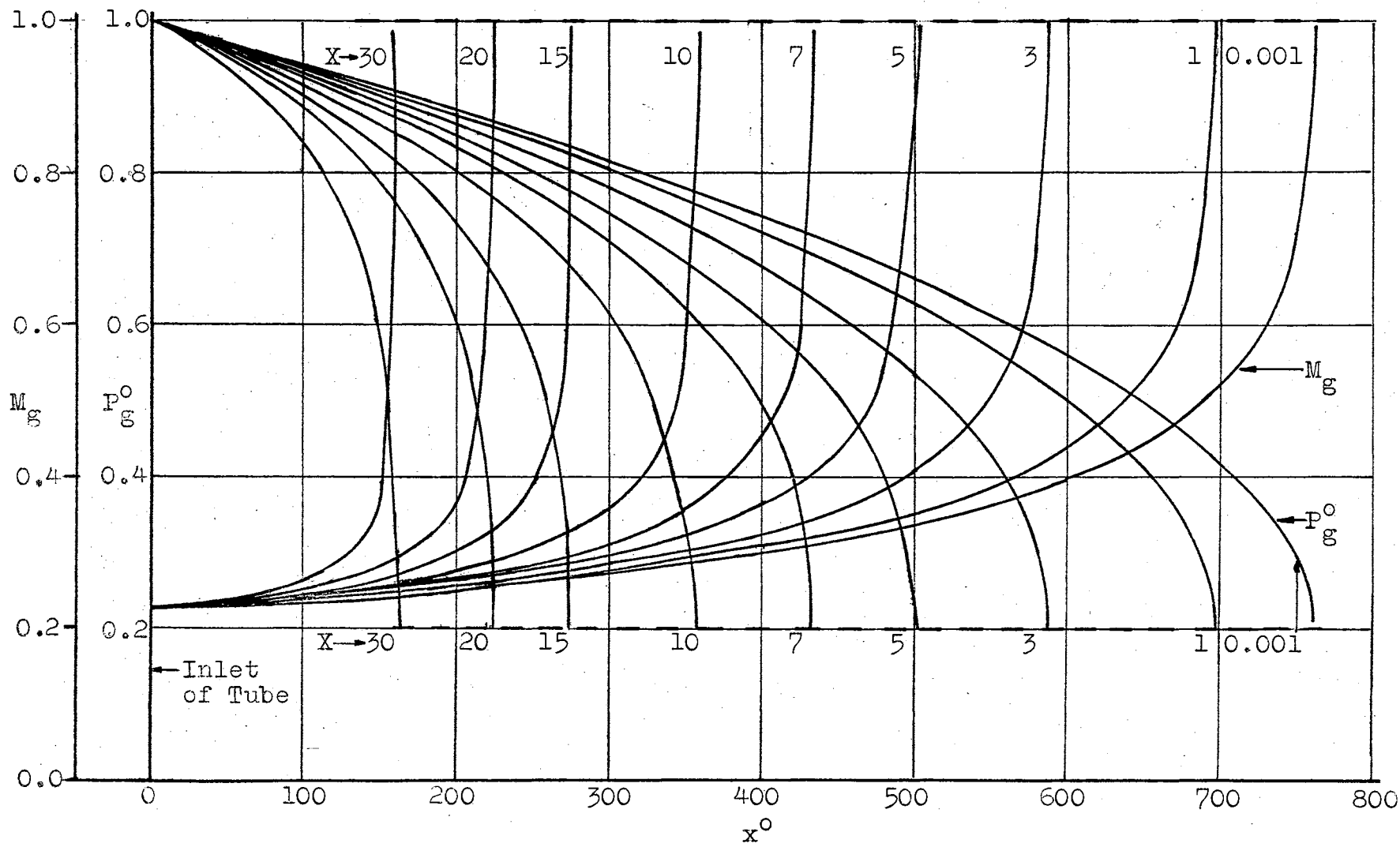


Figure 2. Continued

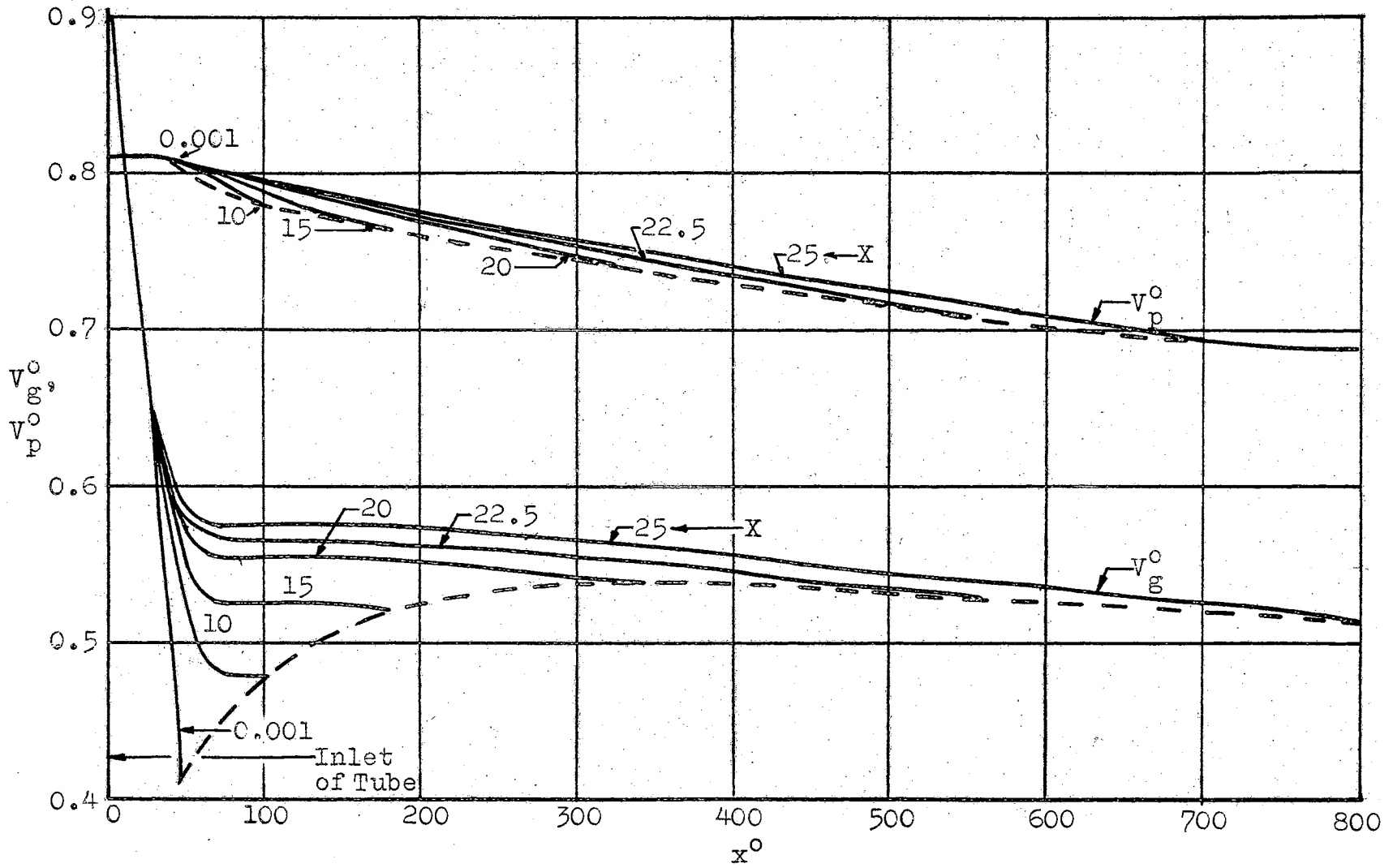


Figure 3. Local Velocity, Temperature, Pressure, and Mach Number Characteristics of Supersonic Gas-Particle Flow

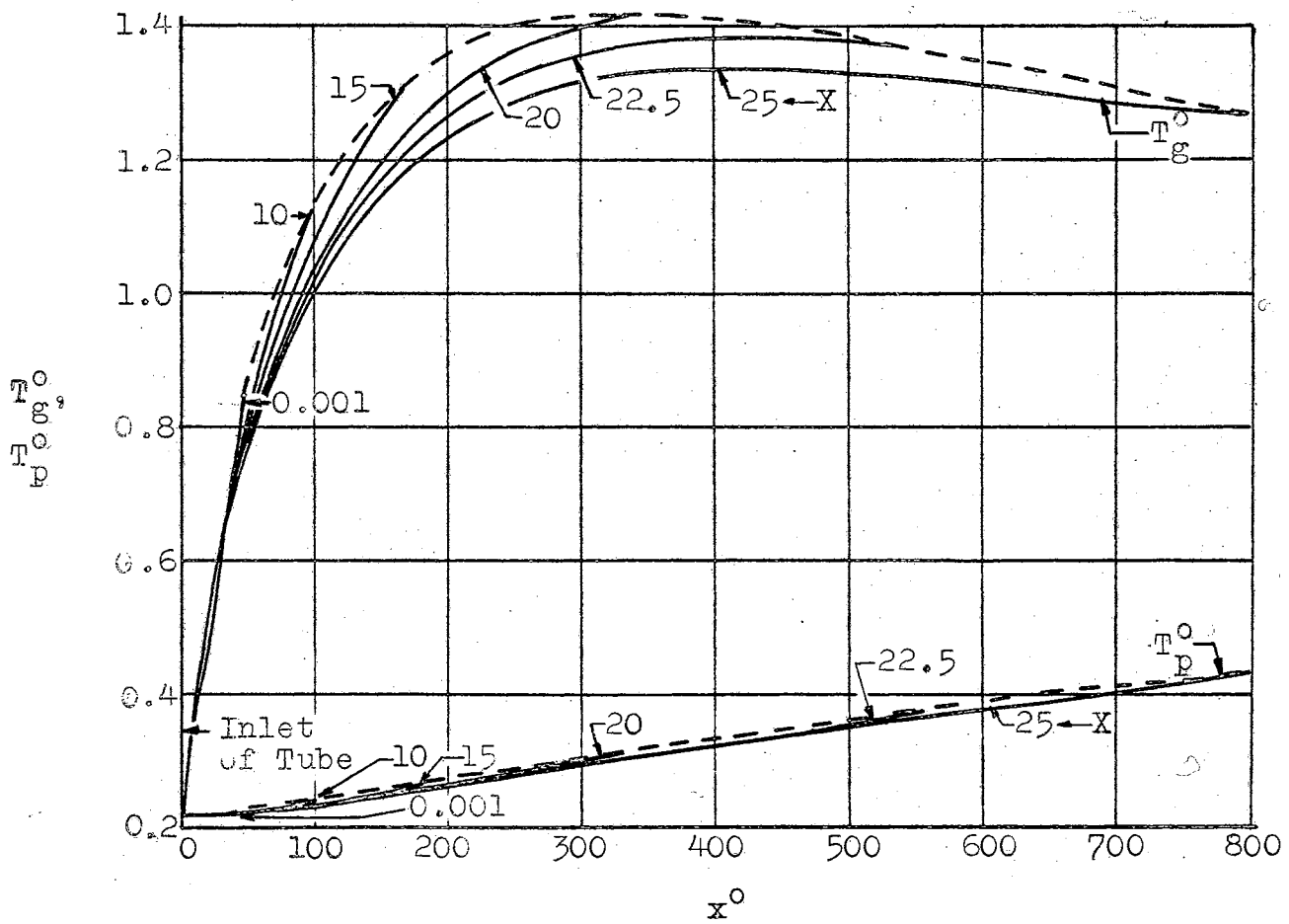


Figure 3. Continued

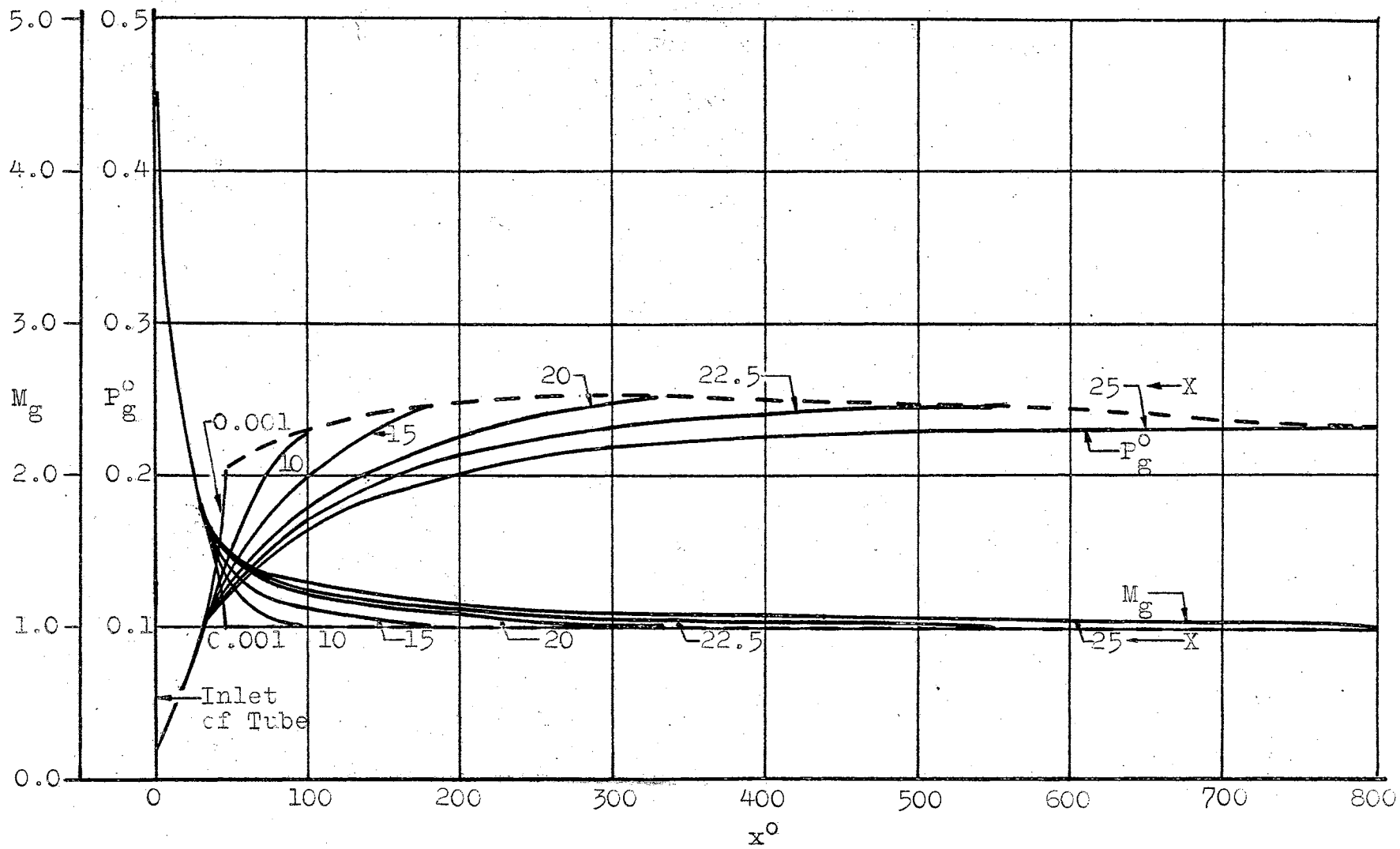


Figure 3. Continued

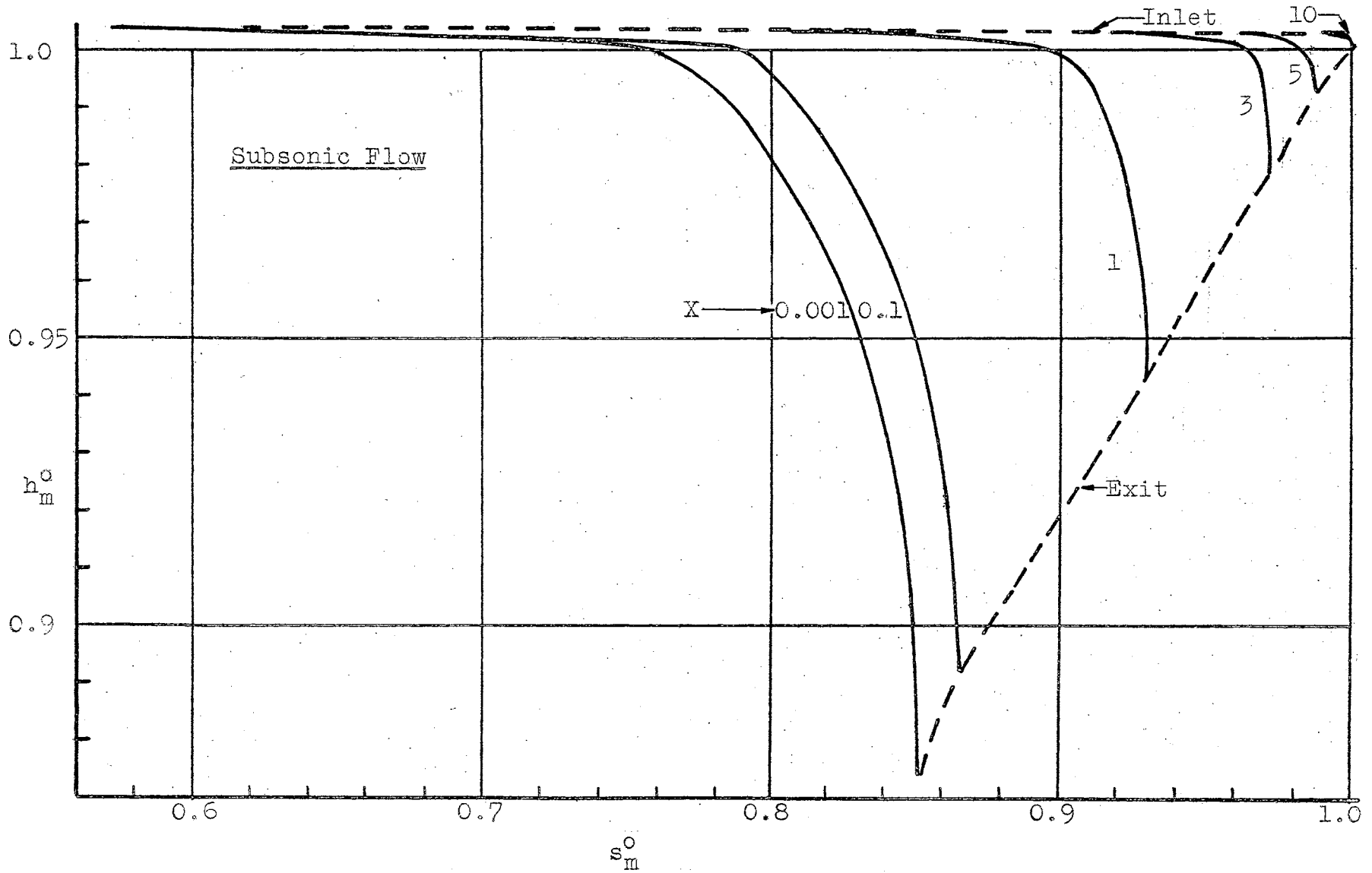


Figure 4. Mixture Enthalpy-Entropy Diagram for Subsonic and Supersonic Gas-Particle Flow

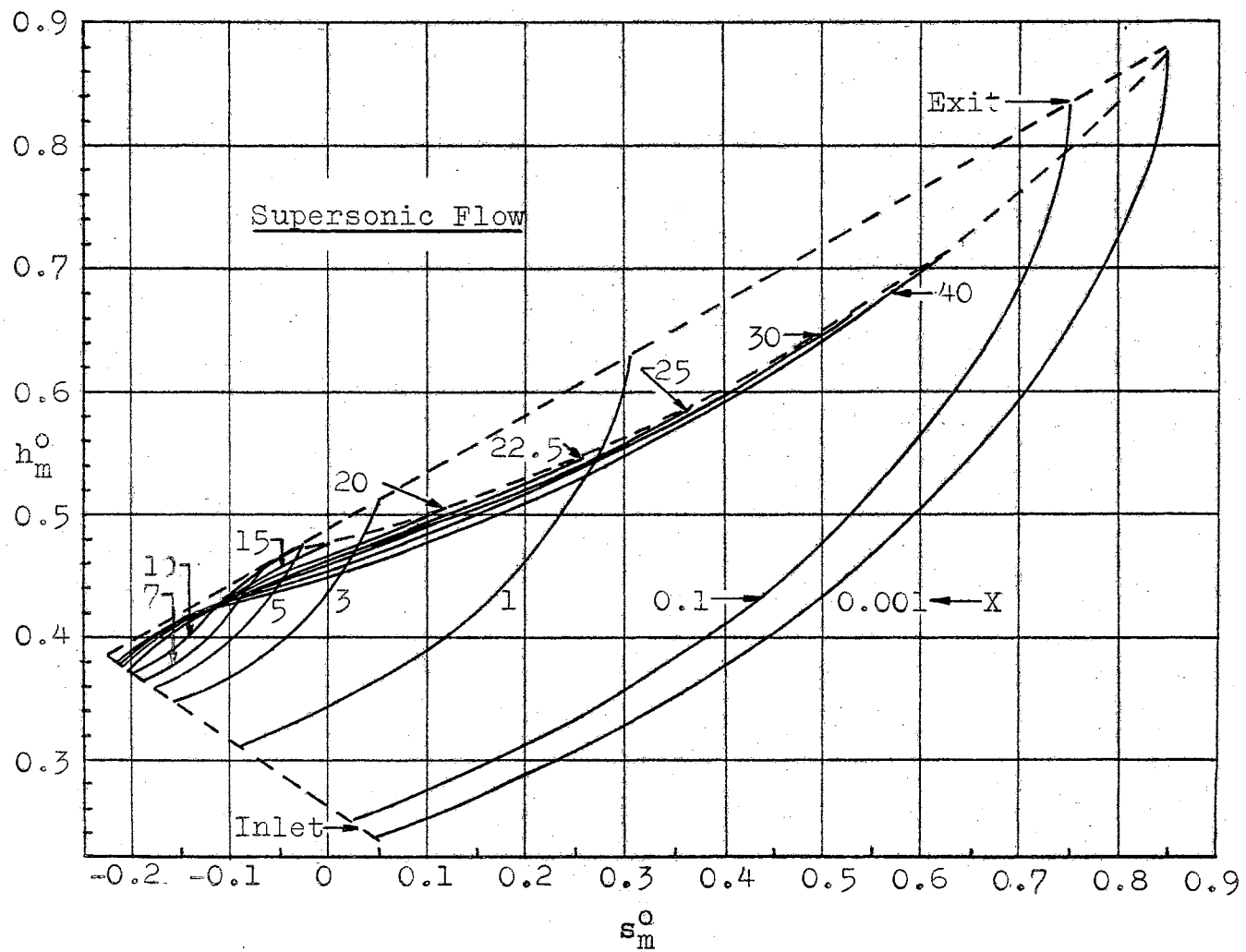


Figure 4. Continued

critical length are shown more clearly in Figure 5 for both low and high inlet particle slip where the particle slip  $S_p$  is defined as the ratio of the particle velocity to that of the air or at the inlet of the tube

$$S_{pi} = \frac{V_{pi}^o}{V_{gi}^o}.$$

The results for the property variation data set for subsonic and supersonic flow are shown in Table I. The subsonic and supersonic critical lengths corresponding to each individual change in starting condition and variable of the system are listed. For comparative purposes, the critical lengths corresponding to the particle mass variation data set at the same value of particle to air mass flow ratio of  $X=10$  are included. In addition, the effects of varying the multi-particle drag coefficient  $C_d$  are shown graphically in Figure 5 for both low and high  $S_{pi}$ .

#### Discussion of Results

The subsonic curves shown in Figure 2 (pages 51-53) for air velocity  $V_g^o$ , temperature  $T_g^o$ , pressure  $P_g^o$ , and Mach number  $M_g$  are similar in shape and characteristics to those for single-phase gaseous flow ( $X = 0.001$ ). As the particle to air mass flow ratio increases, the critical length decreases. It is interesting to note that the exit properties of the air  $V_{ge}^o$ ,  $T_{ge}^o$ ,  $P_{ge}^o$ , and  $M_{ge}$  do not change significantly, especially  $P_{ge}^o$  and  $M_{ge}$  which are essentially



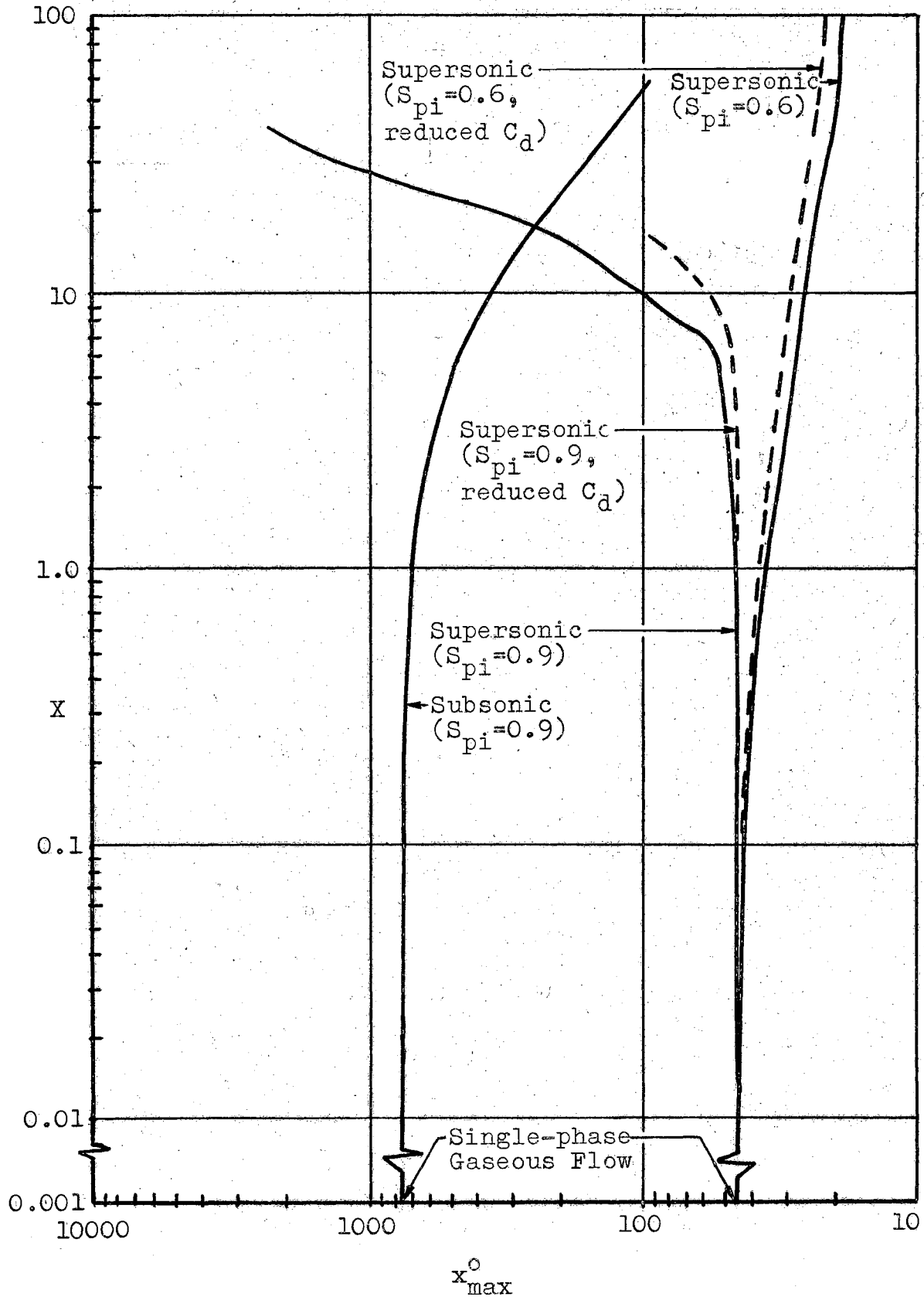


Figure 5. The Effect of Particles on the Subsonic and Supersonic Critical Lengths

TABLE I  
EFFECT OF PROPERTY VARIATIONS ON  
THE CRITICAL LENGTH

X = 10		
Property Variation	Critical Length - $x_{\max}^{\circ}$	
	Subsonic	Supersonic
Data Set 1	359.6	100.0
$c_p$ -Increased	358.8	37.7
$c_p$ (same $M_{gi}$ )	---	100.5
$K_g$ -Increased	354.7	165.0
$c_g$ -Increased	622.1	42.6
$\mu_g$ -Increased	331.5	69.0
$d_t$ -Decreased	401.8	44.5
$d_p$ -Decreased	90.3	882.0
$V_{pi}$ -Decreased	215.1	33.8
$V_{pi}$ (same $M_{gi}$ )	---	50.6
$V_{gi}$ -Increased	277.3	144.5
$T_{pi}$ -Increased	279.5	83.5
$T_{pi}$ (same $M_{gi}$ )	---	98.0
$T_{gi}$ -Increased	889.5	59.0
$P_{gi}$ -Increased	328.4	222.5
$g$ ( $g = 0$ )	363.8	100 <sup>+</sup>
$\gamma$ -Increased	611.5	25.5
$\rho_p$ -Increased	431.8	52.0

constant. Therefore, the limiting exit Mach number is governed by the air only and equals one as in the case of single-phase flow. Of course, as the critical length decreases, the changes in particle velocity  $V_p^0$  and temperature  $T_p^0$  are less because less distance is available for particle acceleration and particle to air heat transfer.

The supersonic curves shown in Figure 3 (pages 54-56) for air velocity  $V_g^0$ , temperature  $T_g^0$ , pressure  $P_g^0$ , and Mach number  $M_g$  are similar in shape and characteristics to those corresponding to single-phase gaseous flow only for low values of particle to air mass flow ratio  $X$  (below  $X = 1$ , approximately) or for tube diameter ratios up to  $x^0 = 25$ . The exit properties of the air  $V_{ge}^0$ ,  $T_{ge}^0$ , and  $P_{ge}^0$  are not constant, but increase and then decrease as the particle to air mass flow ratio  $X$  is increased. Surprisingly enough, though, the exit Mach number of the air is constant and equals one as in the case of single-phase flow and subsonic two-phase flow. The exit slopes of the air properties  $\frac{dV_{ge}^0}{dx^0}$ ,  $\frac{dT_{ge}^0}{dx^0}$ ,  $\frac{dP_{ge}^0}{dx^0}$ , and  $\frac{dM_{ge}}{dx^0}$  do not appear to be infinite, but according to the corresponding computer solutions they approach infinity, as in subsonic flow, very near the exit of the tube (not noticeable on graphs). The changes in particle velocity  $V_p^0$  and temperature  $T_p^0$  are greater as the critical length increases because a greater distance is available for particle deceleration and air to particle heat transfer. An important conclusion for supersonic flow

is that the effect of the particles is to increase the critical length which means that the transportation of a gas-particle mixture over long distances at supersonic speeds is a possibility, an impossible situation for single-phase gaseous flow. In this manner, solid and gaseous fuels, such as coal particles and natural gas, could be transported. As shown later this possibility exists for horizontal flow also.

It is seen from Figure 4 (pages 57 and 58) that the curves of mixture enthalpy versus entropy have discontinuous exit values for all values of particle to air mass flow ratio  $X$  except for the single-phase flow where  $X = 0.001 \approx 0$ . The inlet and exit values for subsonic flow and supersonic flow up to  $X = 10$  lie on different intersecting lines. The exit values for supersonic flow and  $X$  greater than 10 lie on a curved line that approaches the exit enthalpy-entropy for single-phase flow. Generally, as the critical length decreases the changes in entropy and enthalpy are less tending to cause the subsonic curve to approach a point. The same would be true if the critical length decreased for supersonic flow. However, for supersonic flow, the changes in the mixture enthalpy and entropy are greater because the critical length increases. It appears that a limiting exit value could exist, however. This could mean that the increase in critical length is limited to some upper maximum which would be similar to the lower minimum of zero for subsonic flow.

Figure 5 (page 60) shows more clearly the effect of the particles on the critical length to be important only for values of the particle to air mass flow ratio  $X$  greater than one. It is interesting to note that for supersonic flow and low inlet particle slip  $S_{pi} = 0.9$  the critical length is decreased while the results for high inlet particle slip  $S_{pi} = 0.6$  indicate that the supersonic critical length can be decreased if the inlet particle slip  $S_{pi}$  is high enough. This effect and that of reducing the particle drag coefficient are explained later.

To get an insight into the reasons for the subsonic and supersonic critical length characteristics given above, consider single-phase gaseous Fanno flow and Rayleigh flow in a constant area tube (1). Exact one-dimensional Fanno theory shows that wall friction tends to increase the subsonic Mach number by expanding the gas and tends to decrease the supersonic Mach number by compressing the gas both to a limiting exit Mach number equal to one at the critical length. Exact one-dimensional Rayleigh flow shows that heat addition tends to increase the subsonic Mach number by expanding the gas and tends to decrease the supersonic Mach number by compressing the gas both to a limiting exit Mach number equal to one at the critical length. Therefore, the effect of wall friction and heat addition are equivalent in governing the critical length. In both cases, an increase in the inlet Mach number tends to decrease the subsonic critical length and increase the supersonic critical length.

For a given inlet Mach number, the critical length is governed entirely by the amount of wall friction in adiabatic Fanno flow and the rate of heat transfer in frictionless Rayleigh flow. In addition, the inlet Mach number governs entirely the ratios of the inlet properties of the gas to those existing at the critical condition. The ratios are not affected by wall friction or rate of heat transfer in Fanno or Rayleigh flow, respectively.

Then, consider the influence of the particles on the gas. The addition of particles to a gaseous stream tends to affect the momentum transition of the gas and the rate of heat transfer to or from the gas by acting as external forces on the gas and as heat sources or sinks to the gas, respectively. Although the entire flow process was assumed adiabatic, the individual gas-particles processes are not. The air pressure drop over an individual particle, which is referred to as particle pressure drop, resulting from viscous and form drag forces can be defined as the particle drag force  $F_p$  divided by the total cross-sectional area of the tube  $A_t$ . The individual particle pressure drop multiplied by the number of particles passing a given location per unit time  $N$  and divided by the particle velocity  $V_p$  gives the total particle pressure drop per unit length of tube as

$$\Delta P_p = \frac{F_p N}{A_t V_p}. \quad (23)$$

This may be put in terms of the particle drag coefficient  $C_d$  where  $C_d$  is given by

$$C_d = \frac{F_p}{\frac{A_{pf}(V_g - V_p)^2 \rho_g}{2g_c}} .$$

Thus,  $\Delta P_p$  can be expressed by

$$\Delta P_p = \frac{C_d N}{A_t V_p} \frac{A_{pf}(V_g - V_p)^2 \rho_g}{2g_c} . \quad (24)$$

Hariu and Molstad (11) presented a similar equation for  $\Delta P_p$ .

Therefore, for subsonic flow where the particles are generally moving slower than the air, the forces of the particles on the air act in the same direction as wall friction forces. Thus,  $\Delta P_p$  represents an air pressure drop in addition to the pressure drop produced by wall friction which tends to promote a more rapid transition to the critical conditions by effectively increasing wall friction. Also, since the temperature of the particles is generally higher than that of the air, the heat transfer is from the particles to the air. According to Rayleigh flow, the transition to critical conditions is thereby induced more rapidly. Therefore, both effects tend to reduce the critical length as the particle to air mass flow ratio  $X$  is increased because the particle pressure drop and rate of heat transfer from the particles to the air are increased since more particles are present in the system.

It is not as simple to explain the behavior for supersonic flow because as seen from Figure 5 (page 60), the critical length may be increased or decreased, depending on the inlet particle slip  $S_{pi}$ . Consider the air velocity curves  $V_g^0$  versus  $x^0$  shown in Figure 2 (pages 51-53). At first the particles are going slower than the air but after a few tube diameters the air compresses sufficiently so that the particles are eventually traveling faster than the air. In this region where  $V_p < V_g$ , the forces of the particles on the air act in the same direction as wall friction forces. As in subsonic flow, this has the same effect as increasing wall friction but, however,  $\Delta P_p$  represents a pressure increase in addition to the pressure increase caused by wall friction for supersonic flow. Consequently, the critical length tends to decrease in this region as  $X$  is increased. However, when  $V_p > V_g$  the forces of the particles on the air act in the opposite direction as the wall friction forces which tends to reduce the effect of wall friction because  $\Delta P_p$  represents a pressure decrease. The combined effects of the particle pressure drop and the air pressure increase resulting from wall friction forces yields a lower total air pressure increase which tends to retard the transition to critical conditions and increase the critical length.

The effect of low inlet particle slip  $S_{pi} = 0.9$  on the critical length when  $V_p < V_g$  is insignificant and the predominating effect occurs when  $V_p > V_g$  which tends to increase the critical length as explained above. However, for high



inlet particle slip  $S_{pi} = 0.6$ , the air compresses so much that by the time the particles are going faster than the air the transition to critical conditions occurs shortly afterwards. The predominating effect occurs when  $V_p < V_g$  which tends to reduce the critical length. Of course, shock waves would be produced over the particles if  $S_{pi}$  and the Mach number of the air relative to the particles were high enough (effect of shock waves neglected in the analysis). As for subsonic flow, the effect of the particles on  $x_{max}^0$  for both low and high  $S_{pi}$  becomes more pronounced as the particle to air mass flow ratio  $X$  is increased. Also, since the temperature of the particles is generally less than that of the air, the heat transfer is from the air to the particles.

According to Rayleigh theory, the heat rejection from the air would tend to increase the critical length by retarding the transition to critical conditions since heat rejection tends to increase the Mach number of the air. This effect cannot be noticed for the high inlet particle slip  $S_{pi}$  because the particle forces in the region where  $V_p < V_g$  dominate and promote rapid transition to critical conditions. For low  $S_{pi}$ , both effects of particle forces and heat transfer in the region where  $V_p > V_g$  tend to increase the critical length.

The above results for critical gas-particle flow may now be applied to a discussion of choking and sub-critical conditions in gas-particle systems. As mentioned before, choking occurs when the velocity of the gas is insufficient

to support any particles and the particles fill the tube and causes both the flow of gas and particles to cease. A similar condition can occur in horizontal flow as well. Stratification, or fallout of particles from the gas stream, is succeeded by choking in horizontal flow. The gas velocity at which choking occurs is essentially equal to the terminal velocity of the particles  $V_{pt}$  for both horizontal and vertical flow (10). Sub-critical conditions occur when the length of the tube  $x_t^0$  is less than the critical length  $x_{max}^0$  while critical conditions indicate that  $x_t^0 = x_{max}^0$ . It is impossible for  $x_t^0$  to be greater than  $x_{max}^0$ .

Consider a vertical tube of fixed length  $x_t^0$  in which gas and particles flow at supersonic or subsonic conditions. Assume that the only inlet quantity to be varied is the velocity of the gas and that the back pressure is always maintained equal to the pressure at the exit of the tube. In supersonic flow, if the back pressure is higher than the pressure at the exit of the tube, a shock wave is produced in the tube which can cause the tube to operate partly or wholly subsonically and choking to occur.

First, consider critical conditions in supersonic flow. The addition of more particles into the gas-particle stream tends to increase the critical length for low particle slip  $S_{pi}$ . To maintain critical conditions, the inlet velocity of the gas must decrease, i.e., the inlet Mach number of the gas must decrease. According to Fanno theory the critical length decreases. The increase in critical length

must equal to the decrease so that the tube length  $x_t^0$  equals the critical length  $x_{\max}^0$ . As the particle to air mass flow ratio  $X$  is increased further the inlet Mach number of the gas would have to decrease further and approach one to maintain critical conditions. At some inlet Mach number of the gas  $M_{gi}$  greater than one a further increase in  $X$  would probably result in a shock wave causing subsonic flow to exist either partly or entirely in the tube. After the transition to subsonic flow is established critical or sub-critical unchoked conditions may be present or choking may occur if the transition causes the velocity of the gas to be reduced sufficiently so that particles cannot be supported. If choking does not occur, continual increases in  $X$  will eventually cause choking to occur as shown below for subsonic flow. The value of the particle to gas mass flow ratio  $X_c$  at which choking occurs is the maximum. However, the maximum particle mass flow does not occur at choking but at a value of  $X$  somewhere between the value corresponding to the initial conditions and  $X_c$ . If the inlet Mach number of the gas were not decreased, the transition to subsonic flow would not occur because the critical length  $x_{\max}^0$  would be greater than the length of the tube  $x_t^0$ , i.e., sub-critical conditions would result.

For high particle slip  $S_{pi}$  the supersonic critical length decreases as  $X$  is increased as shown before. In this case, the transition to subsonic flow would occur whether the inlet Mach number of the gas were decreased or

held constant since  $x_{\max}^0$  would be less than  $x_t^0$ , an impossible situation. The only way to maintain critical conditions would be to increase the inlet Mach number of the gas, among other things, which would tend to offset the decrease in  $x_{\max}^0$  as  $X$  is increased. However, as  $M_{gi}$  approaches infinity the critical length approaches a finite upper limit. If the inlet Mach number were very high and critical conditions were present, a further increase in  $X$  would cause transition to subsonic flow since  $x_{\max}^0$  would be less than  $x_t^0$ . Sub-critical conditions would occur if  $X$  were maintained constant and  $M_{gi}$  increased. The above discussion would also apply to supersonic flow that is initially sub-critical.

When the gas-particle flow is initially subsonic, choking will eventually occur as the particle to gas mass flow ratio  $X$  is increased. If the flow is initially critical, the addition of more particles tends to reduce the critical length. To maintain critical conditions, the inlet Mach number of the gas must decrease, which tends to increase the critical length so that  $x_t^0 = x_{\max}^0$ . In this case,  $M_{gi}$  cannot remain constant as  $X$  is increased because  $x_{\max}^0$  would be less than  $x_t^0$ , an impossible situation. As  $X$  is continually increased  $M_{gi}$  continues to decrease until choking occurs. If the flow is initially sub-critical, and  $M_{gi}$  maintained constant, an increase in  $X$  would reduce the critical length and critical conditions would be approached ( $x_{\max}^0 \rightarrow x_t^0$ ) resulting in eventual choking as shown

above. Of course, if  $M_{gi}$  is increased, the critical condition is reached more rapidly. If it is decreased, the flow becomes even more sub-critical and choking occurs at a lower value of  $X_c$  than when  $M_{gi}$  is increased or maintained constant.

The above discussion on choking and sub-critical flow is restricted to constant inlet conditions, except for the inlet velocity and Mach number of the gas, and a variable back pressure which is adjusted to equal the pressure at the exit of the tube. In actual practice neither condition is easy to satisfy. Generally, the compressor supplying the gas to the flow passageway has variable characteristics and, in many cases, the gas-particle flow is discharged into an area or device in which the pressure is constant and cannot be varied. Thus, to analyze such a system would be a difficult task. However, it is important to note that the concepts on choking and sub-critical conditions as applied to critical conditions are qualitatively correct for any gas-particle system.

Up to this point, the primary consideration has been the effect of the particle to air mass flow ratio  $X$  on the critical length. To evaluate the effect of the starting conditions and other variables of the system, the property variation data set was considered. The results are shown in Table I (page 61). To evaluate the significance of changing each of the above factors individually on the critical length, the concepts of particle pressure drop and

air-particle heat transfer rates discussed earlier are utilized.

Specific heat of the particles  $c_p$ . The specific heat was increased from 0.2 to 0.4 Btu/lb<sub>m</sub><sup>o</sup>R. As noticed from Table I for subsonic flow, the critical length is decreased slightly (359.6 → 358.8) because the rate of heat transfer from the particles to the air is increased slightly. The temperature drop of the particles per unit length of tube is less for the higher  $c_p$ . Consequently, the local differences in the temperatures of the particles and the air are greater which tends to increase the particle to air convection heat transfer rate. For temperature equilibrium ( $T_g \approx T_p$ ) to exist,  $c_p$  would have to be reduced greatly. For supersonic flow, two critical lengths are given. The first one corresponds to an inlet Mach number of the gas that is lower than the inlet Mach number for the smaller  $c_p$ . This was caused by the method used to calculate the supersonic inlet static temperature and pressure of the air such that the subsonic and supersonic inlet stagnation enthalpies and mixture mass flow rates would be equal. To give a better comparison, the second critical length is based on the same inlet Mach number and mixture mass flow rate but a different inlet stagnation enthalpy. As noted, the critical length increases slightly (100 → 100.5) because the rate of heat transfer from the air to the particles is larger. The reasons for the increased heat transfer rate are similar to those given above for subsonic flow.

Specific heat of the air  $c_g$ . The specific heat was increased from 0.24 to 0.343 Btu/lb<sub>m</sub><sup>o</sup>R. Since the specific heat is given by  $c_g = \gamma R_g / (\gamma - 1)$  for an ideal gas, it was assumed that  $R_g$  increased while  $\gamma$  remained constant. The subsonic critical length increases greatly (359 → 622) even though the wall friction factor increases. Several factors account for the increase such as a decreased inlet Mach number of the gas, reduced particle to air heat transfer rates, and reduced particle pressure drop per unit length. For supersonic flow, the critical length is decreased significantly (100 → 42) primarily because of a reduced inlet Mach number, a greater wall friction factor, and a smaller air to particle heat transfer rate.

Thermal conductivity of the air  $K_g$ . The thermal conductivity was increased from 0.015 to 0.030 Btu/hr<sup>o</sup>F ft. The subsonic critical length is decreased slightly (359 → 354) because the heat transfer rate from the particles to the air is greater. The energy conducted from the surface of the particles is greater for the larger thermal conductivity. The supersonic critical length is increased (100 → 165) because the rate of heat transfer conducted from the air to the surface of the particles is greater.

Viscosity of the air  $\mu_g$ . The viscosity was increased from  $3.76 \times 10^{-7}$  to  $7.52 \times 10^{-7}$  lb<sub>f</sub>sec./ft.<sup>2</sup>. The subsonic critical length decreases (359 → 331) primarily because the wall friction factor increases but the effect is reduced somewhat because of the smaller rate of heat transfer from

the particles to the air. The supersonic critical length is reduced (100 → 69) principally because the wall friction factor  $f$  is greater and the rate of heat transfer from the air to the particles is smaller.

Diameter of tube  $d_t$ . The diameter was decreased from 0.5 to 0.25 inch. The subsonic critical length is increased (359 → 401) even though  $f$  increases. To explain this, consider first the ratio of the mass flow of air for the small tube  $m_{gs}$  to that for the larger tube  $m_{gl}$ . Since the mixture mass flow per unit area  $m_m/A_t$  is the same for both sizes of tube as seen from Equation 16,

$$\frac{m_{gs}}{m_{gl}} = \frac{A_{ts}}{A_{tl}} = \frac{d_{ts}^2}{d_{tl}^2} = \frac{1}{4}.$$

It can also be shown that the ratio of the effective cross-sectional area of the air to that of the particles at the inlet of the tube is the same for both diameters of tube. From continuity of the particles

$$\frac{m_{ps}}{m_{pl}} = \frac{\rho_p \Delta V_p N_s}{\rho_p \Delta V_p N_l}.$$

Since the particle to air mass flow ratio  $X$  is unchanged,

$$\frac{m_{ps}}{m_{pl}} = \frac{m_{gs}}{m_{gl}} = \frac{1}{4}.$$

Therefore, the number of particles passing a given location per unit time in the small tube  $N_s$  is one-fourth that in



the larger tube  $N_1$ . It can be shown that the specific heat transfer to the air and the particle pressure drop per unit length  $\Delta P_p$  do not change significantly. However, the pressure drop of the air per unit length of tube  $\Delta P_g$ , due to wall friction, at the inlet of the smaller tube is more than twice that at the inlet of the larger tube. Thus,  $\Delta P_p/\Delta P_g$  is much less for the smaller tube than for the larger tube which reduces the effect of the particles and thereby tends to increase the critical length. The supersonic critical length is reduced (100  $\rightarrow$  44.5) primarily because of the increased wall friction factor  $f$  and the reduced ratio of  $\Delta P_p/\Delta P_g$ .

Diameter of the particles  $d_p$ . The diameter was decreased from 0.0185 to 0.00185 inch. The subsonic critical length is decreased greatly (359  $\rightarrow$  90). As a result of decreasing the particle size by a factor of 10, the number of particles passing a given location per unit time  $N$  must increase by a factor of  $10^3$  to satisfy particle continuity and the surface area of the particles must increase by a factor of 10. Therefore, the particle-air heat transfer rate and particle pressure drop per unit length  $\Delta P_p$  are greater. Decreasing the diameter of the particles has the same effect as increasing the diameter of the tube, i.e., increasing the tube to particle diameter ratio  $\frac{d_t}{d_p}$ . Another way of verifying that  $\Delta P_p$  is greater is to estimate the relative particle pressure drops quantitatively. From computer data for the smaller particles, the inlet particle

drag coefficient increases (0.44 → 1.176) since the Reynolds number of the particles decreases (1222 → 122.2). Since the inlet quantities  $\rho_{gi}$ ,  $V_{gi}$ , and  $V_{pi}$  are the same for the large and small particles, Equation (24) shows that the ratio of the particle pressure drop for the smaller particles  $\Delta P_{ps}$  to that for the larger particles  $\Delta P_{pl}$  is given by

$$\frac{\Delta P_{ps}}{\Delta P_{pl}} = \frac{C_{ds} N_s^A p_{fs}}{C_{dl} N_l^A p_{fl}} = \frac{(1.176)(1000)}{(0.44)(100)} = 26.4$$

at the inlet of the tube. This ratio reduces to about 10 at the exit of the tube. Therefore, the subsonic critical length decreases because of higher heat transfer rates from the particles to the air and greater particle pressure drops per unit length. The supersonic critical length is increased sharply (100 → 882) primarily because of greater air to particle heat transfer rates and greater particle pressure drops per unit length. The analysis is similar to that for subsonic flow above. For velocity equilibrium ( $V_g \approx V_p$ ) and temperature equilibrium ( $T_g \approx T_p$ ) to exist the diameter of the particles must be decreased greatly. As  $d_p$  approaches zero, the air-particle system behaves as a mixture of ideal gases having equivalent mixture properties. Soo (43) discusses this type of flow in a nozzle. However, the analytical analysis presented herein is not valid for this case because the contribution to the system pressure by the particles was neglected (see page 31).

Inlet velocity of the particles  $V_{pi}$ . The velocity was

decreased arbitrarily from 230 to 179 ft./sec. which corresponds to a increase in the particle slip of from  $S_{pi} = 0.9$  to  $S_{pi} = 0.7$ . The subsonic critical length decreases (359 → 215) principally because the particle pressure drop per unit length is greater as seen from Equation (24) for the same  $C_d = 0.44$ . Since the particle Reynolds numbers is higher because of the increased particle slip, the heat transfer rate from the particles to the air is greater. Both effects, as explained before, tend to decrease the subsonic critical length  $x_{max}^o$  and increase  $x_{max}^o$  for superflow and low inlet particle slip  $S_{pi}$ . For supersonic flow, two critical lengths are given. Similar to the discussion given for the variation of the specific heat of the particles, the critical length based on the same inlet Mach number of the air  $M_{gi}$  has more significance. The critical length corresponding to the same  $M_{gi}$  is reduced (100 → 50.6) for the higher inlet particle slip even though the air to particle heat transfer is greater at the inlet of the tube (See pages 67 and 68). Based on the discussion for particle slip  $S_{pi}$ , the subsonic critical length could be increased if  $S_{pi}$  were greater than one. Also, if  $S_{pi}$  were greater than one, the supersonic critical lengths would be even higher than those corresponding to a particle slip  $S_{pi} = 0.9$ .

Inlet velocity of the air  $V_{gi}$ . The velocity was increased slightly from 255 to 281 ft./sec. The subsonic critical length decreases (359 → 277) since the inlet Mach

number of the air increases even though the wall friction factor decreases slightly. The effect is similar to increasing the inlet Mach number of the air in single-phase gaseous flow. The supersonic critical length is increased (100 → 144.5) since the inlet Mach number of the air increases and the wall friction factor decreases.

Inlet temperature of the particles  $T_{pi}$ . The temperature was increased from 540 to 593°R. The subsonic critical length is decreased (359 → 279) because the particle to air heat transfer rate is increased. The supersonic critical length is reduced (100 → 98) because the smaller differences between the temperatures of the air and particles resulted in lower air to particle heat transfer rates. As done before for  $c_g$  and  $V_{pi}$ , the critical length corresponding to the same inlet Mach number of the air was chosen for a comparison.

Inlet temperature of the air  $T_{gi}$ . The temperature was increased from 540 to 700°R. The subsonic critical length is increased significantly (359 → 889) primarily because the inlet Mach number of the air is reduced and the heat transfer rate is from the air to the particles instead of from the particles to the air. Heat rejected from a gas at subsonic Mach numbers tends to retard the transition to critical conditions. The increase in  $x_{max}^0$  is offset somewhat by an increase in the wall friction factor. The supersonic critical length is reduced (100 → 59) because the wall friction factor is increased and the inlet Mach number of the

air reduced. The decrease in  $x_{\max}^0$  is offset somewhat by the larger rate of heat transfer from the air to the particles.

Inlet pressure of the air  $P_{gi}$ . The pressure was increased from 75 to 150  $\text{lb}_f/\text{in.}^2$ . The subsonic critical length is reduced (359  $\rightarrow$  328) primarily because the particle pressure drop per unit length is greater as seen from Equation (24) for a larger air density  $\rho_g$  and the same  $C_d = 0.44$ . The decrease in  $x_{\max}^0$  is offset partly by a lower wall friction factor. The supersonic critical length is greater (100  $\rightarrow$  222) since the particle pressure drop per unit length is greater and the wall friction factor smaller.

Local acceleration of gravity  $g$ . The local gravity was reduced from  $g \approx |g_c|$  to  $g = 0$  ft./sec. This would correspond to ideal horizontal flow. The subsonic critical length increases slightly (359  $\rightarrow$  363.8) because for no gravity effect the local particle slip is less resulting in a lower particle pressure drop per unit length  $\Delta P_p$ . The critical length was also obtained for a fivefold increase in  $g$ . The above results for  $g = |g_c|$  were not changed significantly. Therefore, the gravity effect is negligible for small particles. As the diameter of the particles and, consequently, the ratio of the gravity to viscous and form drag forces increases, the effect of gravity on the critical length becomes more important. For  $g = 0$  the supersonic critical length was not noticeably affected. However, the local particle slip in the region where  $V_p > V_g$  would be

greater with no gravity effects resulting in a higher  $\Delta P_p$ . Therefore, the critical length would be higher ( $100 \rightarrow 100^+$ ). The critical length obtained for a fivefold increase in  $g$  showed very little difference from  $x_{\max}^0$  for  $g \approx g_c$ .

Specific heat ratio of the air  $\gamma$ . The specific heat ratio was increased from 1.4 to 1.667. Since  $c_g = \gamma R_g / (\gamma - 1)$  for an ideal gas, it was assumed that  $R_g$  increased while  $c_g$  remained constant. The subsonic critical length is larger (359  $\rightarrow$  611) primarily because the inlet Mach number of the air is reduced and the particle pressure drop per unit length  $\Delta P_p$  is decreased as seen from Equation (24) for a lower air density  $\rho_g$  and the same  $C_d = 0.44$ . The supersonic critical length is lower (100  $\rightarrow$  25.5) since the inlet Mach number of the air is less, the wall friction factor greater, and  $\Delta P_p$  less than for the higher specific heat ratio.

Density of the particles  $\rho_p$ . The density was increased from 160 to 320 lb.<sub>m</sub>/ft.<sup>3</sup>. The subsonic critical length increases (359  $\rightarrow$  431). To satisfy particle mass flow continuity, fewer particles pass a given tube location per unit time since the particle density is greater. Thus, the particle pressure drop per unit length  $\Delta P_p$  and the particle to air heat transfer rate are reduced. Both effects tend to reduce the subsonic critical length. The supersonic critical length is lower (100  $\rightarrow$  52) since  $\Delta P_p$  and the rate of heat transfer from the air to the particles are reduced.

There has been some question raised by several

investigators that Equations (20), (21), and (22) for the single-phase wall friction factor  $f$ , single-particle drag coefficient  $C_d$ , and single-particle heat transfer coefficient  $Nu_p$  may not apply to gas-particle systems (see Chapter II). Although little quantitative information is available for multi-particle heat transfer coefficients and two-phase wall friction factors, the effect of any variations on the critical length produced by the presence of the particles can easily be seen from the above discussion on the system variables. However, it was shown in Chapter II that the multi-particle drag coefficient is generally less than for single-particles for values of the particle Reynolds number below 1000. The range of particle Reynolds numbers mostly encountered in this investigation was above 1000. It is assumed that the multi-particle drag coefficient is less than for single-particles in this range also. Qualitatively, a reduced  $C_d$  should increase the subsonic and decrease the supersonic critical length. To evaluate the effects of reducing  $C_d$  on the critical lengths, solutions were obtained for a 50 per cent reduction in  $C_d$ . The results for supersonic flow are shown in Figure 5 (page 60) for both low and high inlet particle slips  $S_{pi} = 0.9$  and  $S_{pi} = 0.6$ , respectively. Subsonic results, not included, verify that the critical length increases. However, for supersonic flow, the reduction in  $C_d$  can cause the critical length to increase or decrease, depending on the inlet particle slip. As mentioned earlier, the forces of the

particles on the air govern the critical length in the region where  $V_p > V_g$  for low inlet particle slip; whereas, for high inlet particle slip, the forces govern the critical length in the region where  $V_p < V_g$ . For the low  $S_{pi}$ , the reduced  $C_d$  results in a lower  $\Delta P_p$  according to Equation (24) and effectively increases wall friction thereby decreasing the critical length. For the high  $S_{pi}$ , the reduced  $C_d$  also results in a lower  $\Delta P_p$ , but effectively decreases wall friction which tends to increase the critical length.

The above discussion of the effect of individually varying each of the governing variables and starting conditions on the critical length may now be applied to the dimensionless parameters and starting conditions given on page 46. It was assumed earlier that the inlet pressure  $P_{gi}$  and temperature  $T_{gi}$  of the air were equal to the reference values  $P_{gl}$  and  $T_{gl}$ , respectively, i.e.,  $P_{gi}^0 = T_{gi}^0 = 1$ . Also, the properties of the air and particles were assumed constant and equal to the reference values, i.e.,  $c_g^0 = c_p^0 = \mu_g^0 = K_g^0 = 1$ . Thus, except for the reference velocity  $V_{gl}$  where  $V_{gl} \neq V_{gi}$ , the reference conditions may be considered the same as the inlet conditions to the tube at  $x^0 = 0$ .

To get a clearer understanding of the effect of the dimensionless parameters and starting conditions on the critical length, the independent dimensionless quantities were required and were obtained by a slight rearranging of the starting conditions. They were formulated from



dimensional analysis and are listed in Table II. From consideration of the discussion given on the property variation data set and particle mass variation data set, the various independent quantities must be altered as shown for the critical length to increase. For example, from Table I (page 61) it can be seen that the particle to air specific heat ratio  $A$  must decrease in order for the subsonic critical length to increase. Some discrepancies may be noted when trying to predict the results of Table II from Table I because the former results involved the individual independent parameters while the latter results concern the individual governing variables and starting conditions of the system.

It is difficult to prescribe a drag, heat transfer, and wall friction parameter since they were considered as variable quantities and functions of  $Re_{pl}$ , in addition to parameters  $D$  and  $Pr_{gl}$ . For example,

$$C_d = g(Re_{pl})$$

$$Nu_p = h(Re_{pl}, Pr_{gl})$$

$$f = i(D, Re_{pl})$$

where  $g$ ,  $h$ , and  $i$  denote functions including only the parameters of the system. Therefore, it can be seen that changing  $Re_{pl}$  affects all of the above quantities.

TABLE II  
EFFECT OF THE PARAMETERS OF THE SYSTEM ON  
THE CRITICAL LENGTH

Parameter Definition		To Increase the Critical Length in	
		Subsonic Flow	Supersonic Flow
Particle to Air Specific Heat Ratio	$A = \frac{c_{pl}}{c_{gl}}$	Decrease A	Increase A
Acceleration of Gravity	$B = \frac{2gd_t}{V_{gl}^2}$	Decrease B	Decrease B
Air to Particle Density Ratio	$C = \frac{\rho_{gl}}{\rho_p}$	Decrease C	Increase C
Tube to Particle Diameter Ratio	$D = \frac{d_t}{d_p}$	Decrease D	Increase D
Reference Reynolds Number of Particles	$Re_{pl} = \frac{d_p V_{gl} \rho_{gl}}{\mu_{gl} g_c}$	Increase $Re_{pl}$	Decrease $Re_{pl}$
Reference Prandtl Number of Particles	$Pr_{gl} = \frac{c_{gl} \mu_{gl}}{K_{gl}}$	Increase $Pr_{gl}$	Decrease $Pr_{gl}$
Inlet Particle to Air Velocity Ratio	$\frac{V_{pi}^o}{V_{gi}^o} = \frac{V_{pi}}{V_{gi}}$	Increase $\frac{V_{pi}^o}{V_{gi}^o}$	Increase $\frac{V_{pi}^o}{V_{gi}^o}$
Inlet Particle to Air Temperature Ratio	$\frac{T_{pi}^o}{T_{gi}^o} = \frac{T_{pi}}{T_{gi}}$	Decrease $\frac{T_{pi}^o}{T_{gi}^o}$	Decrease $\frac{T_{pi}^o}{T_{gi}^o}$
Inlet Mach Number of the Air	$M_{gi} = \frac{V_{gi}^o}{(T_{gi}^o \gamma / Z)^{.5}}$	Decrease $M_{gi}$	Increase $M_{gi}$
Specific Heat Ratio of the Air	$Z = \frac{2\gamma}{(\gamma - 1)}$	Decrease Z	Increase Z
Particle to Air Mass Flow Ratio	$X = \frac{m_p}{m_g}$	Decrease X	Increase X

## CHAPTER V

### EXPERIMENTAL ANALYSIS

To get an insight into the validity of the analytical analysis presented in the last two chapters, an experimental air-particle system was constructed and operated in the Mechanical Engineering Laboratory of the Oklahoma State University. Since the complete study of the effect of the particles on the critical length requires an expensive and complex instrumentation system, the experimental analysis was limited to subsonic air-particle flow in a vertical constant area circular tube of fixed length and to the measurement and subsequent calculation of the pressure of the air  $P_g$ , velocity  $V_g$ , static temperature  $T_g$ , Mach number  $M_g$ , and the air and particle mass flow rates  $m_g$  and  $m_p$ . The air-particle flow in the tube corresponded to critical conditions where the length of the tube  $x_t^0$  equalled the critical length  $x_{max}^0$ .

#### Derivation of Semi-Empirical Equations

Some of the above properties of the air were calculated from semi-empirical equations since direct measurement was difficult because of the presence of the particles. These equations, and others, follow.

### Mass Flow Rate of the Air

The Schematic diagram of the nozzle apparatus employed is shown below in Figure 6. For incompressible flow of air

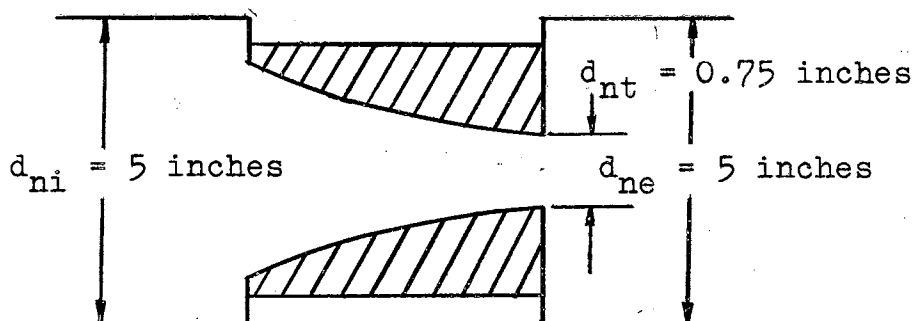


Figure 6. ASME Nozzle

through a nozzle with an inlet to throat diameter  $\frac{d_{ni}}{d_{nt}}$  greater than four, the change in internal energy and density of the air is small and the inlet velocity of the air is negligible. From the energy equation applied between the nozzle inlet (ni) and throat (nt) there results for the velocity of the air at the throat

$$V_{gnt} = \sqrt{\frac{2g_c(P_{gni} - P_{gnt})}{\rho_{gni}}}$$

The one-dimensional mass rate of flow of the air through the nozzle may be expressed by

$$m_g = A_{nt} V_{gnt} \rho_{gnt} \approx \frac{A_{nt} V_{gnt} P_{gni} C_{F_d}}{R_g T_{gni}}$$

where the coefficient of discharge accounts for the non-ideal frictional effects of the air flow. Combining the above equations and substituting in known values for the nozzle and the air, there results

$$m_g = 6.87 C_{F_d} d_{nt}^2 \sqrt{\frac{P_{gni} \Delta P_n}{T_{gni}}} \quad \text{where} \quad (25)$$

$m_g$  = Mass flow rate of air, lb.<sub>m</sub>/min.

$C_{F_d}$  = Coefficient of discharge, dimensionless.

$d_{nt}$  = Diameter of nozzle throat, in.

$P_{gni}$  = Inlet air pressure to nozzle, in. hg.

$T_{gni}$  = Inlet air temperature to nozzle, °R.

$\Delta P_n = P_{gni} - P_{gnt}$  = Air pressure drop across nozzle, in. h<sub>2</sub>O.

Equation (25) is given in the ASME Nozzle Codes (80) for the same nozzle apparatus where values of  $C_{F_d}$  were also obtained.

#### Mass Flow Rate of the Particles

A given mass of particles  $\Delta m_p$  was successively collected and the corresponding time of collection  $\Delta t$  measured. For steady particle flow, the particle mass versus time was

a straight line whose slope equalled the mass flow rate of the particles as given by

$$m_p = \frac{\Delta m_p}{\Delta t} \quad (26)$$

### Mixture Density

Although measurements for the mixture density  $\rho_m$  were not included the equations are important. From the elemental control volume shown in Figure 1 (page 33),  $m_p = A_p V_p \rho_p$ , and  $m_g = A_g V_g \rho_g$  the mixture density  $\rho_m$  may be defined as

$$\rho_m = \frac{\text{Total mass in volume } A_t dx}{\text{Total volume } A_t dx}$$

and may be shown to be

$$\rho_m = \frac{\frac{m_g dt dx}{dx}}{A_t dx} + \frac{\frac{m_p dt' dx}{dx}}{A_t dx} = \frac{\frac{m_g}{V_g} + \frac{m_p}{V_p}}{A_t} \quad \text{where}$$

$dt$  = Incremental time interval for the air.

$dt'$  = Incremental time interval for the particles.

Since  $A_t = A_g + A_p$ , the above equation becomes

$$\rho_m = \rho_g + \frac{A_p}{A_t} (\rho_p - \rho_g) \quad \text{or} \quad (27)$$

$$\rho_m = \rho_p + \frac{A_g}{A_t} (\rho_g - \rho_p). \quad (28)$$

To show the effect of particle slip, the equation involving

$V_g$  and  $V_p$  may be rearranged to give

$$\rho_m = \frac{m_g}{V_g} \frac{(1 + \frac{XV_g}{V_p})}{(A_g + A_p)} = \frac{m_g}{V_g} \frac{(1 + \frac{XV_g}{V_p})}{(\frac{m_g}{V_g \rho_g} + \frac{m_p}{V_p \rho_p})} \quad \text{or}$$

$$\rho_m = \frac{(1 + \frac{XV_g}{V_p})}{(\frac{XV_g}{\rho_p V_p} + \frac{1}{\rho_g})}. \quad (29)$$

Equations (27), (28), and (29) or in similar form have been used by several investigators (11, 39, 43, 48).

#### Velocity and Temperature of Air and Particles

From the one-dimensional steady flow continuity equation for the air acting as an ideal gas

$$m_g = \left(1 - \frac{A_p}{A_t}\right) \frac{V_g P_g A_t}{R_g T_g} \quad \text{from which}$$

$$T_g = \left(1 - \frac{A_p}{A_t}\right) \frac{V_g P_g A_t}{m_g R_g}.$$

Since  $\frac{A_g}{A_t} = \frac{\rho_m - \rho_p}{\rho_g - \rho_p}$  from Equation (28), the equation for  $m_g$

becomes

$$m_g = \left(\frac{\rho_m - \rho_p}{\rho_g - \rho_p}\right) \frac{V_g P_g A_t}{R_g T_g} \quad \text{from which}$$

$$V_g = \frac{m_g}{A_t \rho_m} \frac{\left( \frac{\rho_p R T_{og}}{P_g} - 1 \right)}{\left( \frac{\rho_p}{\rho_m} - 1 \right)}$$

From the energy equation for the stagnation temperature of the air

$$T_{og} = T_g + \frac{V_g^2}{2g_c c_g} \quad \text{from which}$$

$$T_g = T_{og} - \frac{V_g^2}{2g_c c_g}$$

Two equations for  $V_g$  may result. First, substituting the first equation for  $T_g$  into the equation for  $T_{og}$  yields a quadratic equation in  $V_g$  from which

$$V_g = -\left(1 - \frac{A_p}{A_t}\right) \frac{g_c c_g P_g A_t}{R_g m_g} + \sqrt{\left[\left(1 - \frac{A_p}{A_t}\right) \frac{g_c c_g P_g A_t}{R_g m_g}\right]^2 + 2g_c c_g T_{og}}$$

Knowing  $P_g$ ,  $A_p$ ,  $T_{og}$ ,  $m_g$ , and the remaining properties of the air and system from laboratory measurements, the average velocity of the air  $V_g$  can be found. If the mixture density is measured instead of the effective cross-sectional area of the particles  $A_p$ , then substituting the second equation for  $T_g$  into the equation for  $V_g$  gives a quadratic equation in  $V_g$  from which

$$V_g = -\left(1 - \frac{\rho_m}{\rho_p}\right) \frac{g_c c_g P_g A_t}{R_g m_g} + \sqrt{\left[\left(1 - \frac{\rho_m}{\rho_p}\right) \frac{g_c c_g P_g A_t}{R_g m_g}\right]^2 + 2g_c c_g T_{og} \left(1 - \frac{\rho_{og}}{\rho_p}\right)}$$



where

$$\rho_{og} = \frac{P_g}{R_g T_{og}}$$

The static temperature of the air can then be found from

$$T_g = T_{og} - \frac{V_g^2}{2g_c c_g}$$

From direct measurement of  $A_p$ , the average velocity of the particles can be found from

$$V_p = \frac{\dot{m}_p}{A_p \rho_p}$$

Of course,  $A_p$  could be calculated from Equation (27) where  $\rho_m$  is obtained from direct measurements or  $V_p$  could be measured directly. The static temperature of the particles  $T_p$  would be best determined by experiment although it could be found from the energy equation knowing  $V_g$ ,  $V_p$ ,  $T_g$ , and  $x$  at a given location and all of the properties of the air and particles at some reference location. The direct measurement of  $V_g$ ,  $V_p$ ,  $T_g$ ,  $T_{og}$ , and  $T_p$  by the insertion of a measuring device directly in the air-particle stream at high velocities of the air and particles is difficult because the bombardment of the particles would tend to destroy the device.

In the above equations the properties of the air may be found without measuring  $A_p$ ,  $\rho_m$ , or  $V_p$  if the particle to

air mass flow ratio  $X$  is kept small. For a small  $X$ ,  $\frac{A_p}{A_t} \rightarrow 0$  and  $\rho_m \rightarrow \rho_g$ . The first equation given above for the average velocity of the air reduces to

$$V_g = - \frac{g_c c_g P A_t}{R_g m_g} + \sqrt{\left( \frac{g_c c_g P A_t}{R_g m_g} \right)^2 + 2g_c c_g T_{og}} \quad (30)$$

This equation was used to find  $V_g$  since the properties of the particles were not measured. Then the static temperature of the air is given by

$$T_g = T_{og} - \frac{V_g^2}{2g_c c_g} \quad (31)$$

Since the flow between the inlet of the ASME nozzle and the exit of the vertical tube was essentially adiabatic and the change in stagnation temperature of the air is insignificant for values of  $X$ , it was assumed that the local stagnation temperature of the air  $T_{og}$  was constant and equalled the static temperature of the air at the inlet of the nozzle  $T_{gni}$ .

#### Mach Number of the Air

For air acting as an ideal gas, the Mach number is given by

$$M_g = \frac{V_g}{c_{gs}} = \frac{V_g}{49.08\sqrt{T_g}} \quad (32)$$

where  $V_g$  is in ft./sec. and  $T_g$  in  $^{\circ}\text{R}$ .

Equations (25), (26), (30), (31), and (32) are based on measured values of  $P_g$ ,  $P_{gni}$ ,  $T_{gni}$ ,  $\Delta P_n$ ,  $\Delta m_p$ , and  $\Delta t$  and the knowledge of  $CF_d$ ,  $d_{nt}$ ,  $A_t$ ,  $c_g$ ,  $R_g$ , and  $g_c$ . The dimensionless quantities  $V_g^{\circ}$ ,  $T_g^{\circ}$ , and  $P_g^{\circ}$  are defined the same way as in the analytical analysis.

### The Experimental System

The experimental apparatus consisted of a vertical plastic tube with an average inside diameter  $d_t = 0.495$  in. and a length of  $x_t = 21.5$  ft. through which air and solid spherical glass particles flowed. The air, supplied by a double-acting single-stage reciprocating compressor, was filtered to remove any water or oil droplets and passed thru an ASME nozzle apparatus before entering the tube at the bottom. An air flow control valve and pressure regulator were installed between the nozzle apparatus and the compressor. The spherical glass particles, purchased from the Minnesota Mining and Manufacturing Company, had an average diameter of  $0.0185$  inch  $\pm 6$  per cent and were stored in a pressure tight particle reservoir from which they were injected into the tube at the bottom. The particle injection into the air stream was accomplished by ordinary gravity feed and by maintaining the reservoir pressure higher than the air pressure at the point of injection. The particles entered the tube through a five-sixteenth inch hole in the tube and were dispersed by a fine, high speed

jet of air supplied by a copper tube installed at the tube opening, flush with the inside of the tube, and at a 45 degree angle to the axis of the tube. To insure that a developed velocity distribution of the air and particles existed over the cross-section of the tube at the first measuring station, the particles were injected approximately fifty tube diameters upstream of the first measuring station (considered as the inlet of the tube).

From the tube inlet to the tube exit, there were 10 pressure measuring stations, each one spaced two feet apart so that the tenth one was at the exit of the tube. The tube was encased in a six inch diameter steel tube and held concentric by plexiglass discs spaced at one foot intervals along the tube so as to reduce heat transfer effects and electrical noises and to maintain a straight vertical tube. The 10 measuring stations were left exposed. Since the length of the tube  $x_t^0$  was constant and critical conditions were maintained, the critical length of the tube equalled the tube length, i.e.,

$$x_t^0 = x_{\max}^0 = \frac{18(12)}{0.495} = 436.5 \text{ diameters.}$$

After the air and particles passed from the inlet to exit of the tube, a return line was used to divert the flow and return the air and particles to a lower level near the bottom of the tube whereupon the air was separated from the particles and re-entered the atmosphere and the particles

were collected in a container which rested on a beam scale. Thus, neither the air nor the particles were continuously recirculated.

The instrumentation consisted of a Heise gage to measure the pressure of the air  $P_g$  at the 10 measuring stations. A surge tank and pressure switching circuit were necessary to accomplish the individual measurements. A separate Bourdon tube pressure gage was employed to measure the static pressure of the air at the inlet to the nozzle  $P_{gni}$ . Both gages were calibrated to insure their accuracy. A copper-constantan thermocouple was installed at the inlet of the nozzle to measure the static temperature of the air at the inlet to the nozzle  $T_{gni}$  and a milli-voltmeter was selected to measure the voltage output of the thermocouple. The pressure tap and thermocouple location, and the length and diameter of tube approaching the nozzle inlet and departing the nozzle exit, were in accordance with ASME nozzle specifications. The thermocouple reference junction was maintained at  $32^{\circ}\text{F}$  by a container filled with ice. The air pressure drop across the ASME nozzle  $\Delta P_n$  was measured by a vertical water manometer. Other thermocouples were installed at each measuring station in stainless steel hypodermic needles which extended three-sixteenth inch into the tube. They were used to measure any variation in the stagnation temperature of the air.

Also installed at each of the measuring stations were piezoelectric crystals and stainless steel electrical

capacitors that were to be used for measuring the speed of sound of the mixture and the mixture density  $\rho_m$ , respectively. No speed of sound measurements were taken. The measurements for  $\rho_m$  were unreliable because of electrical noises and instabilities that were observed in the measurement system.

In each of the experimental test runs, the air flow rate was maintained at a sufficient value so that critical conditions existed at the exit of the tube. To insure this the exit pressure of the air  $P_{ge}$  was always kept two or three psig above atmospheric pressure  $P_a$  ( $P_{ge} \geq P_a$  for critical conditions). After steady flow and equilibrium prevailed in the tube, the test procedure was to record the local pressure of the air  $P_g$ , the pressure and temperature of the air at the nozzle inlet  $P_{gni}$  and  $T_{gni}$ , respectively, and the average air pressure drop across the nozzle  $\Delta P_n$ . Regulation of  $P_{gni}$  was accomplished by the air control valve. The fluctuations in  $\Delta P_n$  were approximately  $\pm 0.05$  in  $h_2O$ . During the test run, a known weight of particles (2.5 lb.<sub>m</sub>) was successively collected and the time of collection measured by an electrical timer. The change in the stagnation temperature of the air from the inlet to the exit of the tube was observed. The maximum change was about  $6^\circ F$  which was probably attributed to the differences in shape of the junctions of the individual thermocouples and in the recovery factors of the individual thermocouples. The particle to air mass flow ratio was varied from  $X = 0$ ,

which corresponded to single-phase gaseous flow, to the maximum obtainable for the system. Several test runs were made for both the single-phase flow and two-phase flow.

Photographs of the experimental apparatus are shown in Figures 7, 8, and 9. Figure 7 shows the basic instrumentation board, which includes the Heise gage, thermocouple switching circuit, pressure switching circuit, and Bourdon tube gage, and the milli-voltmeter, particle collection container, scale and timer, air-particle return line, and the encased vertical constant area tube. Figure 8 includes the air filter, pressure regulator and flow control valve, nozzle apparatus with before and after air straightener sections, and the vertical water manometer. Figure 9 gives the over-all view of the apparatus and the relative position of the components of the system. Not shown is the compressor which was housed outside of the laboratory.

A portion of the experimental data taken and a list of the experiment equipment used is given in Appendix B. The properties of the air and particles corresponding to the experimental data are given in Appendix A.

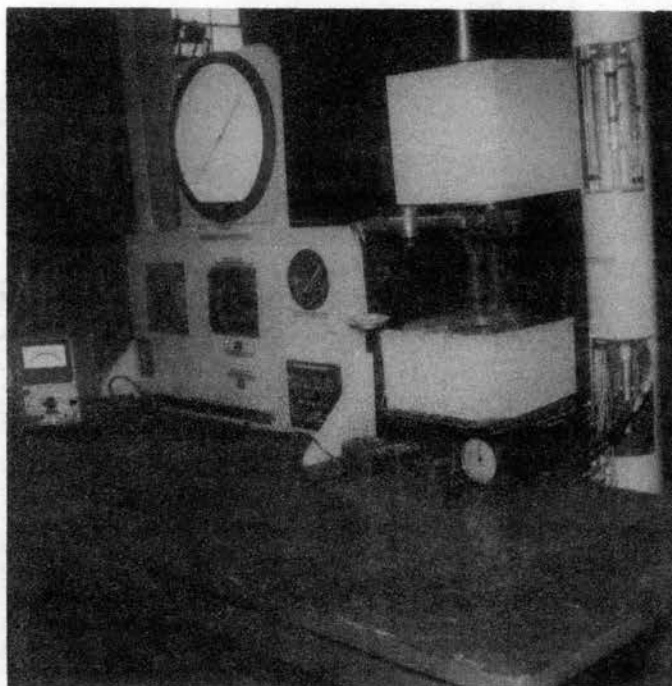


Figure 7. Instrumentation and Test Section

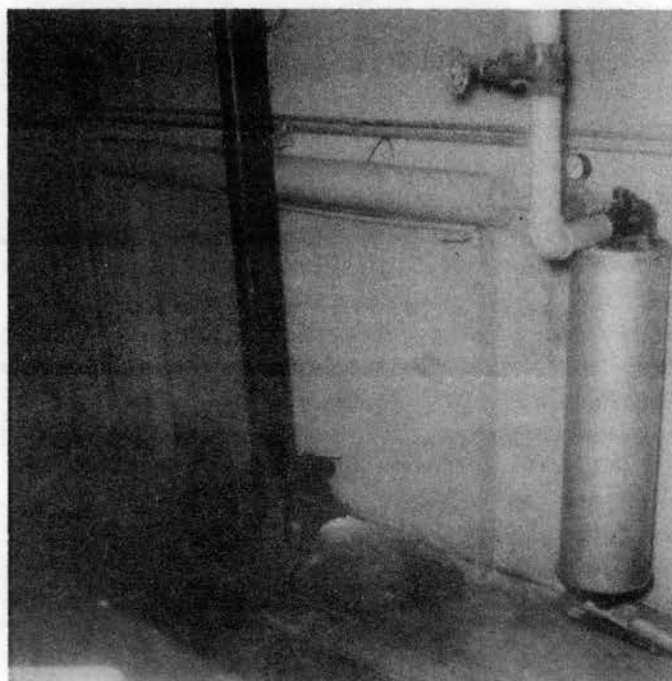


Figure 8. Air Flow Nozzle Apparatus and Air Filter



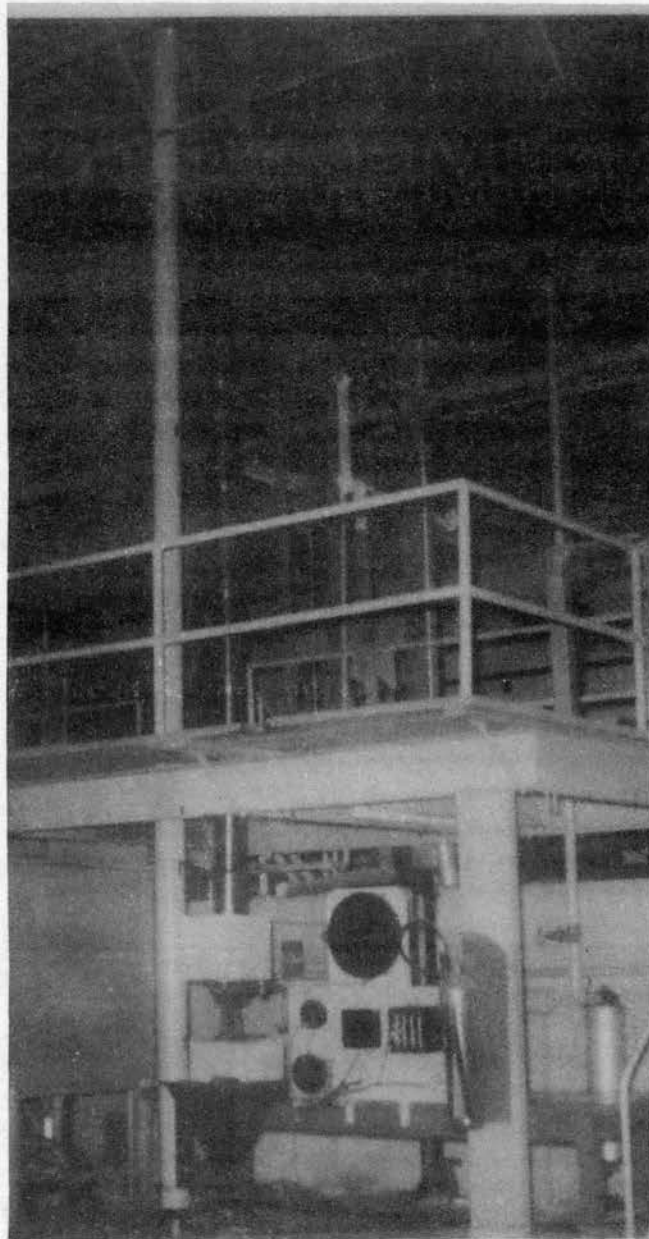


Figure 9. Overall View of Experimental Apparatus

## CHAPTER VI

### EXPERIMENTAL RESULTS

From the observed experimental data for air-particle flow in a vertical constant area tube and the semi-empirical equations presented in the last chapter, the average velocity of the air  $V_g$ , static temperature of the air  $T_g$ , and the Mach number of the air  $M_g$  were calculated at each of the 10 measuring stations along the tube for the single-phase and two-phase air-particle test runs. Also evaluated were the mass flow rates of the air and the particles  $m_g$  and  $m_p$ , respectively. Only the results for one single-phase test run and two air-particle test runs are included. The corresponding values for the particle to air mass flow ratios are  $X = 0, 0.114, \text{ and } 0.1531$ , respectively, where the latter value was the maximum allowed by the system. No data on choking or sub-critical conditions was taken.

#### Presentation of Results

The results corresponding to the above test runs are given in graphical form in Figures 10, 12, and 13. The abscissa for each curve is the dimensionless tube position  $x^0$  where it was shown earlier that the length of the tube  $x_t^0$  equalled the critical length  $x_{\max}^0$  for critical conditions

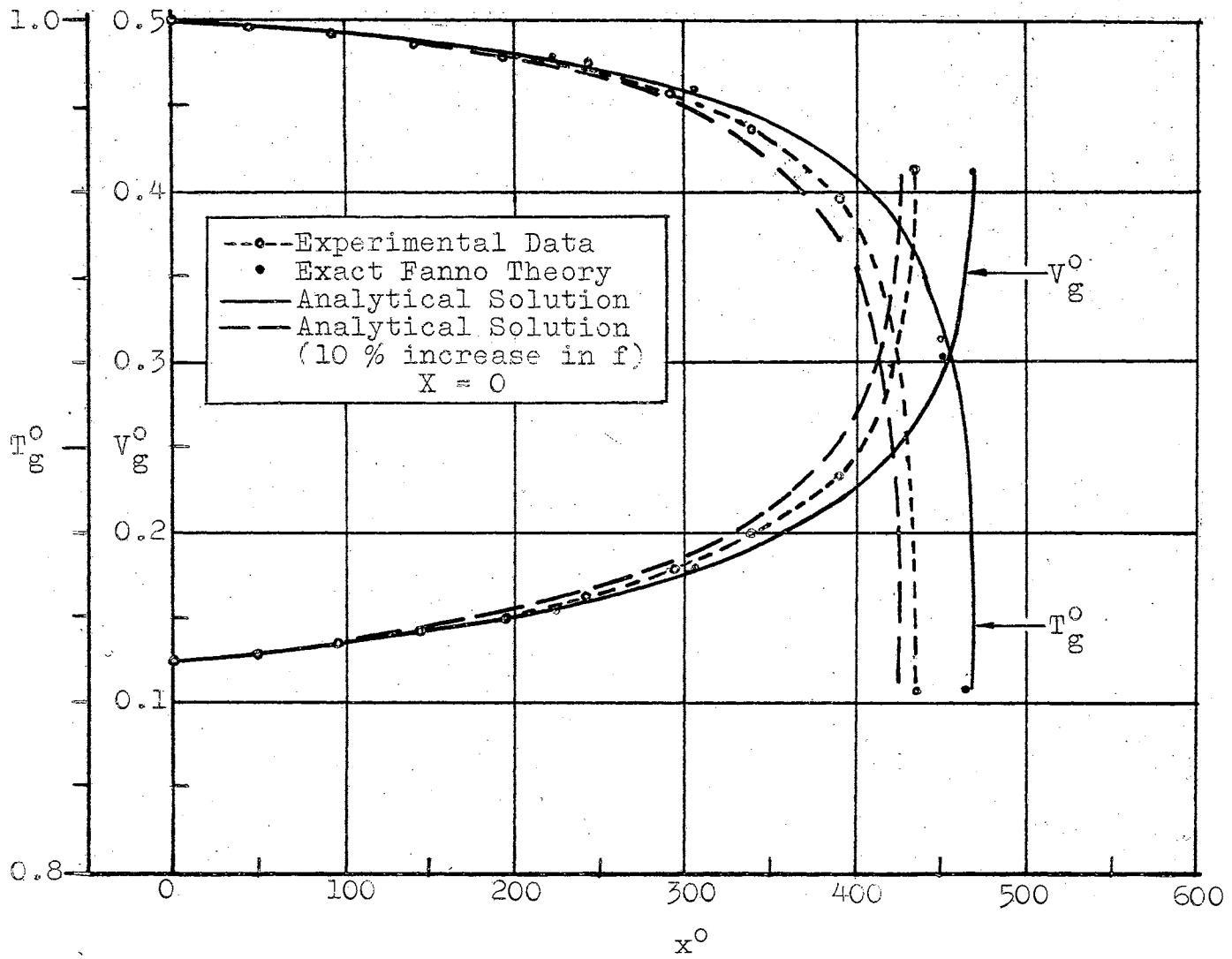


Figure 10. Local Velocity, Temperature, Pressure, and Mach Number Characteristics of Subsonic Air Flow

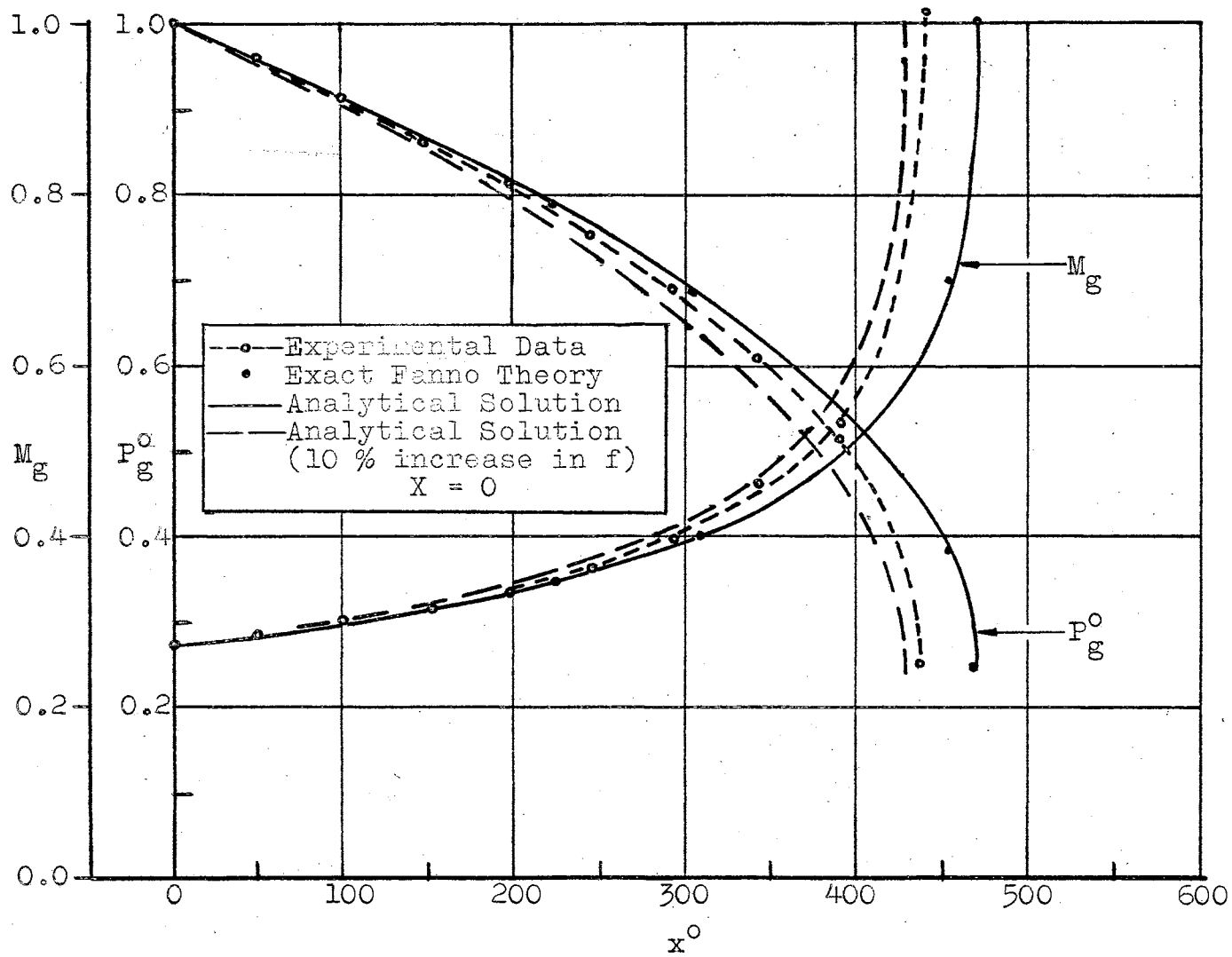


Figure 10. Continued

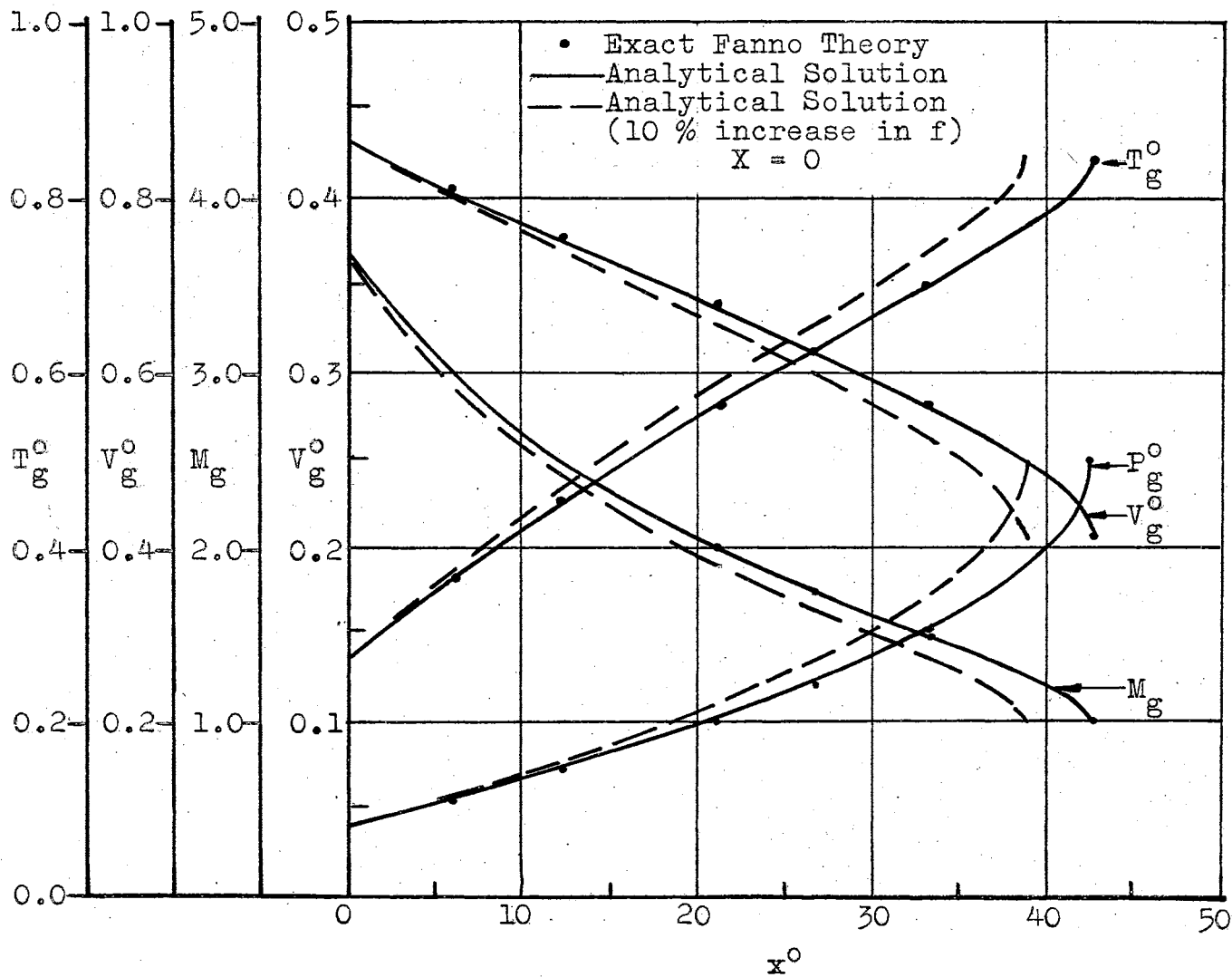


Figure 11. Local Velocity, Temperature, Pressure, and Mach Number Characteristics of Supersonic Air Flow

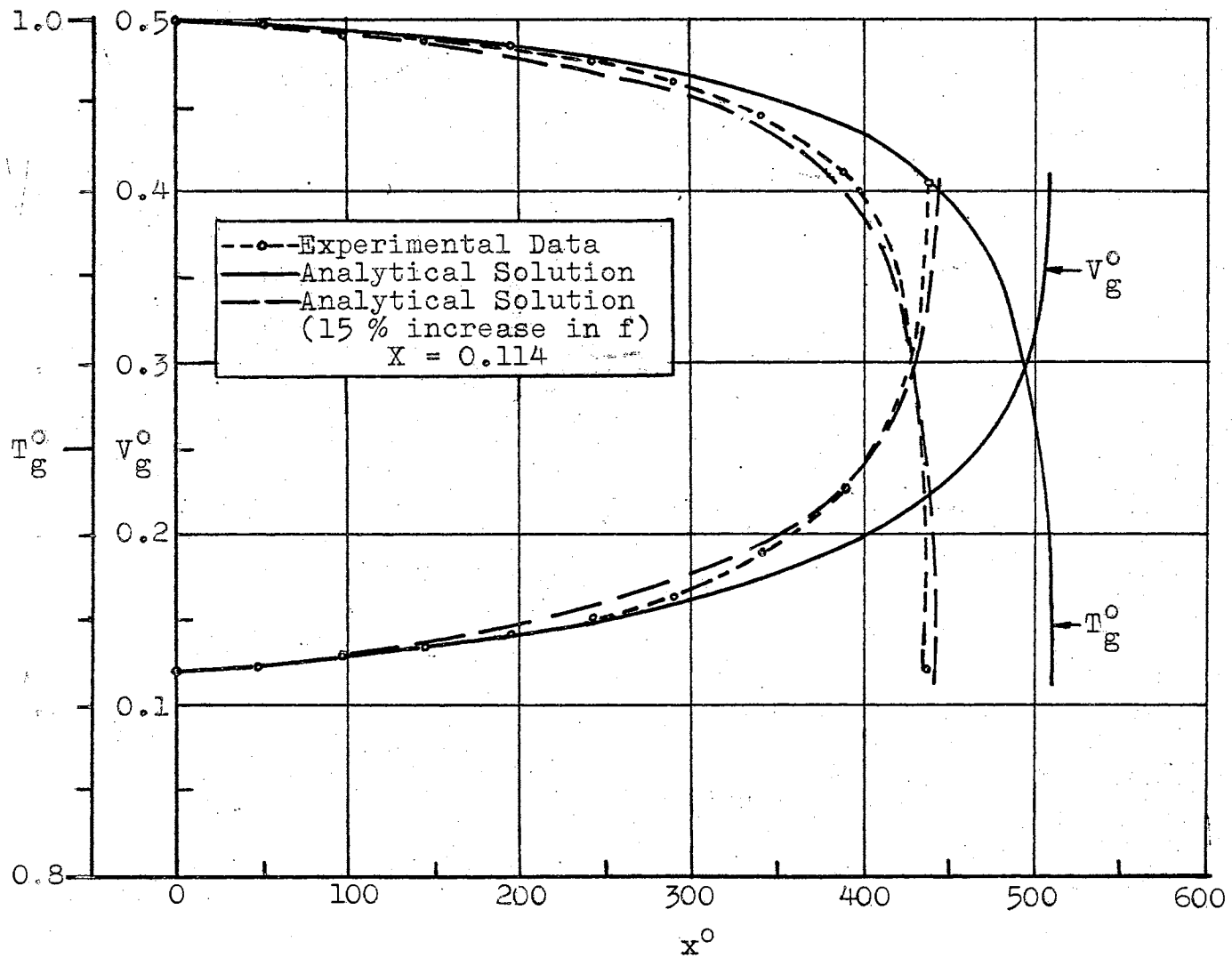


Figure 12. Local Velocity, Temperature, Pressure, and Mach Number Characteristics of Subsonic Air-Particle Flow

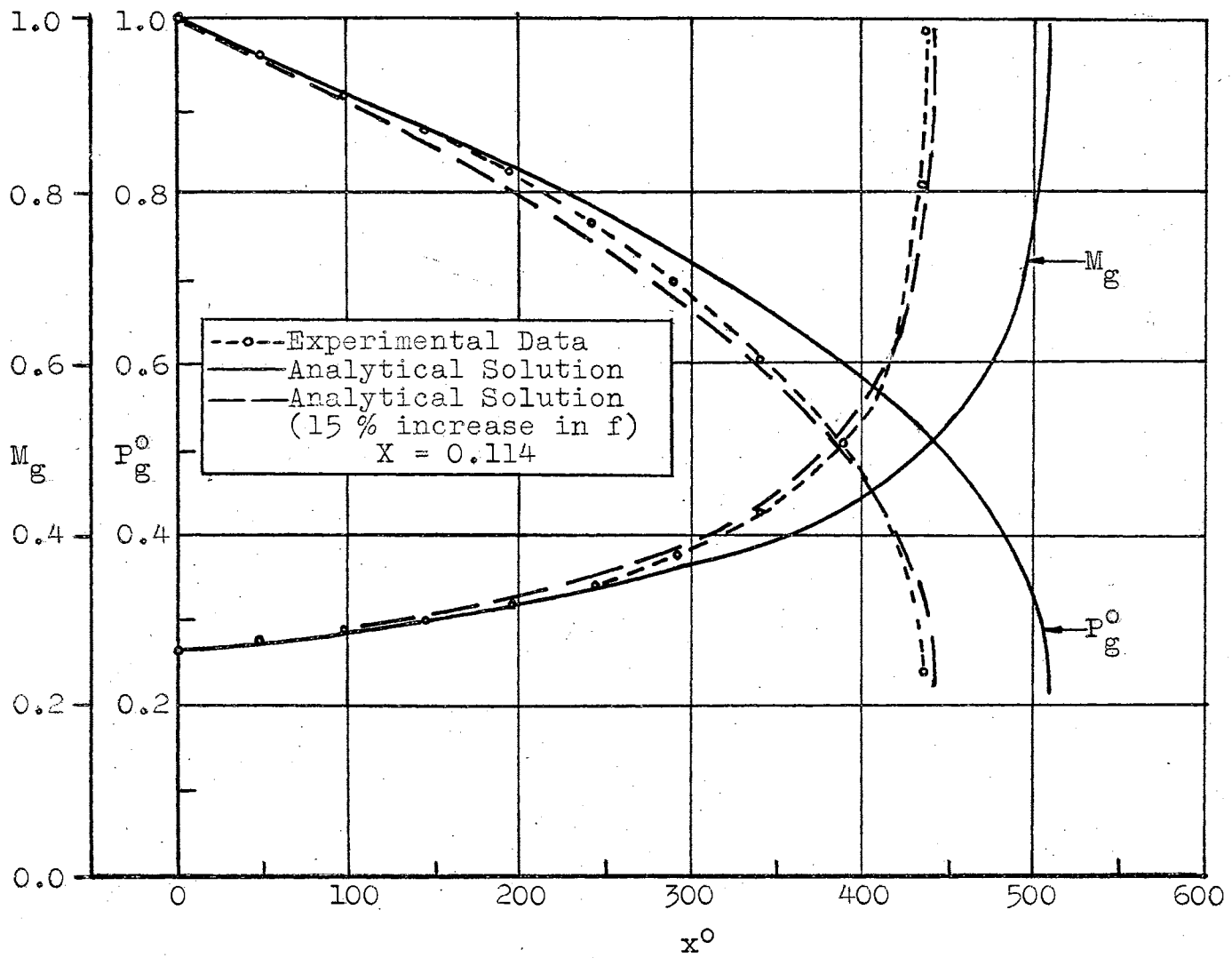


Figure 12. Continued

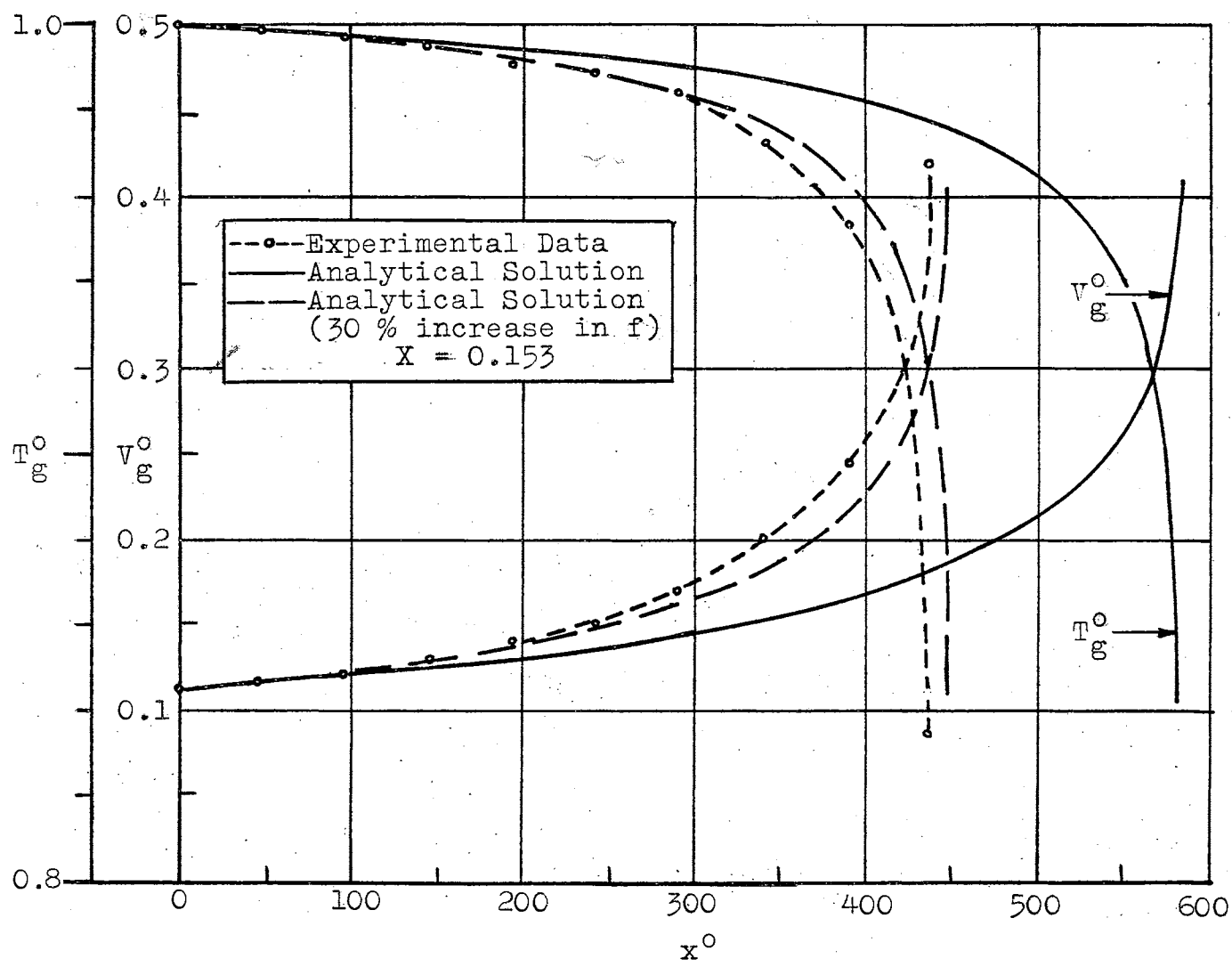


Figure 13. Local Velocity, Temperature, Pressure, and Mach Number Characteristics of Subsonic Air-Particle Flow



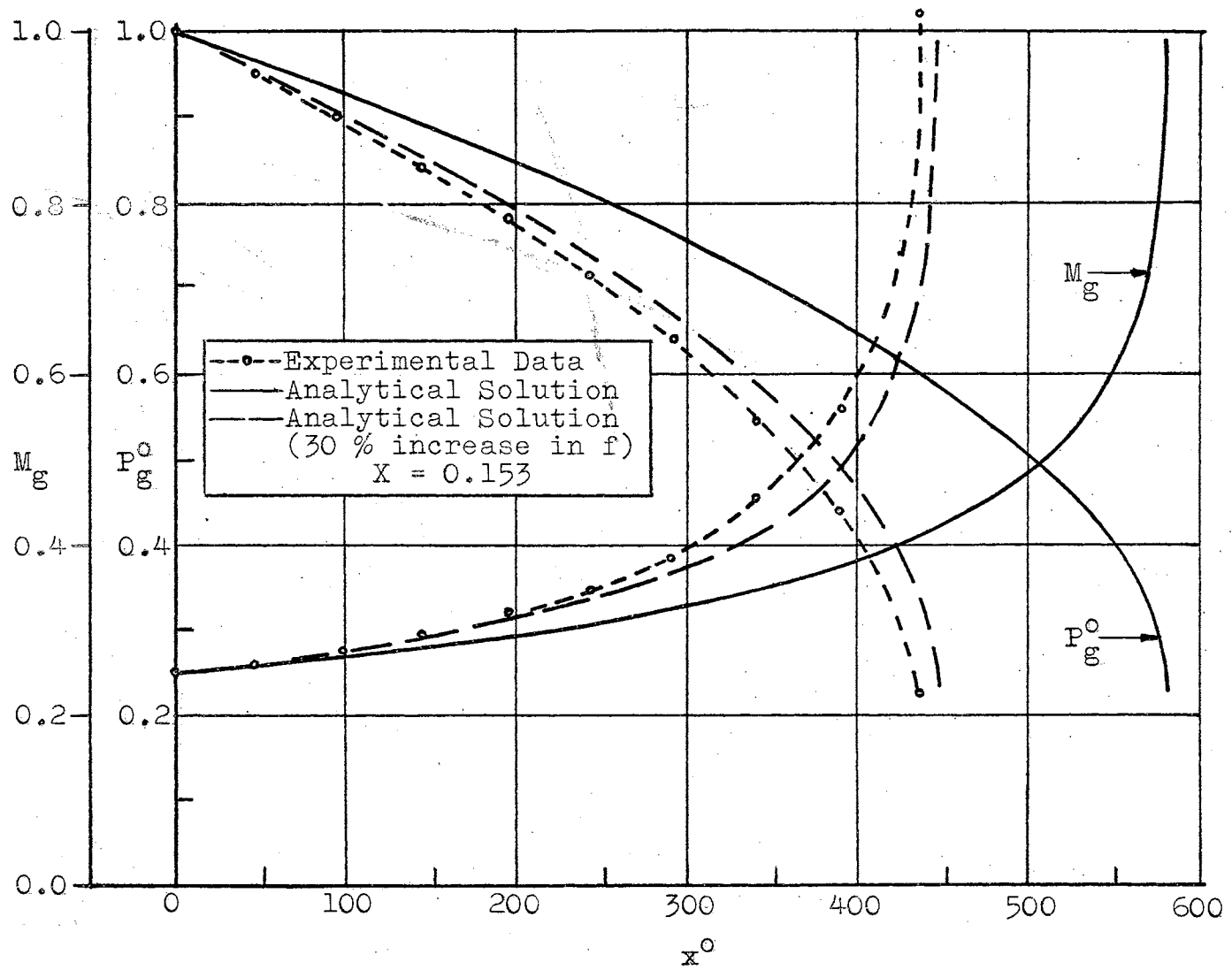


Figure 13. Continued

and  $x_{\max}^0 = x_t^0 = 436.5$  diameters. The ordinates are the dimensionless velocity of the air  $V_g^0$ , pressure of the air  $P_g^0$ , static temperature of the air  $T_g^0$ , and Mach number of the air  $M_g$ . The particle velocity and temperature are not shown since no measurements for them were taken. Also shown on the figures are the corresponding analytical solutions. Although no data was taken for supersonic flow, the analytical solution and exact Fanno solution are shown for supersonic flow in Figure 11 (page 104). The exact subsonic Fanno solution is also given in Figure 10 (pages 102 and 103).

#### Discussion and Comparison to Analytical Solutions

It is noticed from Figures 10 and 11 that the exact Fanno solutions for subsonic and supersonic flow agree very well with the corresponding analytical solutions. The particle to air mass flow ratio  $X$  was set equal to 0.0001 and 0.001 instead of 0.0 so as to include the two-phase terms in the differential equations. The effects were negligible so that the analytical solutions correspond essentially to those for single-phase gaseous flow. The exact Fanno solutions given are for horizontal flow, but are essentially the same as for vertical flow since the potential energy changes of a gas are small even for relatively large elevation changes.

In comparing the single-phase analytical and

experimental results shown in Figure 10, the local agreement is very good up to a Mach number  $M_g = 0.4$  where  $x^0 = 300$ , approximately. The exit properties of the air agree closely, but the critical lengths do not ( $466 \neq 436.5$ ). Several factors could account for the disagreement in critical lengths.

First of all, for given inlet conditions and a constant wall friction factor  $f$ , the critical exit properties of the air are fixed and the governing agent in determining the critical length is  $f$ . As mentioned earlier, the standard wall friction factor curve for incompressible flow and smooth tubes was utilized in the analytical solutions. Since one-dimensional steady flow of a gas with constant properties through a constant cross-sectional area was assumed, the standard curve yielded constant values of  $f$  in all analytical solutions.

However, the use of the standard curve for  $f$  was somewhat unreliable. The thermocouples, piezoelectric crystals, and pressure taps located at each of the ten measuring stations effectively increased the roughness of the wall to some degree and, consequently, increased  $f$ . The surface of the tube, although apparently smooth, could have had the friction characteristics of a rougher tube. This would tend to increase  $f$  also. From the slope of the air pressure curve, the inlet friction factor was calculated from

$$f = \frac{dP_g}{dx} \frac{2g_c d_t}{\rho_g V^2 g} \quad (\text{Reference 79})$$

and gave a value of  $f = 0.0169$  compared to  $f = 0.01418$  obtained from the standard curve. This method of calculating the local value of  $f$  was not reliable because not enough pressure taps were installed along the tube and because the above equation is valid only for non-accelerating flow.

Chen (21) considered the effect of compressibility on the wall friction factor in circular tubes and showed that  $f$  was a function of both the Mach number of the air and the Reynolds number of the tube. For incompressible flow, or low Mach numbers,  $f$  was shown to be a function of only the Reynolds number of the tube which has been verified by others. His results are shown qualitatively below in Figure 14. It is seen that  $f$  is generally higher than the

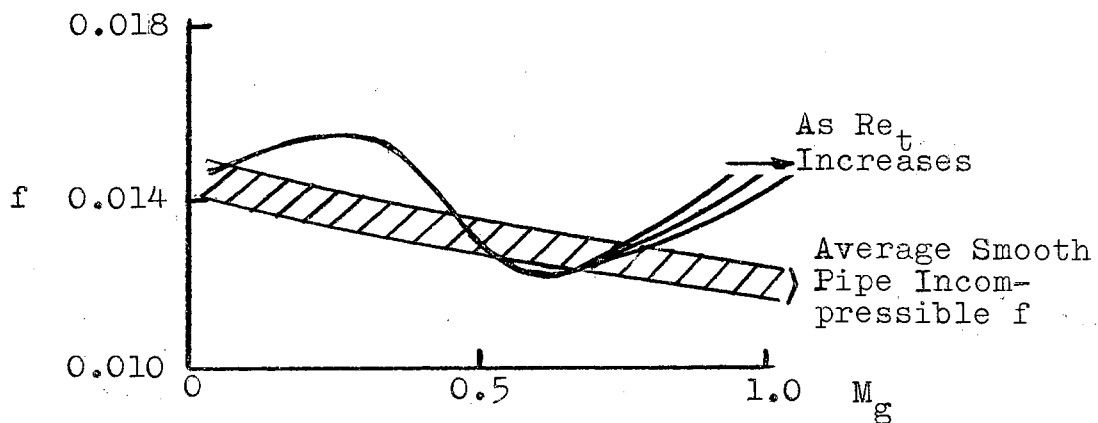


Figure 14. Dependency of the Wall Friction Factor on the Mach Number of the Air

incompressible curve, depending on the Mach number of the air  $M_g$ . It is lower in the range from  $M_g = 0.5$  to  $M_g = 0.75$ ,

approximately. No quantitative correlation of data to find  $f = g(\text{Re}_t, M_g)$  was attempted since his results were not conclusive.

Since the above factors tend to increase  $f$ , analytical solutions for a ten per cent increase in  $f$  are shown in Figure 10 (pages 102 and 103). The critical lengths agree more closely but the local agreements in the properties of the air are not as good under  $M_g = 0.4$ . Thus, it appears that  $f$  is not constant.

Another factor for consideration is the low inlet Mach number of the air that was employed ( $M_g = 0.276$ ). For low Mach numbers, a small change in  $M_g$  would cause a large change in the critical length  $x_{\text{max}}^0$ . For example, if the inlet Mach number of the air were  $M_{gi} = 0.281$  instead of the calculated value of  $M_{gi} = 0.276$ , the critical length would be reduced from 466 to 447, approximately.

The viscosity of the air  $\mu_g$  decreased but it was assumed constant in the analytical solutions. From Equations (19) and (22), it is seen that the wall friction factor would decrease. This, however, would cause the critical length corresponding to the analytical solution to be greater than 466 if variable viscosity were considered.

A final factor that can account for the difference in critical lengths is the effect of the boundary layer of the air in the tube. One-dimensional flow is closely approximated in the center of the tube, but near the walls the flow is two-dimensional. This has the same effect as

reducing the diameter of the tube  $d_t$ . If the laboratory critical length were based on this reduced diameter, the effective critical length would be higher than  $x_{\max}^0 = 436.5$ . The analytical solutions for the reduced diameter of the tube would yield a critical length lower than  $x_{\max}^0 = 466$  since the wall friction factor  $f$  would be higher.

The two-phase experimental results and the corresponding analytical solution are shown in Figures 12 and 13 (pages 105-108) for particle to air mass flow ratios of  $X = 0.114$  and  $X = 0.153$ , respectively. For both values of  $X$  the local agreement in the properties of the air are good only at low Mach numbers  $M_g$  beyond which the agreement is unsatisfactory. The critical exit properties of the air agree closely but the critical lengths do not. Comparing the disagreement in critical lengths from Figures 10, 12, and 13, it becomes worse as the particle to air mass flow ratio  $X$  is increased. Thus, it appears that the two-phase wall friction factor is higher than for single-phase flow and is a function of the presence of the particles in addition to the Mach number of the air and the Reynolds number of the tube. Therefore, analytical solutions corresponding to increased wall friction factors  $f$  are included in Figures 12 and 13. The increase in  $f$  is greater for the larger particle to air mass flow ratio  $X$  than for the lower. Roughening of the walls of the tube because of particle-wall collisions during the two-phase test runs partly accounts for the increase in  $f$ . The agreements in the

critical lengths are satisfactory for both values of  $X$ .

Of course, the factors affecting the agreement in critical lengths for the single-phase test runs also apply to the air-particle test runs. However, the effect of the particles on the velocity profile of the air is not known although it has been shown to be insignificant for low values of  $X$  (66).

Since particle velocities were not measured, an inlet particle slip of  $S_{pi} = 0.6$  was assumed for the analytical solutions. Solutions were also obtained for a slip of  $S_{pi} = 0.3$ . The results differed from the analytical solutions presented in Figures 12 and 13 by less than one per cent. Similar solutions were obtained for a 50 per cent decrease in the drag coefficient of the particles  $C_d$ . The results differed by less than one-half per cent.

It is important to note that the critical exit Mach number of the air  $M_{ge}$  is equal to one as in the case of single-phase flow. Soo (43) showed analytically that for small values of  $X$  (0.3), the speed of sound in a gas-particle mixture, with or without particle slip, is significantly lower than the speed of sound in the gas only. For homogeneous flow (no particle slip), the Mach number of a gas-particle mixture can be defined as

$$M_{gm} = \frac{(V_g = V_p)}{c_{gs}(\text{mixture})}$$

It is seen that  $M_{gme}$  is larger than one. Consequently, the

critical condition is governed by the Mach number of the air rather than by the Mach number of the mixture, which is also valid for particle slip conditions. For particle slip, no satisfactory definition of mixture Mach number exists. Based on the analytical solutions presented earlier for the particle mass variation data set, a correlation was attempted, considering such factors as particle slip  $S_p$  and particle to gas mass flow ratio  $X$ , but no satisfactory equation for  $M_{gm}$  was obtained.

#### Comparison of Results From the Literature to Analytical Solutions

No data was found for high Mach number or critical gas-particle flow. The most complete findings for comparison were presented by Hariu and Molstad (11) who studied sub-critical gas-particle flow in a vertical glass tube. The tube had a diameter of  $d_t = 0.267$  inch and a length of  $x_t = 2.67$  feet. The flowing mediums were air and sand where the average diameter of the sand was  $d_p = 0.0197$  inch. The total pressure drop of the air was measured and from semi-empirical expressions, they calculated such values as the individual pressure drop components of the air and particles and the drag coefficients of the particles. From measured values of the dispersed solids density, the velocity of the particles was determined. The particle to air mass flow ratio  $X$  was varied from 6 to 30 while the inlet conditions, especially the inlet velocity and Mach



number of the air, were maintained constant. Their results for one test run and the corresponding analytical solution obtained from the analysis given in Chapter III are shown below in Figure 15. Based on their data, the computer input

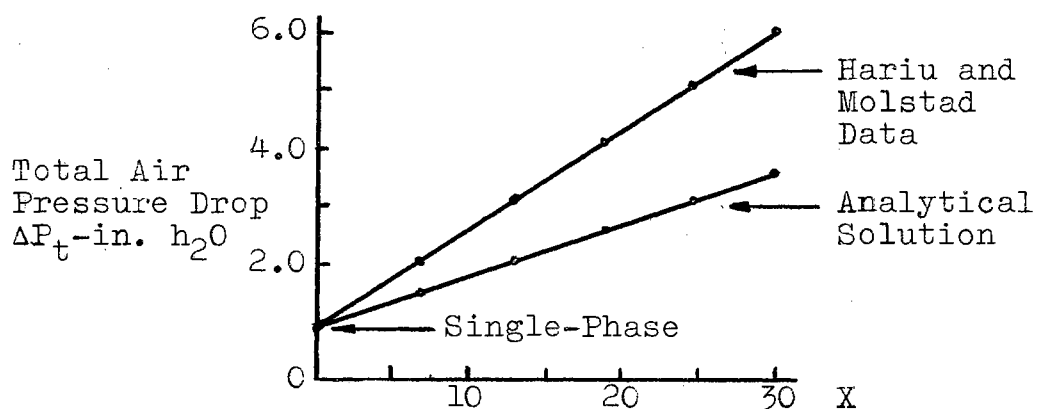


Figure 15. Dependency of Air-Particle Pressure Drop on the Particle to Air Mass Flow Ratio

data is shown in Appendix A for  $X = 6.95$ . Although the results agree qualitatively, their results for the pressure drop of the air as affected by the particle to air mass flow ratio  $X$  are underestimated by the analytical solutions. The two curves do intersect at the single-phase conditions where  $X = 0.0$ . From the gas pressure curves given in Figure 2 (pages 51-53), it can be seen that for their tube length of  $x_t^0 = 120$ , the corresponding critical length

would be less than would be obtained from the analytical solution because the local measured air pressures are less than those corresponding to the analytical solution. The critical length of their tube for a low inlet Mach number would be of the order of 5,000 tube diameters; whereas, the analytical solution would yield a critical length greater than 5,000. Consequently, it is again probable that the two-phase wall friction factor is not only greater than that for single-phase flow, but also increases as  $X$  is increased. This may be seen more clearly by considering the method by which they calculated the drag coefficient of the particles  $C_d$ . The pressure drop due to the air only  $\Delta P_a$  was subtracted from the total air pressure drop  $\Delta P_t$ . The difference was due to the air pressure drop over the particles  $\Delta P_p$ . In calculating  $\Delta P_a$ , they assumed that the particles did not affect the wall friction factor  $f$ . From semi-empirical equations, they calculated values of  $C_d$  that were somewhat higher than the standard drag curve. However, it was shown before in Chapter II that the drag coefficients of multi-particles were less than those given for single particles from the standard drag curve even though the particles may be irregularly shaped. Based on this,  $\Delta P_p$  would be lower as seen from Equation (24). Then, the pressure drop due to the air only  $\Delta P_a = \Delta P_t - \Delta P_p$  would be greater indicating that the two-phase wall friction factor is higher than for single-phase flow.

The data presented by Boatright (13) for air and sand

flowing in a vertical tube was also considered because the inlet Mach numbers were up to  $M_{gi} = 0.13$ . The corresponding analytical solutions again underestimated the total pressure losses of the air and, consequently, overestimated the critical length. His tube diameter was  $x_t^0 = 400$  which is still far short of the critical length corresponding to an inlet Mach number of  $M_{gi} = 0.13$ .

Other data was not considered because complete experimental information was not given in regards to particle velocities, air and particle inlet conditions, two-phase wall friction factors, or multi-particle characteristics.

## CHAPTER VII

### INTERPRETATION OF RESULTS

#### Summary and Conclusions

The solutions to the governing one-dimensional differential equations for subsonic and supersonic adiabatic gas-particle flow in a constant area tube have been presented to show the effect of the governing variables and starting conditions of the system on the critical length and the local and critical exit properties of the gas and particles. The critical length is the maximum length that a gas-particle mixture may be transported. An experimental system was designed and operated for air and spherical glass particles flowing in a vertical constant area tube. Critical conditions were maintained for all test runs. The experimental results for the critical conditions were compared to corresponding analytical solutions.

The analytical results for the particle mass variation data set as the particle to air mass flow ratio  $X$  was increased may be summarized as follows:

1. From Figure 2 (page 51) the subsonic curves of the velocity  $V_g^0$ , temperature  $T_g^0$ , pressure  $P_g^0$ , and Mach number  $M_g$  of the air versus the local

tube position  $x^0$  are similar in shape and characteristics to those for single-phase gaseous flow ( $X = 0.001$ ), while from Figure 3 (page 54) for supersonic flow, the curves are similar only for low values of  $X$ .

2. The critical exit properties of the air  $V_{ge}^0$ ,  $T_{ge}^0$  and  $P_{ge}^0$  are essentially constant for subsonic flow, but are variable for supersonic flow.
3. From Figure 5 (page 60), the subsonic critical length decreases while for supersonic flow the critical length increases for low inlet particle slip  $S_{pi}$ .
4. The critical exit Mach number  $M_{ge}$  for particle to air mass flow rates up to  $X = 30$  is governed by the air only and equals one for both subsonic and supersonic flow as in the case of single-phase gaseous flow.

The analytical results for the property variation data set for  $X = 10$  may be summarized as follows:

1. Increasing the inlet particle to air velocity ratio and reducing the acceleration of gravity parameter and inlet particle to air temperature ratio increases both the subsonic and supersonic critical length.
2. Increasing the inlet Mach number of the air and the tube to particle diameter ratio decreases

the subsonic critical length and increases the supersonic critical length. The effects of other parameters of the systems and the variables of the system may be seen from Tables II and I, respectively.

Two observations regarding the particle mass variation data set and the property variation data set are:

1. Any factor that increases the particle pressure drop per unit length  $\Delta P_p$  tends to decrease the subsonic critical length and increase the supersonic critical length.
2. Any factor that increases the particle to air or air to particle heat transfer rate tends to decrease the subsonic critical length and increase the supersonic critical length, respectively.

The experimental results and the corresponding analytical solutions presented in this study may be summarized as follows:

1. The analytical finite difference computer solutions agreed well with exact single-phase Fanno theory as shown in Figures 10 and 11 (pages 102-104).
2. From Figure 10, the single-phase experimental results for the critical exit properties of the air  $V_{ge}^0$ ,  $P_{ge}^0$ ,  $T_{ge}^0$  and  $M_{ge}$  agreed well with the analytical solutions. The local values agreed only at low Mach numbers.

3. The single-phase critical length  $x_{\max}^0 = 436.5$  did not agree with the critical length of  $x_{\max}^0 = 466$  obtained from the analytical solution. This was probably due to the use of unreliable values for the wall friction factor  $f$  resulting from the dependency of  $f$  on the Mach number of the air as well as on the Reynolds number of the tube  $Re_t$ .
4. From Figures 12 and 13 (pages 105-108); the two-phase experimental results for the critical exit properties of the air agreed well with the analytical solutions. The local values agreed only at low Mach numbers.
5. The critical lengths of  $x_{\max}^0 = 507$  and  $x_{\max}^0 = 577$  obtained from the analytical solutions for particle to air mass flow ratios of  $X = 0.114$  and  $X = 0.153$ , respectively, did not agree with the critical length of the tube  $x_{\max}^0 = 436.5$ . This was probably due to the use of unreliable values for  $f$  resulting from the dependency of  $f$  on the particle to air mass flow ratio as well as on the Mach number of the air and the Reynolds number of the tube.
6. The experimental results given by Hariu and Molstad (11) and the corresponding analytical solutions agreed qualitatively but the analytical results predicted lower total air

pressure drops as seen from Figure 15 (page 116). Although the data was for sub-critical conditions, it is probable that the critical lengths would not agree because of the increased dependency of  $f$  on the particle to air mass flow ratio  $X$ .

#### Suggestions for Future Study

It is recommended that additional analytical and experimental work be done in the following areas:

1. Two-phase wall friction factors at low and high Mach numbers and particle to gas mass flow ratios.
2. Multi-particle drag and heat transfer coefficients at low and high particle slips, Mach numbers of the gas, and particle to gas mass flow ratios.
3. The effect of particles on the velocity distribution of a gas flowing in a tube.
4. Instrumentation system for the complete measurement of the properties of the gas and particles for flow in vertical and horizontal tubes.
5. Complete analytical solutions for the critical length as a function of the independent parameters of the system.



6. Subsonic and supersonic gas-particle critical length measurements for low and high particle to gas mass flow ratios.

If the above work is accomplished, the complex mechanism of gas-particle flow in vertical (and horizontal) tubes would be more completely understood and the practical design of such systems could be more accurately accomplished.

## BIBLIOGRAPHY

1. Shapiro, A. H. The Dynamics and Thermodynamics of Compressible Fluid Flow. New York: Ronald Press Co., Volume I, 1953, pp. 159, 190.
2. Croft, H. O. Thermodynamics Fluid Flow and Heat Transmission. New York and London: McGraw-Hill Co., 1938.
3. Waddell, H. "The Coefficient of Resistance as a Function of Reynolds Number for Solids of Various Shapes," J. Franklin Inst., Volume 217, 1934, p. 459.
4. Alves, G. E. "Cocurrent Liquid-Gas Flow in Pipe Line Contactor," Chem. Engr. Progress, Vol. 50, No. 9, 1954, p. 449.
5. Leva, M., M. Grummer, M. Weintraub, and M. Pollchik. "Fluidization of Solid Non-Vesicular Particles," Chem. Engr. Progress, Vol. 44, No. 8, 1948, p. 619.
6. Wilhelm, R. H. and M. Kwauk. "Fluidization of Solid Particles," Chem. Engr. Progress, Vol. 44, No. 3, 1948, p. 201.
7. Wen, C. Y. and R. F. Hashinger. "Elutriation of Solid Particles From a Dense-Phase Fluidized Bed," A.I.Ch.E. Journal, Vol. 6, No. 2, 1960, p. 220.
8. Zenz, F. A. "Two-Phase Fluid-Solid Flow," Ind. and Engr. Chem., Vol. 41, No. 12, 1948, p. 2801.
9. Hanratty, T. J., G. Latinen, and R. H. Wilhelm. "Turbulent Diffusion in Particulately Fluidized Beds of Particles," A.I.Ch.E. Journal, Vol. 2, No. 3, 1956, p. 372.
10. Vogt, E. G. and R. R. White. "Friction in the Flow of Suspensions," Ind. and Engr. Chem., Vol. 40, No. 9, 1948, p. 1731.

11. Hariu, O. H. and M. C. Molstad. "Pressure Drop in Vertical Tubes in Transport of Solids by Gases," Ind. and Engr. Chem., Vol. 41, No. 6, 1949, p. 1148.
12. Farbar, L. "Flow Characteristics of Solids-Gas Mixtures," Ind. and Engr. Chem., Vol. 41, No. 6, 1949, p. 1184.
13. Boatright, K. E. "Transportation of Solid Particles in a Gas Flow Stream," Thesis, Oklahoma State University, 1959.
14. Boggs, J. H. and E. C. Fitch. "Reconnaissance Survey of Two-Phase, Two-Component Fluid Flow and Transportation of Solid Particles in Fluid Streams," Fluid Dynamics Project, Contract No. 1, Report No. 1, Carter Oil Co., Tulsa, Oklahoma, 1957.
15. Richardson, J. F. and M. McLeman. "Pneumatic Conveying Part II-Solids Velocities and Pressure Gradients in a One-inch Horizontal Pipeline," Trans. Instn. Cnem. Engrs., Vol. 38, 1960, p. 257.
16. Khudiakow, G. N. and Z. F. Chukanov. Doklady Akad. Nauk. S.S.S.R., Vol. 78, 1951, p. 681.
17. Soo, S. L. "Fully Developed Turbulent Pipe Flow of a Gas-Solid Suspension," Ind. and Engr. Chem. Fund., Vol. 1, No. 1, 1962, p. 33.
18. Soo, S. L. and J. A. Regalbuto. Can. J. Chem., Vol. 38, 1960, p. 160.
19. Hino, M. "Turbulent Flow With Suspended Particles," J. Hydraulics Div., Proc. A.S.C.E., Vol. 89, No. HY4, 1963, p. 161.
20. Lebedev, V. V. and A. Y. Makirov. "Determination of the Parameters of Particle-Size Distribution," Izvestiya Vysshikh Uchebnykh Zavedeniy, Fizika, Nr. 4, 1960, p. 60. Translation by Tech. Documents Liason Office, Wright Patterson AFB, Ohio, 1961.
21. Chen, A. C. H. "An Investigation of Compressible Subsonic Adiabatic Turbulent Flow in Smooth Circular Pipes of Constant Cross Section," Thesis, Oklahoma State University, 1964.

22. Farbar, L. and M. J. Morley. "Heat Transfer to Flowing Solids-Gas Mixtures in a Circular Tube," Ind. and Engr. Chem., Vol. 49, No. 7, 1957, p. 1143.
23. Depew, C. A. "Heat Transfer to Flowing Gas-Solids Mixtures in a Vertical Circular Duct," Phd Thesis, University of California, 1960.
24. Tien, C. L. "Heat Transfer by a Turbulently Flowing Fluids-Solids Mixture in a Pipe," J. of Heat Transfer, Trans. A.S.M.E., Series C, Vol. 83, No. 2, 1961, p. 183.
25. Zurakowski, S. "Heat-Transfer Efficiency in Gas-Solid Suspension Systems," International Chem. Engr., Vol. 3, No. 2, 1963, p. 178.
26. Depew, C. A. and L. Farbar. "Heat Transfer to Pneumatically Conveyed Glass Particles of Fixed Size," J. of Heat Transfer, Trans. A.S.M.E., Paper No. 62-HT-14, 1962.
27. Farbar, L. and C. A. Depew. "Heat Transfer Effects to Gas-Solids Mixtures Using Solid Spherical Particles of Uniform Size," Ind. and Engr. Chem. Fund., Vol. 2, No. 2, 1963, p. 130.
28. Tien, C. L. and V. Quan. "Local Heat Transfer Characteristics of Air-Glass and Air-Lead Mixtures in Turbulent Pipe Flow," Trans, A.S.M.E., Paper No. 62-HT-15, 1963.
29. Abel, W. T., D. E. Bluman, and J. P. O'Leary. "Gas-Solids Suspensions as Heat Carrying Mediums," Trans. A.S.M.E., Paper No. 63-WA-210, 1964.
30. Netzer, D. W. "Calculation of Flow Characteristics for Two-Phase Flow in Annular Converging-Diverging Nozzles," Contract No. onr 1100(21), Report No. TM-62-3, Jet Propulsion Center, Purdue University, 1962.
31. Smigielski, J. "Monodimensional Adiabatic Flow of a Two-Phase Medium," Polska An, Instytut Maszyn Przeplywowych, Prace, Nr. 10, 1962, p. 3. Translation by the Foreign Technology Division, Wright Patterson AFB, Ohio, 1963.

32. Karplus, H. B. "The Velocity of Sound in a Liquid Containing Gas Bubbles," Armour Research Foundation Project No. A-097, Atomic Energy Comm. Contract No. AF(11-1)-528, 1958.
33. Karplus, H. B. "Propogation of Pressure Waves in a Mixture of Water and Steam," Armour Research Foundation Project No. D132A13, AEC Contract No. AT(11-1)-528, 1961.
34. Vogrin, J. A. Jr. "An Experimental Investigation of Two-Phase, Two-Component Flow in a Horizontal, Converging-Diverging Nozzle," Argonne National Laboratory Report No. ANL-6754, 1963.
35. Fauske, H. K. "Two-Phase Critical Flow with Application to Liquid-Metal Systems," Argonne National Laboratory Report No. ANL-6779, 1963.
36. Murdock, J. W. and J. M. Bauman. "The Critical Flow Function for Superheated Steam," J. of Basic Engr., Trans. A.S.M.E., Paper No. 63-WA-19, 1963.
37. Stepanoff, A. J. "Pumping Solid-Liquid Mixtures," Trans. A.S.M.E., Paper No. 63-WA-102, 1963.
38. Levy, S. "Prediction of Two-Phase Pressure Drop and Density Distribution From Mixing Length Theory," J. of Heat Transfer, Trans. A.S.M.E., Paper No. 62-HT-6, 1962.
39. Hoglund, R. F. "Recent Advances in Gas-Particle Nozzle Flows," ARS, Solid Propellant Rocket Conference, Baylor University, Waco, Texas, Paper No. 2331-62, 1962.
40. Travis, L. P. "Heat Transfer and Particle Trajectories in Solid Propellant Rocket Nozzles," Aerojet-General Corp., Sacramento, Calif., Report No. 0162-01TN-17, 1962.
41. Gilbert, M., J. J. Allport, R. Dunlap, C. T. Crowe, B. G. Wrenn, and M. Rogers. "Dynamics of Two-Phase Flow in Rocket Nozzles," United Technology Corp., Sunnyvale, Calif., Contract No. NOW 61-0760-c, Fifth Quarterly Report, 1962.
42. Glauz, R. D. "Combined Subsonic-Supersonic Gas-Particle Flow," ARS Preprint 1717-61, 1961.

43. Soo, S. L. "Gas Dynamic Processes Involving Suspended Solids," A.I.Ch.E. Journal, Vol. 7, No. 3, 1961, p. 384.
44. Kriebel, A. R. "Analysis of Normal Shock Waves in Particle Laden Gas," J. of Basic Engr., Trans. A.S.M.E., Paper No. 63-WA-13, 1963.
45. Carrier, G. F. "Shock Waves in a Dusty Gas," J. of Fluid Mech., Vol. 4, Part 4, 1958, p. 376.
46. Dobbins, R. A. and S. Temkin. "Measurements of Particulate Attenuation," AIAA Journal, Vol. 2, No. 6, 1964, p. 1106.
47. Chu, B. T. "Wave Propagation in a Reacting Mixture," Heat Transfer and Fluid Mechanics Inst., Stanford University Press, Stanford, Calif., 1958.
48. Wood, A. B. A Textbook of Sound. New York: Macmillan, 1941.
49. Soo, S. L. "Effect of Transport Processes on Attenuation and Dispersion in Aerosols," J. of Acoustical Soc. of America, Vol. 32, No. 8, 1960, p. 943.
50. Knudsen, V. O., J. V. Wilson, and N. S. Anderson. "The attenuation of Audible Sound in Fog and Smoke," J. of Acoustical Soc. of America, Vol. 20, No. 6, 1948, p. 849.
51. Epstein, P. S. and R. R. Carhart. "The Absorption of Sound in Suspensions and Emulsions-Part I-Water Fog in Air," J. of Acoustical Soc. of America, Vol. 25, No. 3, 1953, p. 553.
52. Bradfield, G. "Relation Between Velocity Change and Absorption of Sound," International Conference on Ultrasonics, 1951.
53. Zink, J. W. "The Attenuation and Dispersion of Sound by Solid Particles Suspended in a Gas," Phd Thesis, University of Calif., Los Angeles, Calif., 1957.
54. Chu, B. T. and J. Y. Parlange. "A Macroscopic Theory of Two-Phase Flow With Mass, Momentum, and Energy Exchange," Contract No. DA-19-020-ORD-4761, Report No. 4, Div. of Engr., Brown Univ., Providence, R. I., 1962.

55. Scott, W. G. Jr. "Measurement of Turbine Nozzle Flow Area by Capacitance Methods," Thesis, Oklahoma State Univ., 1959.
56. Shapiro, A. H. and J. L. Dussourd. "Deceleration Probe for Measuring Stagnation Pressure and Velocity of a Particle Laden Stream," Heat Transfer and Fluid Mechanics Inst., Univ. of Calif., Los Angeles, Calif., 1955.
57. Millikan, R. A. "The General Law of Fall of a Small Spherical Body Through a Gas, and its Bearing Upon the Nature of Molecular Reflection from Surfaces," Physical Review, Vol. 22, No. 1, Second Series, 1923.
58. Corrsin, S. and J. Lumley. "On the Equation of Motion for a Particle in a Turbulent Fluid," Applied Science Review, Section A, Vol. 6, 1956, p. 114.
59. Peskin, R. L. "Some Effects of Particle-Particle and Particle-Fluid Interaction in Two-Phase Flow Systems," Proc. of the Heat Transfer and Fluid Mechanics Inst., 1960, p. 192.
60. Rubinow, S. I. and B. Keller. "The Transverse Force on a Spinning Sphere in a Viscous Fluid," J. of Fluid Mech., Vol. 11, Part 3, 1961, p. 447.
61. Haberman, W. L. "Subsonic Potential Flow Past a Sphere Inside a Cylindrical Duct," J. of Aerospace Sciences, March, 1962, p. 356.
62. Soo, S. L., C. L. Tien, and V. Kadambi. "Determination of Turbulence Characteristics of Solid Particles in a Two-Phase Stream by Optical Autocorrelation," Review of Scientific Instruments, Vol. 30, No. 9, 1959, p. 821.
63. Soo, S. L. and C. L. Tien. "Effect of the Wall on Two-Phase Turbulent Motion," J. of Applied Mech., Trans. A.S.M.E., Series E, Vol. 27, No. 1, 1960, p. 5.
64. Soo, S. L., H. K. Ihrig Jr., and A. F. El Kouh. "Experimental Determination of Statistical Properties of Two-Phase Turbulent Motion," Trans. A.S.M.E., Paper No. 59-A-59, 1959.
65. Ranz, W. E., G. R. Talandis, and B. Gutterman. "Mechanics of Particle Bounce," A.I.Ch.E. Journal, Vol. 6, No. 1, 1960, p. 124.

66. Torobin, L. B. and W. H. Gauvin. "Fundamental Aspects of Solids-Gas Flow," Can. J. of Chem. Engr., Part I, Vol. 37, 1959, p. 129; Part II, Vol. 37, 1959, p. 167; Part III, Vol. 37, 1959, p. 224; Part IV, Vol. 38, 1960, p. 142; Part V, Vol. 38, 1960, p. 189; Part VI, Vol. 38, 1960, p. 142.
67. Kada, H. and T. J. Hanratty. "Effects of Solids on Turbulence in a Fluid," A.I.Ch.E. Journal, Vol. 6, No. 4, 1960, p. 624.
68. Torobin, L. B. and W. H. Gauvin. "Turbulent Flow Ballistics for Particle Momentum Studies," A.I.Ch.E. Journal, Vol. 7, No. 3, 1961, p. 406.
69. Torobin, L. B. and W. H. Gauvin. "The Drag Coefficients of Single Spheres Moving in Steady and Accelerated Motion in a Turbulent Fluid," A.I.Ch.E. Journal, Vol. 7, No. 4, 1961, p. 615.
70. Drake, R. M. Jr. Discussion, J. of Heat Transfer, Trans. A.S.M.E., Series C, Vol. 83, 1961, p. 170.
71. Yuge, T. "Experiments on Heat Transfer From Spheres Including Combined Natural and Forced Convection," J. of Heat Transfer, Trans. A.S.M.E., Series C, Vol. 82, 1960, p. 214.
72. Pasternak, I. S. and W. H. Gauvin. "Turbulent Convective Heat and Mass Transfer From Accelerating Particles," A.I.Ch.E. Journal, Vol. 7, No. 2, 1961, p. 254.
73. Johnson, C. H. J. "Heat Transfer and Mass Transfer From the Sphere at Low Reynolds Number," Australian Journal of Physics, Vol. 15, No. 2, 1962, p. 143.
74. Yen, Y. C. and G. Thodos. "Heat, Mass, and Momentum Transfer in the Flow of Gases Past Single Spheres," A.I.Ch.E. Journal, Vol. 8, No. 1, 1962, p. 34.
75. Klyachko, L. S. "Heat Transfer Between a Gas and a Spherical Surface With the Combined Action of Free and Forced Convection," J. of Heat Transfer, Trans. A.S.M.E., Paper No. 62-WA-114, 1962.
76. Runge, C. Mathematische Annalen, Vol. 46, 1895.



77. Kutta, W. Zeitschrift fur Math und Phys., Vol. 46, 1901.
78. Schlichting, H. Boundary Layer Theory. New York: McGraw-Hill Co., 1960, p. 16.
79. Eckert, E. R. G. and R. M. Drake Jr. Heat and Mass Transfer. New York: McGraw-Hill Co., 1959, p. 155.
80. A.S.M.E. Power Test Codes, "Measurement of Quantity of Materials," Part 5, 1949.

## APPENDIX A

### COMPUTER PROGRAM AND INPUT DATA

In order to use the Runge-Kutta finite difference method for a computer solution, the four derivatives

$$\frac{dV_p^{\circ}}{dx^{\circ}}, \quad \frac{dT_p^{\circ}}{dx^{\circ}}, \quad \frac{dV_g^{\circ}}{dx^{\circ}}, \quad \frac{dT_g^{\circ}}{dx^{\circ}}$$

in terms of the variables of the system must be found from Equations (7), (10), (11), and (12).

From Equation (11),

$$\frac{dV_p^{\circ}}{dx^{\circ}} = \frac{3CDC_d G (V_g^{\circ} - V_p^{\circ})^2}{4V_g^{\circ} \left( \frac{A^{\circ} V_p^{\circ}}{XC} - 1 \right)} - \frac{B}{2V_p^{\circ}} = f_1(V_g^{\circ}, V_p^{\circ}, T_g^{\circ}, T_p^{\circ}).$$

From Equation (12),

$$\frac{dT_p^{\circ}}{dx^{\circ}} = \frac{6CDNu_p}{ARe_{pl} Pr_{gl} V_p^{\circ}} (T_g^{\circ} - T_p^{\circ}) = f_2(V_g^{\circ}, V_p^{\circ}, T_g^{\circ}, T_p^{\circ}).$$

From Equation (10),

$$\frac{dT_g^0}{dx^0} = cT_g^0 - \frac{aT_g^0}{V_p^0} \frac{dV_p^0}{dx^0} + \frac{bT_g^0}{V_g^0} \frac{dV_g^0}{dx^0}.$$

From Equation (7),

$$\frac{dT_g^0}{dx^0} + 2V_g^0 \frac{dV_g^0}{dx^0} + AX \frac{dT_p^0}{dx^0} + 2XV_p^0 \frac{dV_p^0}{dx^0} + (1+X)B = 0.$$

Substituting  $\frac{dT_g^0}{dx^0}$  from Equation (10) into the above equation yields

$$\frac{dV_g^0}{dx^0} = \frac{-\left[(1+X)B + AX \frac{dT_p^0}{dx^0} + \left(2XV_p^0 - \frac{aT_g^0}{V_p^0}\right) \frac{dV_p^0}{dx^0} + cT_g^0\right]}{\left(2V_g^0 + \frac{bT_g^0}{V_g^0}\right)}$$

$$= f_3(V_g^0, V_p^0, T_g^0, T_p^0, a, b, c).$$

Finally, from Equation (10),

$$\frac{dT_g^0}{dx^0} = cT_g^0 - \frac{aT_g^0}{V_p^0} \frac{dV_p^0}{dx^0} + \frac{bT_g^0}{V_g^0} \frac{dV_g^0}{dx^0} = f_4(V_g^0, V_p^0, T_g^0, T_p^0, a, b, c).$$

It is noted that in each of the above four functions  $f_1$ ,  $f_2$ ,  $f_3$ , and  $f_4$  the independent variable  $x^0$  does not appear.

Choosing  $V_g^0, V_p^0, T_g^0$ , and  $T_p^0$  as the dependent variables and the local tube position  $x^0$  as the independent variable, the variables at  $x^0 + dx^0$  may be found as follows:

$$\text{Let } D = f_1(V_g^0, V_p^0, T_g^0, T_p^0)$$

$$E = f_2(V_g^0, V_p^0, T_g^0, T_p^0)$$

$$F = f_3(V_g^0, V_p^0, T_g^0, T_p^0, a, b, c)$$

$$G = f_4(V_g^0, V_p^0, T_g^0, T_p^0, a, b, c)$$

$$A = a = g_1(V_g^0, V_p^0, T_g^0, T_p^0)$$

$$B = b = g_2(V_g^0, V_p^0, T_g^0, T_p^0)$$

$$C = c = g_3(V_g^0, V_p^0, T_g^0, T_p^0).$$

Then,

$$A(n+1) = g_1[V_g^0 + F(n)dx^0/2, V_p^0 + D(n)dx^0/2,$$

$$T_g^0 + G(n)dx^0/2, T_p^0 + E(n)dx^0/2]$$

$$B(n+1) = g_2[V_g^0 + F(n)dx^0/2, V_p^0 + D(n)dx^0/2,$$

$$T_g^0 + G(n)dx^0/2, T_p^0 + E(n)dx^0/2]$$

$$C(n+1) = g_3[V_g^0 + F(n)dx^0/2, V_p^0 + D(n)dx^0/2,$$

$$T_g^{\circ} + G(n)dx^{\circ}/2, T_p^{\circ} + E(n)dx^{\circ}/2]$$

$$D(n+1) = f_1[V_g^{\circ} + F(n)dx^{\circ}/2, V_p^{\circ} + D(n)dx^{\circ}/2,$$

$$T_g^{\circ} + G(n)dx^{\circ}/2, T_p^{\circ} + E(n)dx^{\circ}/2]$$

$$E(n+1) = f_2[V_g^{\circ} + F(n)dx^{\circ}/2, V_p^{\circ} + D(n)dx^{\circ}/2,$$

$$T_g^{\circ} + G(n)dx^{\circ}/2, T_p^{\circ} + E(n)dx^{\circ}/2]$$

$$F(n+1) = f_3[V_g^{\circ} + F(n)dx^{\circ}/2, V_p^{\circ} + D(n)dx^{\circ}/2,$$

$$T_g^{\circ} + G(n)dx^{\circ}/2, T_p^{\circ} + E(n)dx^{\circ}/2,$$

$$A(n+1), B(n+1), C(n+1)]$$

$$G(n+1) = f_4[V_g^{\circ} + F(n)dx^{\circ}/2, V_p^{\circ} + D(n)dx^{\circ}/2,$$

$$T_g^{\circ} + G(n)dx^{\circ}/2, T_p^{\circ} + E(n)dx^{\circ}/2,$$

$$A(n+1), B(n+1), C(n+1)].$$

The above equations must be solved four times from  $n = 1$  to  $n = 4$ . If  $n = 4$ ,  $dx^{\circ} = 2dx^{\circ}$ . For the starting condition  $n = 1$ ,  $D(1) = E(1) = F(1) = G(1) = 0$ .

Finally,

$$V_g^{\circ}(x^{\circ} + dx^{\circ}) = V_g^{\circ}(x^{\circ}) + [F(2) + 2F(3) + 2F(4) + F(5)]dx^{\circ}/6$$

$$V_p^0(x^0 + dx^0) = V_p^0(x^0) + [D(2) + 2D(3) + 2D(4) + D(5)]dx^0/6$$

$$T_g^0(x^0 + dx^0) = T_g^0(x^0) + [G(2) + 2G(3) + 2G(4) + G(5)]dx^0/6.$$

$$T_p^0(x^0 + dx^0) = T_p^0(x^0) + [E(2) + 2E(3) + 2E(4) + E(5)]dx^0/6.$$

The values  $F(2)$ ,  $D(2)$ ,  $G(2)$ , and  $E(2)$  are the derivatives at the previous tube location  $x^0$ .

TABLE III  
 PROPERTIES OF GAS-PARTICLE MIXTURES

Property of Air or Particles	Particle Variation Data Set	Property Variation Data Set	Lab Data X=0.0	Lab Data X=0.114	Lab Data X=0.153	Hariu and Molstad Data X=6.95
$c_p$ -Btu/lb. <sub>m</sub> °R	0.2	0.4	0.2	0.2	0.2	0.195
$c_g$ -Btu/lb. <sub>m</sub> °R	0.24	0.343	0.24	0.24	0.24	0.24
$K_g$ -Btu/hr. °F ft.	0.015	0.030	0.015	0.015	0.015	0.015
$\mu_g$ -lb. <sub>f</sub> sec./ft. <sup>2</sup>	3.76E-7	7.52E-7	3.76E-7	3.76E-7	3.76E-7	3.83E-7
$d_t$ -inches	0.5	0.25	0.495	0.495	0.495	0.267
$d_p$ -inches	.0185	.00185	.0185	.0185	.0185	.0197
$V_{pi}$ -ft./sec.	230	179	281	181	170	6.2
$V_{gi}$ -ft./sec.	255	281	312	299	283.5	21.9
$T_{pi}$ -°R	540	593	532.2	530.7	538.2	537
* $T_{gi}$ -°R	540	700	532.2	530.7	538.2	537
* $P_{gi}$ -lb. <sub>f</sub> /in. <sup>2</sup> (Abs.)	75.0	150.0	71.3	73.36	73.6	14.7
$g$ -ft./sec. <sup>2</sup>	32.0	0.0	32.2	32.2	32.2	32.2
$\gamma$ -Dimensionless	1.4	1.67	1.4	1.4	1.4	1.4
$\rho_p$ -lb. <sub>m</sub> /ft. <sup>3</sup>	160	320	160	160	160	165

TABLE III (Continued)

Property of Air or Particles	Particle Variation Data Set	Property Variation Data Set	Lab Data X=0.0	Lab Data X=0.114	Lab Data X=0.153	Hariu and Molstad Data X=6.95
$V_{gl}$ -ft./sec.	2550	Variable	2531	2530	2542	2541
$R_g$ -ft.lb. <sub>f</sub> /lb. <sub>m</sub> <sup>o</sup> R	53.3	Variable	53.3	53.3	53.3	53.3

\* $T_{gi} = T_{gl}$ ,  $P_{gi} = P_{gl}$

Note: The values in the property variations column apply to each individual property variation given in Table I.



TABLE IV  
COMPUTER INPUT DATA

Input Data	Particle Variation Data Set	Property Variation Data Set								
		$c_p$	$c_g$	$K_g$	$\mu_g$	$d_t$	$d_p$	$V_{pi}^o$	$V_{gi}^o$	$T_{pi}^o$
A	0.833	1.668	0.583							
B	4.13E-7		2.89E-7			2.065E-7				
C	0.00234		.001636							
D	27.0					13.5	270.0			
E	5.38E-6	2.69E-6	4.5E-6	1.076E-5		2.69E-6	5.38E-4			
EP	122,200		102,200		61,100		12,220			
EPP	0.7		1.0	0.35	1.4			0.7		
EPPP	0.9									
VR	9.0									
VRR	0.1		.0836						0.11	
TR	1.0									1.1
TRR	1.0									1.1
TRRF	0.9629									
PRRF	0.196									
PA	958.0		802.8							
Z	7.0									
dx1	Variable	2.0	2.0	2.0	2.0	2.0	2.0	2.0	2.0	2.0
dx2	Variable	0.5	0.5	0.5	0.5	0.5	0.2	0.2	0.5	0.5
XMR	.001, .1,	10	10	10	10	10	10	10	10	10
Remarks	1, 3, 5, 7, 8.5, 10, 15, 20, 22.5, 25, 30, 40	Incr.	Incr. ( $\gamma$ const., $R_g$ incr.)	Incr.	Incr.	Decr.	Decr.	Decr.	Incr.	Incr.

Note: Blank columns indicate same value as Particle Variation Data Set

TABLE IV (Continued)

Input Data	Property Variation Data Set						Lab Data X=0.0	Lab Data X=0.114	Lab Data X=0.153	Hariu and Molstad Data X=6.95
	T <sup>o</sup> <sub>gi</sub>	P <sup>o</sup> <sub>gi</sub>	g	Y	ρ <sub>p</sub>	C <sub>d</sub>				
A							.833	.833	.833	.813
B	3.19E-7		0.0	.001672			4.16E-7	4.17E-7	4.12E-7	2.22E-7
C	.001805	.00468			.00117		.002265	.002334	.00231	.000449
D							26.8	26.8	26.8	13.5
E	4.725E-6				2.69E-6		5.38E-6	5.38E-6	5.35E-6	2.54E-6
EP	107,300	244,400		87,300			117,000	119,860	119,300	25,000
EPP							.687	.687	.687	.71
EPPP							.90	.60	.60	.284
VR							7.0	7.0	7.0	9.0
VRR	.0877						.123	0.1182	.1114	0.00862
TR							1.0	1.0	1.0	1.0
TRR	.772						1.0	1.0	1.0	1.0
TRRF	.743						0.978	0.979	0.965	1.0
PRRF		0.098					0.206	0.2004	0.1945	1.0
PA	840.0	1916.0		684.0			918.0	941.7	939.0	188.0
Z				5.0			7.0	7.0	7.0	7.0
dx1	2.0	2.0	2.0	2.0	2.0	2.0	5.0	2.0	2.0	2.0
dx2	0.5	0.5	0.5	0.5	0.5	0.5	0.5	0.5	0.5	5.0
XMR	10	10	10	10	10	10	.0001	.114	.1531	6.95
Remarks	Incr.	Incr.	Decr.	Incr. (c <sub>g</sub> const., R incr.) g	Incr.	C <sub>d</sub> de- creased 50%				

TABLE V  
COMPUTER PROGRAM

Symbol Used in Computer Program	Corresponding Symbol Used in Text
A	A
B	B
C	C
D	D
E	$\frac{6 C D}{A Re_{pl} Pr_{gl}}$
EP	$Re_{pl}$
EPP	$Pr_{gl}$
EPPP	$\frac{V_o}{V_{gi}}$ (subsonic)
EPPPP	$\frac{T_o}{T_{gi}}$ (supersonic)
VR	$\frac{V_o}{V_{gi}}$ (subsonic)
VRR	$\frac{V_o}{V_{gi}}$ (supersonic)
TR	$\frac{T_o}{T_{gi}}$ (subsonic)
TRR	$\frac{T_o}{T_{gi}}$ (supersonic)
TRRF	$\frac{T_R}{T_{gl}}$ ( $T_R = 520^\circ R$ )
PRRF	$\frac{P_R}{P_{gl}}$ ( $P_R = 14.7 \text{ lb.}_f/\text{in.}^2$ )
PA	$V_{gl} \rho_{gl}$
Z	Z
XMR	$X_o$
VRRG	$V_g$
VRRP	$V_p$
TRRG	$T_o$
TRRP	$T_g$
PRRG	$P_o$
	$P_g$

TABLE V (Continued)

Symbol Used in Computer Program	Corresponding Symbol Used in Text
AR	$A^{\circ}$
PAM	$m_m/A_t$
RN	$Re_p$
PR	$Pr_g$
RNT	$Re_t$
CR	$f$
GM	$M_g$
HMX	$h_m$
SMX	$s_m$
DC	$C_d$

(Continued-Next page)

```

MON$$ JOB 252740027
MON$$ COMT TWO-PHASE FANNO FLOW PROBLEM
MON$$ ASGN MGO,A2
MON$$ ASGN MJB,A3
MON$$ ASGN MW1,A4
MON$$ ASGN MW2,A5
MON$$ MODE GO,TEST
MON$$ EXEQ FORTRAN,,,10,,,FLOW
C      PROGRAM FOR THE STUDY OF TWO-PHASE FANNO FLOW
C      IN A VERTICAL CONSTANT-SECTION DUCT
C
C      *****
C
C      DAVID ADAMS * * * MECHANICAL ENGINEERING
C
C
C      INTEGER PAGE,FAIL
C      DIMENSION AA(5),BB(5),CC(5),DD(5),EE(5),FF(5),GG(5)
C      COMMON RNABS,DC,NTIMES,DX,DX3,DX4,M
101 FORMAT(/10X,22HSIGN CHANGE -- DDVGX = ,1PE14.5)
102 FORMAT(1HK,10X,12HPROGRAM EXIT,12,39H -- ABSOLUTE VALUE OF REYNOLD
IS NUMBER =,1PE12.5//)
103 FORMAT(1HL,10X,25HSUBSONIC INLET CONDITIONS// 9X,1PE14.5/16X,1P8E1
14.5/(16X,1P7E14.5))
104 FORMAT(1HL,10X,27HSUPERSONIC INLET CONDITIONS//9X,1PE14.5/16X,1P8E
114.5/(16X,1P7E14.5))
105 FORMAT(1HL,10X,1PE12.5)
106 FORMAT(16X,1P7E14.5)
107 FORMAT(16X,1P7E14.5)
108 FORMAT(1H1,32X,59H* * * T W O P H A S E F A N N O F L O
1W * * *,20X,4HPAGE,I4)
109 FORMAT (I5)
110 FORMAT(F12.5,60X,A8)
111 FORMAT(1H2,10X,10HINPUT DATA///(16X,A8,1X,1H=,1PE14.5))
112 FORMAT(/10X,22HDDVGX DISORDER-DDVGX =,1PE14.5)
113 FORMAT(/10X,16HTEST FAILURE NO.,I2)
114 FORMAT(/10X,16HENTROPY DECREASE)
115 FORMAT(/10X,22HGM DISORDER ---- GM =,1PE14.5)
C
C      **      INPUT DATA ---
C      **      NINETEEN (19) -- EACH WITH ONE (1) F-TYPE NUMBER
C      **      LOCATED IN COLUMNS 2 - 12
C      **      ALL DECIMAL POINTS MUST BE INCLUDED IN THE NUMBERS
C
2 READ(1,110)A,AN,B,BN,C,CN,D,DN,E,EN,EP,EPN,EPP,EPPN,EPPP,EPPPN,VR,
1 VRN,VRR,VRRN,TR,TRN,TRR,TRRN,TRRF,TRRFN,PRRF,PRRFN,PA,PAN,Z,ZN
2 ,DX1,DX1N,DX2,DX2N,XMR,XMRN
WRITE(3,111)AN,A,BN,B,CN,C,DN,D,E,EN,E,EPN,EP,EPPN,EPP,EPPPN,EPPP,VR
1N,VR,VRRN,VRR,TRN,TR,TRRN,TRR,TRRFN,TRRF,PRRFN,PRRF,PAN,PA,ZN,Z,DX
21N,DX1,DX2N,DX2,XMRN,XMR
C
C      LINES=0
C      PAGE=0

```

```

AA(1)=0.0
BB(1)=0.0
CC(1)=0.0
DD(1)=0.0
EE(1)=0.0
FF(1)=0.0
GG(1)=0.0
DX3=DX1/50.0
DX4=DX2/50.0

```

C  
C  
C  
C  
C

```

* * * * *

```

```

**      BEGIN SUBSONIC INLET CONDITIONS CALCULATIONS

```

```

X=0.0
M=1
IDO=0
IDID=0
DX=DX1
NTIMES=3
VRRG=VRR
VRRP=EPPP*VRR
TRRG=1.0
TRRP=TRR
PRRG=1.0
AR=(1.0/VRR)*(1.0+((XMR*C)/EPPP))
PAM=(PA*(1.0+XMR)/AR)
EPPPP=((1.0+(A*XMR*TRR))+((VRR*VRR)*(1.0+(XMR*EPPP*EPPP)))*(1.0-(V
LR*VR)))/(1.0+(A*XMR*TR))
RN=VRR*(1.0-EPPP)*EP
RNABS=ABS(RN)
IF(RNABS.LE.1.0E+05)GO TO 4
K=1
WRITE(3,102)K,RNABS
CALL EXIT
4 CALL REYNUM
IF(RN.LT.0.0)DC=-DC
PR=2.0+0.495*(RNABS**0.55)*(EPP**0.33)
RNT=(VRR*D*EP)
IF(RNT.LE.1.0E+05)GO TO 5
CR=0.1382/((RNT)**0.177)
GO TO 3
5 CR=0.316/((RNT)**0.25)
3 GAMMA=1.4
GM=(VRR/((GAMMA/Z)**0.5))
HMI=((A*XMR*(TRR-TRRF))+(1.0-TRRF))/(1.0+XMR) +1.0
SMI=((A*XMR*ALOG(TRR/TRRF))+ALOG(1.0/TRRF)-((2.0/Z)*ALOG(1.0/PRRF)
1))/((1.0+XMR) +1.0)
SM=SMI
G=((AR*VRR)/(XMR*C))-1.0/EPPP
TRRPO=TRRP
TRRGO=TRRG
PRRGO=PRRG
PAGE=PAGE+1

```

```

REWIND 4
WRITE(3,108)PAGE
WRITE(3,103)X, VRRG, VRRP, TRRG, TRRP, PRRG, RN, AR, PAM, DC, PR, CR, GM, HMI, S
LMI, G
C
C   **      BRANCH TO SUBSONIC FINITE DIFFERENCES
C
C   GO TO 10
C
C   **      BEGIN SUPERSONIC INLET CONDITIONS CALCULATIONS
C
6 X=0.0
M=2
IDO=0
IDID=0
DX=DX2
NTIMES=3
VRRG=VR*VRR
VRRP=VR*VRR*EPP
TRRG=EPPPP
TRRP=TR*EPPPP
PRRG=1.0/(((XMR*C*(VR-1.0))/(EPPPP*EPPP))+ (VR/EPPPP))
AR=(EPPPP/(PRRG*VR*VRR))*(1.0+((XMR*C*PRRG)/(EPPP*EPPPP)))
PAM=(PA*(1.0+XMR)/AR)
RN=(VR*VRR*(1.0-EPPP)*EP*PRRG)/EPPPP
RNABS = ABS(RN)
IF(RNABS.LE.1.0E+05)GO TO 8
K=2
WRITE(3,102)K, RNABS
CALL EXIT
8 CALL REYNUM
IF(RN.LT.0.0)DC=-DC
PR=2.0+0.459*(RNABS**0.55)*(EPP**0.33)
RNT=(VR*VRR*PRRG*D*EP/EPPPP)
IF(RNT.LE.1.0E+05)GO TO 9
CR=0.1382/((RNT)**0.177)
GO TO 7
9 CR=0.316/((RNT)**0.25)
7 GAMMA=1.4
GM=(VR*VRR/((EPPPP*GAMMA/Z)**0.5))
HMI=((A*XMR*(TR*EPPPP-TRRF))+ (EPPPP-TRRF))/(1.0+XMR) +1.0
SMI=((A*XMR*ALOG(TR*EPPPP/TRRF))+ALOG(EPPPP/TRRF)-((2.0/Z)*ALOG(PR
LRG/PRRF)))/(1.0+XMR) +1.0
SM=SMI
G=(PRRG/EPPPP)*(((AR*VR*VRR)/(XMR*C))- (1.0/EPPP))
TRRPO=TRRP
TRRGO=TRRG
PRRGO=PRRG
LINES=0
PAGE=PAGE+1
REWIND 4
WRITE(3,108)PAGE
WRITE(3,104)X, VRRG, VRRP, TRRG, TRRP, PRRG, RN, AR, PAM, DC, PR, CR, GM, HMI, S
LMI, G

```

C  
C  
C  
C  
C  
C  
C

```

**      CONTINUE ON TO SUPERSONIC FINITE DIFFERENCES
* * * * *
**      BEGIN FINITE DIFFERENCES CALCULATIONS

10 DO 11 N=1,4
    DP=DX
    IF(N.EQ.4)DP=DX*2.0
    AA(N+1)=(1.0/(1.0-((VRRP+(DD(N)*DP/2.0))*AR)/(XMR*C)))+(1.0-(XMR*C
1) /((VRRP+(DD(N)*DP/2.0))*AR))*Z*XMR*((VRRG+(FF(N)*DP/2.0))*(VRRP+
2(DD(N)*DP/2.0)))/(TRRG+(GG(N)*DP/2.0)))
    BB(N+1)=1.0-((1.0-((XMR*C)/((VRRP+(DD(N)*DP/2.0))*AR)))*Z*((VRRG+
1(FF(N)*DP/2.0))*(VRRG+(FF(N)*DP/2.0)))/(TRRG+(GG(N)*DP/2.0)))
    CC(N+1)=-(((CR*Z*(VRRG+(FF(N)*DP/2.0))*(VRRG+(FF(N)*DP/2.0)))/(2.0
1*(TRRG+(GG(N)*DP/2.0)))+(1.0-((XMR*C)/((VRRP+(DD(N)*DP/2.0))*AR))
2)*((B*Z*(VRRG+(FF(N)*DP/2.0)))/(2.0*(TRRG+(GG(N)*DP/2.0)))*((XMR/
3(VRRP+(DD(N)*DP/2.0)))+(1.0/(VRRG+(FF(N)*DP/2.0))))))
    DD(N+1)=((0.75*C*D*DC*G*((VRRG+(FF(N)*DP/2.0))-(VRRP+(DD(N)*DP/2.
10))))**2)/((VRRG+(FF(N)*DP/2.0))*((AR*(VRRP+(DD(N)*DP/2.0)))/(XMR
2*C))-1.0))-B/(2.0*(VRRP+(DD(N)*DP/2.0)))
    EE(N+1)=((E*PR)/(VRRP+(DD(N)*DP/2.0)))*((TRRG+(GG(N)*DP/2.0))-(TRR
1P+(EE(N)*DP/2.0)))
    FF(N+1)=-(((1.0+XMR)*B+(A*XMR*EE(N+1)))+(2.0*XMR*(VRRP+(DD(N)*DP/2
1.0)))-(AA(N+1)*(TRRG+(GG(N)*DP/2.0))/(VRRP+(DD(N)*DP/2.0)))*DD(N+
21)+(TRRG+(GG(N)*DP/2.0))*CC(N+1)))/((BB(N+1)*(TRRG+(GG(N)*DP/2.0
3))/(VRRG+(FF(N)*DP/2.0))+2.0*(VRRG+(FF(N)*DP/2.0)))
11 GG(N+1)=((CC(N+1)*(TRRG+(GG(N)*DP/2.0)))-(AA(N+1)*(TRRG+(GG(N)*DP/
12.0)))/(VRRP+(DD(N)*DP/2.0)))*DD(N+1)*(BB(N+1)*(TRRG+(GG(N)*DP/2.0
2)/(VRRG+(FF(N)*DP/2.0)))*FF(N+1))
    DVRGX=(FF(2)+2.0*FF(3)+2.0*FF(4)*FF(5))/6.0
    DVRPX=(DD(2)+2.0*DD(3)+2.0*DD(4)+DD(5))/6.0
    DTRGX=(GG(2)+2.0*GG(3)+2.0*GG(4)+GG(5))/6.0
    DTRPX=(EE(2)+2.0*EE(3)+2.0*EE(4)+EE(5))/6.0
    VRRG=VRRG+(DVRGX*DX)
    VRRP=VRRP+(DVRPX*DX)
    TRRG=TRRG+(DTRGX*DX)
    TRRP=TRRP+(DTRPX*DX)
    PRRG=(TRRG*VRRP*G)/(VRRG*((AR*VRRP)/(XMR*C))-1.0)
    DEF2=((BB(2)*(TRRG+(GG(1)*DX/2.0)))/((VRRG+(FF(1)*DX/2.0))*(VRRG+1
1FF(1)*DX/2.0)))+2.0
    DFF3=((BB(3)*(TRRG+(GG(2)*DX/2.0)))/((VRRG+(FF(2)*DX/2.0))*(VRRG+1
1FF(2)*DX/2.0)))+2.0
    DFF4=((BB(4)*(TRRG+(GG(3)*DX/2.0)))/((VRRG+(FF(3)*DX/2.0))*(VRRG
1+(FF(3)*DX/2.0)))+2.0
    DFF5=((BB(5)*(TRRG+(GG(4)*DX/1.0)))/((VRRG+(FF(4)*DX/1.0))*(VRRG
1+(FF(4)*DX/1.0)))+2.0
    DDVGX=(DFF2*DFF3*DFF4*DFF5)
    WRITE(3,107)DVRGX,DVRPX,DTRGX,DTRPX,DDVGX,FF(2),RNT
    LINES=LINES+1
    IF(LINES.LE.8)GO TO 12
    PAGE=PAGE+1
    WRITE(3,108)PAGE

```



```

LINES=0
12 IF(X.EQ.0.0)GO TO 38
   IF(IDID.EQ.0)GO TO 14
   IF(IDO.EQ.1)GO TO 14
   IDO=1
   DDVGXP=DDVGX
   GMP=GM
C
C   TESTS TO DETERMINE FINITE DIFFERENCE CALCULATION SHUTOFF POINT
C
C   TEST 1-SIGN CHANGE OF DENOMINATOR OF GAS DERIVATIVE
C
14 PREV=SIGN(1.0,DDVGXP)
   CURNT=SIGN(1.0,DDVGX)
   IF(PREV.EQ.CURNT)GO TO 16
   WRITE(3,101)DDVGX
   GO TO 48
C
C   TEST 2-DISORDER OF DENOMINATOR OF GAS DERIVATIVE
C
16 IF(DDVGX.LE.DDVGXP)GO TO 18
   WRITE(3,112)DDVGX
   GO TO 48
C
C   TEST 3-DISORDER OF GAS MACH NUMBER
C
18 IF(M.EQ.1)GO TO 20
   IF(GM.LE.GMP)GO TO 30
   GO TO 22
20 IF(GM.GE.GMP)GO TO 30
22 WRITE(3,115)GM
   GO TO 48
C
C   TESTS 4 THRU 6-FAILURE OF SYSTEM PROPERTIES TO BE GREATER THAN 0
C
30 IF(TRRP.GT.0.0)GO TO 32
   FAIL=1
   WRITE(3,113)FAIL
   GO TO 48
32 IF(TRRG.GT.0.0)GO TO 34
   FAIL=2
   WRITE(3,113)FAIL
   GO TO 48
34 IF(PRRG.GT.0.0)GO TO 38
   FAIL=3
   WRITE(3,113)FAIL
   GO TO 48
C
C   TEST 7-ENTROPY MAXIMUM (SEE00044)
C
38 DDVGXP=DDVGX
   GMP=GM
   AR=(TRRG/(PRRG*VRRG))*(1.0+((XMR*C*PRRG*VRRG)/(VRRP*TRRG)))
   RN=(VRRG/TRRG)*(1.0-(VRRP/VRRG))*PRRG*EP

```

```

RNABS=ABS(RN)
IF(RNABS.LE.1.OE+05)GO TO 40
K=3
WRITE(3,102)K,RNABS
CALL EXIT
40 CALL REYNUM
IF(RN.LT.0.0)DC=-DC
PR=2.0+(0.459*(RNABS**0.55))*(EPP**0.33)
RNT=(VRRG*PRRG*D*EP/TRRG)
IF(RNT.LE.1.OE+05)GO TO 41
CR=0.1382/((RNT)**0.177)
GO TO 43
41 CR=0.316/((RNT)**0.25)
43 GM=(VRRG/((TRRG*GAMMA/Z)**0.5))
HMX=HMI+(((XMR*A)*(TRRP-TRRPO)+(TRRG-TRRGO))/(1.0+XMR))
SMX=SMI+((XMR*A*ALOG(TRRP/TRRPO))+ALOG(TRRG/TRRGO)-((2.0/Z)*ALOG(P
LRRG/PRRGO)))/(1.0+XMR)
G=(PRRG/TRRG)*(((AR*VRRG)/(XMR*C))-(VRRG/VRRP))
X=X+DX
WRITE(3,105)X
WRITE(3,106)VRRG,VRRP,TRRG,TRRP,PRRG,RN,AR,DC,PR,CR,GM,HMX,SMX,G
WRITE(4)X,VRRG,VRRP,TRRG,TRRP,PRRG,RN,AR,DC,PR,CR,GM,HMX,SMX,G
44 IF(SMX.LE.SM)GO TO 46
SM=SMX
IF(IDID.EQ.0)GO TO 10
IF(M.EQ.2)GO TO 45
IF(GM.GE.0.95)DX=DX3/5.0
GO TO 10
45 IF(GM.LE.1.01)DX=DX4/5.0
GO TO 10

C
C ** BRANCH --
C ** IF SUBSONIC FINITE DIFF. JUST COMPLETED -- TO SUPERSONIC
C ** IF SUPERSONIC FINITE DIFF. COMPLETED -- TO END
C
46 WRITE(3,114)
C
C INSTRUCTIONS FOR BACKING PROGRAM UP TO REAPPROACH SHUTOFF POINT
C WITH FINER INCREMENTS
C
48 IF(M.EQ.2)GO TO 50
GO TO 52
50 XMRNB=9.0
IF(XMR.GE.XMRNB)GO TO 54
52 IF(IDID.EQ.1)GO TO 54
IDID=1
CALL BACKUP
READ(4)X,VRRG,VRRP,TRRG,TRRP,PRRG,RN,AR,DC,PR,CR,GM,HMX,SMX,G
WRITE(3,105)X
WRITE(3,106)VRRG,VRRP,TRRG,TRRP,PRRG,RN,AR,DC,PR,CR,GM,HMX,SMX,G
SM=SMX
GO TO 10

C
54 M1=M

```

```

GO TO(6,56),M1
56 READ(1,109)MORE

```

C  
C  
C  
C  
C

```

**      HAVE CONTROL DATA CARD READY IF NEW DATA IS TO FOLLOW ...
**      TO READ NEW DATA, PUT A -1- IN COL. 5.
**      USE A CONTROL CARD WITH -0- IF NO NEW DATA FOLLOWS.

```

```

IF(MORE.EQ.1)GO TO 2
CALL EXIT
END

```

```

MON$$      EXEQ FORTRAN, , , 10
SUBROUTINE REYNUM

```

C  
C  
C  
C

```

**      SUBROUTINE FOR CALCULATING *DC* FOR VARIOUS RANGES
**      OF REYNOLDS NUMBER

```

```

COMMON RNABS,DC,NTIMES,DX,DX3,DX4,M
IF(RNABS.LE.1000.0)GO TO 58
DC=0.44
RETURN

```

```

58 IF(RNABS.LE.10.0)GO TO 60
DC=13.0/SQRT(RNABS)
RETURN

```

```

60 IF(RNABS.LE.1.0)GO TO 62
DC=24.0/(RNABS**0.75)
RETURN

```

```

62 DC=24.0/RNABS
RETURN
END

```

```

MON$$      EXEQ FORTRAN, , , 10
SUBROUTINE BACKUP

```

C  
C  
C  
C

```

SUBROUTINE FOR BACKING PROGRAM UP TO REAPPROACH SHUTOFF POINT
WITH FINER INCREMENTS

```

```

COMMON RNABS,DC,NTIMES,DX,DX3,DX4,M
DO 64 J=1,NTIMES
64 BACKSPACE 4
DX=DX3
IF(M.EQ.2)DX=DX4
RETURN
END

```

```

MON$$      EXEQ LINKLOAD
           PHASEENTIREPGM
           CALL FLOW

```

```

MON$$      EXEQ ENTIREPGM,MJB

```

## APPENDIX B

### EXPERIMENTAL DATA

The measured experimental laboratory data and resulting calculated quantities for one single-phase and two air-particle test runs are shown in Tables VI, VII, and VIII, respectively. Table IX includes the list of experimental equipment used in this investigation.

TABLE VI  
EXPERIMENTAL SINGLE-PHASE DATA

(X=0.0)

Station	x°	P <sub>g</sub> -lb. <sub>f</sub> /in. <sup>2</sup>	lb. <sub>f</sub> /in. <sup>2</sup> -ab.	V <sub>g</sub> -ft./sec.	T <sub>g</sub> -°R	V <sub>g</sub> <sup>o</sup>	T <sub>g</sub> <sup>o</sup>	P <sub>g</sub> <sup>o</sup>	M <sub>g</sub>
1-Inlet	0	57.0	71.3	312.0	532.2	.123	1.0	1.0	.276
2	48.5	54.2	68.5	324.3	531.7	.128	.999	.962	.2858
3	97.0	50.8	65.1	341.9	530.3	.1351	.997	.913	.3025
4	145.5	47.2	61.5	360.0	529.0	.142	.994	.863	.319
5	194.0	43.6	57.9	380.8	528.2	.1485	.9925	.813	.338
6	242.5	39.3	53.6	409.0	526.2	.162	.989	.752	.363
7	291.0	34.9	49.2	444.0	523.7	.1757	.983	.689	.396
8	339.5	28.7	43.0	513.0	518.9	.2025	.974	.604	.460
9	388.0	22.1	36.4	586.0	510.1	.232	.958	.511	.529
10-Exit	436.5	3.4	17.7	1052.0	448.7	.416	.8425	.248	1.01

Nozzle Inlet Pressure P<sub>gni</sub>: lb.<sub>f</sub>/in.<sup>2</sup>(gage)-70.5  
lb.<sub>f</sub>/in.<sup>2</sup>(abs.)-84.8

Particle Mass Flow Rate: m<sub>p</sub> = 0.0

Nozzle Inlet Temperature T<sub>gni</sub>: mv-1.07  
(System Stagnation Temp.) °R-540.5

Air Mass Flow Rate: m<sub>g</sub> = 9.27 lb.<sub>m</sub>/min.

Pressure Drop Across Nozzle ΔP<sub>n</sub>: in.h<sub>2</sub>O-19.0(Av.)

$$m_g = KCF_d d_{nt}^2 \sqrt{P_{gni} \Delta P_n / T_{gni}} \quad \text{where}$$

$$CF_d = .987 \text{ (ASME Nozzle Codes)}$$

$$d_{nt} = .75 \text{ in. (Nozzle Throat Diameter)}$$

Atmospheric Pressure P<sub>a</sub>: lb.<sub>f</sub>/in.<sup>2</sup>-14.3

Atmospheric Temperature T<sub>a</sub>: °F-80.0

Reference Conditions: P<sub>gl</sub> = 71.3 lb.<sub>f</sub>/in.<sup>2</sup>

$$T_{gl} = 532.2 \text{ } ^\circ\text{R}$$

$$V_{gl} = \sqrt{2g_c c_{gl} T_{gl}} = 2531 \text{ ft./sec.}$$

$$K = 6.87$$

TABLE VII  
EXPERIMENTAL TWO-PHASE DATA

(X-0.114)

Station	$x^\circ$	$P_g$ -lb. <sub>f</sub> /in. <sup>2</sup>	lb. <sub>f</sub> /in. <sup>2</sup> -ab	$V_g$ -ft./sec.	$T_g$ - <sup>o</sup> R	$V_g^\circ$	$T_g^\circ$	$P_g^\circ$	$M_g$
1-Inlet	0	59.0	73.36	299.0	530.7	.1182	1.0	1.0	.264
2	48.5	56.3	70.66	309.0	530.5	.1221	.999	.962	.273
3	97.0	53.3	66.66	324.3	528.95	.1272	.996	.909	.287
4	145.5	49.6	63.96	336.3	528.1	.1319	.995	.872	.298
5	194.0	46.0	60.36	357.5	527.4	.1412	.994	.822	.317
6	242.5	41.6	55.96	383.0	525.7	.1515	.990	.763	.340
7	291.0	36.6	50.96	418.0	523.0	.1640	.985	.694	.373
8	339.5	30.1	44.46	475.0	518.8	.1877	.977	.606	.426
9	388.0	22.7	37.06	562.5	512.0	.2225	.964	.505	.506
10-Exit	436.5	2.6	17.96	1022.0	450.6	.4040	.848	.245	.982

Nozzle Inlet Pressure  $P_{gni}$ : lb.<sub>f</sub>/in.<sup>2</sup> (gage)-70.0  
lb.<sub>f</sub>/in.<sup>2</sup> (abs.)-84.36

Particle Mass Flow Rate:  $m_p = 1.03$  lb.<sub>m</sub>/min.

Nozzle Inlet Temperature  $T_{gni}$ : mv-1.01  
(System Stagnation Temp.) <sup>o</sup>R-538.0

Air Mass Flow Rate:  $m_g = 9.06$  lb.<sub>m</sub>/min.

Pressure Drop Across Nozzle  $\Delta P_n$ : in.h<sub>2</sub>O-17.75(av.)

$$m_g = K C F_d d_{nt}^2 \sqrt{P_{gni} \Delta P_n / T_{gni}} \quad \text{where}$$

$C F_d = .987$  (ASME Nozzle Codes)  
 $d_{nt} = .75$  in. (Nozzle Throat Diameter)  
 $K = 6.87$

Atmospheric Pressure  $P_a$ : lb.<sub>f</sub>/in.<sup>2</sup>-14.36

Atmospheric Temperature  $T_a$ : <sup>o</sup>F-78.5

Reference Conditions:  $P_{g1} = 73.36$  lb.<sub>f</sub>/in.<sup>2</sup>

$T_{g1} = 530.7$  <sup>o</sup>R

$V_{g1} = \sqrt{2g_c c_{g1} T_{g1}} = 2530$  ft./sec.

TABLE VIII  
EXPERIMENTAL TWO-PHASE DATA

(X=0.153)

Station	$x^\circ$	$P_g$ -lb. <sub>f</sub> /in. <sup>2</sup>	lb. <sub>f</sub> /in. <sup>2</sup> -ab.	$V_g$ -ft./sec.	$T_g$ - $^\circ$ R	$V_g^\circ$	$T_g^\circ$	$P_g^\circ$	$M_g$
1-Inlet	0	59.3	73.6	283.5	538.2	.1114	1.000	1.000	.249
2	48.5	55.6	69.9	299.0	537.6	.1175	.9985	.950	.2625
3	97.0	51.9	66.2	314.0	536.7	.1234	.997	.899	.2764
4	145.5	47.5	61.8	336.0	535.4	.1320	.995	.839	.2963
5	194.0	43.1	57.4	362.0	533.9	.1422	.990	.781	.320
6	242.5	38.2	52.5	390.0	532.3	.1532	.988	.713	.3443
7	291.0	32.7	47.0	432.5	529.4	.1700	.984	.639	.383
8	339.5	25.8	40.1	510.1	523.3	.2020	.972	.544	.454
9	388.0	18.0	32.3	620.0	513.0	.2437	.953	.438	.558
10-Exit	436.5	2.0	16.3	1068.5	449.4	.4195	.834	.2215	1.026

Nozzle Inlet Pressure  $P_{gni}$ : lb.<sub>f</sub>/in.<sup>2</sup> (gage)-70.0  
lb.<sub>f</sub>/in.<sup>2</sup> (abs.)-84.3

Particle Mass Flow Rate:  $m_p = 1.317$  lb.<sub>m</sub>/min.

Nozzle Inlet Temperature  $T_{gni}$ : mv-1.17

Air Mass Flow Rate:  $m_g = 8.62$  lb.<sub>m</sub>/min.

(System Stagnation Temp.)  $^\circ$ R-544.9

Pressure Drop Across Nozzle  $\Delta P_n$ : in.h<sub>2</sub>O-16.3(av.)

$$m_g = KCF_d d_{nt}^2 \sqrt{P_{gni} \Delta P_n / T_{gni}} \quad \text{where}$$

Atmospheric Pressure  $P_a$ : lb.<sub>f</sub>/in.<sup>2</sup>-14.3

$CF_d = .987$  (ASME Nozzle Codes)

Atmospheric Temperature  $T_a$ :  $^\circ$ F-85.0

$d_{nt} = .75$  in. (Nozzle Throat Diameter)

Reference Conditions:  $P_{g1} = 73.6$  lb.<sub>f</sub>/in.<sup>2</sup>

$K = 6.87$

$T_{g1} = 538.2$   $^\circ$ R

$V_{g1} = \sqrt{2g_c c_{g1} T_{g1}} = 2542$  ft./sec.

TABLE IX  
EXPERIMENTAL EQUIPMENT

Instrument	Manufacturer	Range	Division
Bourdon-type pressure gage	Heise	0-175 psig	0.2 psig
Bourdon-type pressure gage	Ashcroft	0-100 psig	1.0 psig
Vertical water manometer	Meriam	0-60 in.h <sub>2</sub> O	0.1 in.h <sub>2</sub> O
Milli-Voltmeter	Hewlett-Packard	0-3 mv	.05 mv
Scale balance	Fairbanks	0-70 lbs.	.02 lb.
Air pressure regulator	Schrader	0-100 psig	2.0 psig
No. 30 Copper-Constantan thermocouple wire	Minneapolis-Honeywell		
Double-acting single-stage air compressor	Chicago Penumatic Tool Co.	Capacity-200 CFM maximum at standard conditions at 110 psig outlet pressure	



VITA

David Michael Adams

Candidate for the Degree of

Doctor of Philosophy

Thesis: THE EFFECT OF PARTICLES ON THE CRITICAL LENGTH IN  
SUBSONIC AND SUPERSONIC GAS-PARTICLE FLOW IN A  
VERTICAL CONSTANT AREA TUBE

Major Field: Mechanical Engineering

Biographical:

Personal Data: Born at Chicago, Illinois, September 4,  
1936, the son of Nicholas M. and Juliana Adams.

Education: Attended grade school in Chicago, Illinois;  
graduated from Central YMCA High School in 1954;  
received the Bachelor of Science degree from Texas  
A. and M. University, with a major in Mechanical  
Engineering, in August, 1959; received the Master  
of Science degree from Texas A. and M. University,  
with a major in Mechanical Engineering, in August,  
1960; completed the requirements for the Doctor of  
Philosophy degree in January, 1965.

Experience: Employed as gas station mechanic and oil  
plant worker during high school; employed as  
maintenance man and assistant chemist for Oil  
Products and Chemical Company, Chicago, Illinois,  
during the summers of 1954 thru 1957; employed as  
general technician and laboratory instructor for  
the Hydraulics Laboratory at the Illinois Insti-  
tute of Technology, in Chicago, Illinois, from  
January, 1958 to June, 1958; employed as research  
engineer at Oklahoma State University, in  
Stillwater, Oklahoma, from June, 1961 to January,  
1962; employed as graduate assistant at Oklahoma  
State University, in Stillwater, Oklahoma, from  
January, 1961 to June, 1964.

Professional and Honorary Organizations: AIAA, Pi Tau  
Sigma.